EXPERIMENTAL AND NUMERICAL INVESTIGATIONS ON THE HEAT TRANSFER PERFORMANCE OF A STACKED DOUBLE LAYER MICROCHANNEL

Thesis Submitted to

UNIVERSITY OF CALICUT

in fulfilment for the award of the degree of

DOCTOR OF PHILOSOPHY

UNDER THE FACULTY OF ENGINEERING

By

SAGAR M. NARAYANAN

(U.O.NO. 2340/2015/Admn. Dated 03.03.2015)

Under the supervision and guidance of

Dr PRADEEP M. KAMATH
Associate Professor,
Department of Mechanical Engineering,
Government Engineering College Trichur, Thrissur.
UNIVERSITY OF CALICUT, KERALA – INDIA.

December 2019

DECLARATION

I hereby declare that this thesis entitled "**Experimental and Numerical Investigations on the Heat Transfer Performance of a Stacked Double Layer Microchannel"** submitted to the University of Calicut, for the award of Degree of Doctor of Philosophy under the Faculty of Engineering is an independent work done by me under the supervision of Dr Pradeep M. Kamath, Associate Professor, Department of Mechanical Engineering, Government Engineering College Trichur, Thrissur, University of Calicut.

I also declare that this thesis contains no material which has been accepted for the award of any degree or diploma of any University or Institution and to the best of my knowledge and belief, it contains no material previously published by any other person, except where due references are made in the text of the thesis

Thrissur
10.12.2019

SAGAR M. NARAYANAN
(U.O.NO. 2340/2015/Admn. Dated 03.03.2015)

Certified that the suggestions/corrections from the adjudicators as per Ref. No. 246425/RESEARCH-C-ASST-1/2019/Admn Dated 14-07-2020 from the Director of Research, University of Calicut, have been incorporated in this thesis.

Thrissur
10.09.2020

SAGAR M. NARAYANAN
(U.O.NO. 2340/2015/Admn. Dated 03.03.2015)

DEPARTMENT OF MECHANICAL ENGINEERING

GOVERNMENT ENGINEERING COLLEGE,THRISSUR
Engineering College P.O., Ramavarmapuram,
Thrissur, Kerala, India, PINCODE – 680009.
Phone No. 0487-2334144 Fax : 0487-2336124
Website : www.gectcr.ac.in

CERTIFICATE

This is to certify that the research work reported in this thesis entitled "**Experimental and Numerical Investigations on the Heat Transfer Performance of a Stacked Double Layer Microchannel"** is being submitted by Mr. SAGAR M. NARAYANAN for the award of the Degree of Doctor of Philosophy to the University of Calicut is based on the bonafide research work carried out by him under my supervision and guidance in the Department of Mechanical Engineering, Government Engineering College Trichur, Thrissur, University of Calicut. The results embodied in this thesis have not been included in any other thesis submitted previously for the award of any degree or diploma of any University or Institution.

Thrissur
10.12.2019

Dr. Pradeep M. Kamath
Supervising Teacher/Associate Professor
Department of Mechanical Engineering,
Government Engineering College Trichur.
University of Calicut

Certified that the suggestions/corrections from the adjudicators as per Ref. No. 246425/RESEARCH-C-ASST-1/2019/Admn Dated 14-07-2020 from the Director of Research, University of Calicut, have been incorporated in this thesis.

Thrissur
10.09.2020

Dr. Pradeep M. Kamath
Supervising Teacher/Associate Professor
Department of Mechanical Engineering,
Government Engineering College Trichur.
University of Calicut

ABSTRACT

The modern technology is attaining a significant upgrade in the electronic system performance after the use of very large scale integration techniques. The high circuit density and faster operation of electronic devices result in a huge amount of heat to be dissipated. Conventional methods of heat removal fail in such a scenario. Heat dissipation using a double layer circular microchannel heat sink is a promising solution for the above problem.

In the present study the heat transfer characteristics, flow parameters and flow mal-distribution of a double layer circular microchannel heat sink for different flow configurations are studied both numerically and experimentally. The research work is conducted by initially conducting an experimental study on a double layer stacked microchannel.

Experiments were also conducted on a single layer microchannel for comparison with a stacked microchannel. Lower mass flow rates are achieved by a gravity feed system and higher mass flow rates are obtained using the peristaltic pump. Different series of flow configurations are also studied by changing the locations of inlet and outlet.

The experimental study is followed by numerical investigation using the commercial Ansys Fluent 16.1 software. The numerical results are validated with the results of the experiment. Further, a parametric study is conducted numerically and also the effect of mal-distribution is studied. It can be concluded that the double layer microchannel has higher heat removal rate than the single-layer microchannel with a lower pressure drop. The counter flow configuration with the upper inlet is found to be a better performer than the rest of the configurations studied. The present configuration gave a base temperature lower than 55^0C (which is the optimum operating temperature of electronics for safe operation and long life) even for a heat load of $25W/cm^2$.

Dedicated

First, to almighty

GOD

who keep me alive, without his support and guidance

My PhD. *program*

would not have moved forward to the end.

Second, to my beloved

father, ***Narayanan M. K.***

mother, ***Vijayalakshmi C. N.***

wife, ***Reema K. R.***

daughter, ***Medha M.***

and

son, ***Madhav M.***

who sacrificed a lot for my dream to come true.

ACKNOWLEDGEMENT

Before everything, I would like to thank **God Almighty** for all support in this research work and all in my life.

I would like to express sincere gratitude to my research supervisor and guide **Dr. Pradeep M. Kamath,** Associate Professor, Government Engineering College, Trichur for his continuous support, guidance and valuable suggestions throughout the research. His trust, enthusiasm, motivation and efficient discussions helped me throughout this research and the writing of the thesis. I think this study would not be completed without his intellectual advice and support.

I also express my sincere thanks to all my doctoral committee members **Dr. Mohandas V. P.,** Professor and Head Department of Mechanical Engineering and Chairman of the Doctoral Committee, **Dr. Pradeep Kumar P.**, Associate Professor, Aerospace Engineering, IIST Valiamala, Thiruvananthapuram and **Dr. Jithesh P. K.**, Assistant Professor, Department of Mechanical Engineering, Government Engineering College Kozhikkode, for their valuable support and suggestions during this research work.

I would like to thank **Dr. Sheeba V. S.**, Principal, **Dr. Jayanand B.**, **Dr. Indiradevi K. P.** and **Dr. Vijayakumar K.,** former principals, **Dr. Vijayan P.**, Chairman, Engineering Research Council and **Dr. Nandakumar M.**, former Chairman, Engineering Research Council, Government Engineering College Thrissur, for extending the facilities in the research centre. I also like to express my special thanks to **Dr. Jayadevan K.R.**, former Chairman of the Doctoral Committee for his support and motivation for the research work.

I would like to thank **Dr. Ramesh A.**, **Dr. Sunilkumar C. P.**, and **Prof. E. C. Ramakrishnan,** former head of the department, all faculty members and non-teaching staffs in the Department of Mechanical Engineering, Government Engineering College, Thrissur for their valuable suggestions, support and help during this research work.

I would like to express special thanks to all fellow research scholars in my department and our research center for guiding me in the right direction throughout the research. My sincere thanks to **Mr. Shajiraj K. V.,** Mechanical Engineering department for the extended support in this research work. Special thanks to **Mr. Hareesh S.**, **Mr. Mohamed Fuhad Sanil M. V.**, and **Mr. Sidharth R.**, Postgraduate scholars in ICTM, Department of Mechanical Engineering for their effort and support to make this research work a success.

I express my sincere thanks to **Mr. Sunil Krishna V.**, Proprietor Kshethropasana, Konikkara, Thrissur and **Mr. Dinesh Kumar V. R.**, Proprietor STC Engineering, Peringandoor, Thrissur for the great support in connection with the research work.

I express my sincere thanks to **Dr. Krishnakumary M. P.**, Professor, Retired, Department of Literature, Vimala College, Thrissur for the support in connection with the thesis correction of this research work.

I would like to thank the **Technical Education Quality Improvement Programme (TEQIP Phase II)** in Government Engineering College Thrissur, under Ministry of Human Resources, Government of India for the financial support given to me.

Finally, I would like to thank **my family, my parents, my relatives and my friends** for continued patience, support, understanding and inspiration throughout this research work. Thank you all for your sacrifices by allowing me to pursue my PhD dream to come true.

CONTENTS

LIST OF TABLES

LIST OF FIGURES

LIST OF ABBREVIATIONS

CF	Counter Flow
DL-MCHS	Double Layer Microchannel Heat Sink
LC	Lower Channel
LIC	Lower Inlet Counter
LIP	Lower Inlet Parallel
MCHS	Microchannel Heat Sink
MFR	Mass Flow Rate
OHPs	Oscillating Heat Pipes
PF	Parallel Flow
SL-MCHS	Single Layer Microchannel Heat Sink
Ti	Inlet Temperature
To	Outlet Temperature
TDP	Thermal Design Power
UC	Upper Channel
UIC	Upper Inlet Counter
UIP	Upper Inlet Parallel

NOMENCLATURE

A	Cross-sectional area of the microchannel in m^2
A_1	Cross-sectional area of the collecting vessel in m^2
A_2	Surface Area of the Convective Wall in m^2
C_p	Specific Heat Capacity in J/kg K
d	Diameter of the microchannel in m
d_1	Diameter of the collecting vessel in m
f	Friction Factor
h	Convective Heat Transfer Coefficient in W/m^2K
h_1	Height of water collected in m
k	Thermal Conductivity in W/m K
L	Length of the microchannel in m
$\dot{m}$	Mass flow rate in kg/s
p	Pressure drop in Pascal
P	Power in Watts
Q	Discharge of the fluid in m^3/s
Re	Reynolds Number
t	Time taken for collecting de-ionized water in seconds
T	Temperature in K
ΔT	Difference in Temperature
u	Velocity in m/s
W	Watt
ρ	Density in kg/m^3

CHAPTER 1
INTRODUCTION

1.1 INTRODUCTION

With the invention of large scale integration techniques, technologies attain a significant upgrade in the electronic system performance. This resulted in a high circuit density and faster operation, leading to a large amount of heat dissipation. It affects the life of the electronic components. The long life of the electronic equipment is obtained by adopting an efficient cooling method. This is achieved by reducing the component temperature as well as the surrounding temperature. For that, a systematized, efficient, and effective electronic cooling technique is needed. Certain active and passive techniques are used in the twentieth century. The proper thermal management of the electronic equipment steer the high lifespan, reduced operational cost, and attains good performance.

The necessity of heat removal from the electronic components massively increases with recent years. Moore (1998) conducted a study related to the number of the transistor in a chip. This shown in Fig. 1.1, from this it can be found that the transistor number per chip increases doubly every one and a half years. This increases the number of transistors used, resulting in a large amount of heat is dissipated from the surface of the component. In the early stages, the heat was removed by natural convection techniques by the use of fins, which increase the surface area.

Nowadays due to the increased operational power of the electronic components, these cooling methods are inadequate. The cooling method using a liquid as the coolant is one of the best ways to remove a high amount of dissipated heat. This gives a high heat removal rate compared to conventional techniques. This technique can be used by properly rectifying the leakage problems otherwise it will lead to permanent damage to the electronic components. The channel through which the liquid passes is categorized based on the hydraulic diameter. They are microchannels, mini channels, and conventional channels respectively with increasing hydraulic diameter [Kandlikar and Grande (2003)]

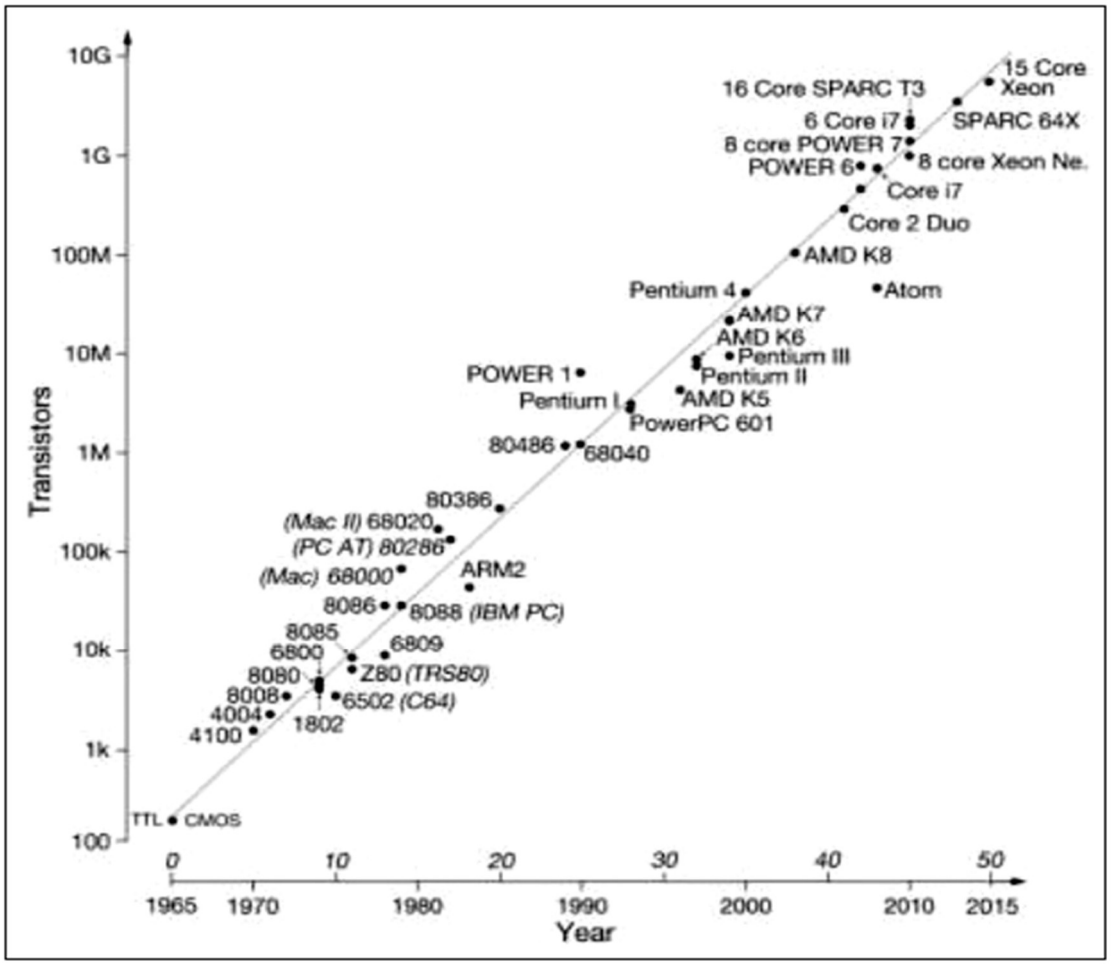

Fig 1.1 Moore's law with time **(Moore G.1998)**

An improvement in the cooling of such electronic devices is obtained after the use of microchannel cooling techniques. A high-performance cooling is evinced in this new technique.

Figure1.2 represents the miniaturization of microprocessor size with the calendar year, which is studied by Thompson and Parthasarathy (2014). This shows that nanotechnology is to be used for the manufacturing of chips during 2020 due to the size reduction to a nanometer.

Tuckerman and Pease (1981) used a microchannel heat sink (MCHS) for cooling purposes. The channel consists of a rectangular cross-section silicon wafer. The heat given at the base of the substrate is uniform.

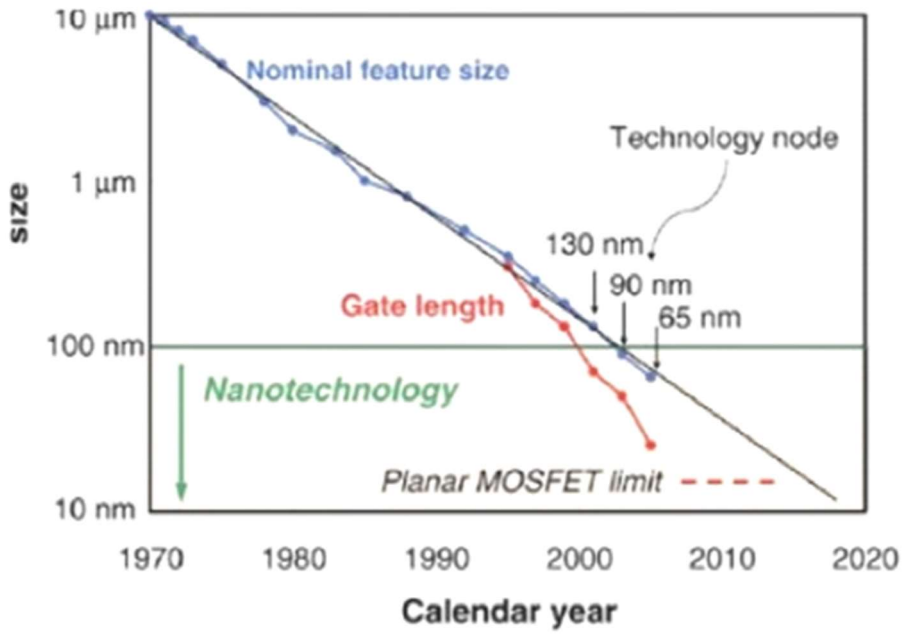

Fig 1.2 Miniaturization of the microprocessor **(Thompson and Parthasarathy.2014)**

They found that small geometric sizes have higher heat transfer characteristics and lower cooling fluid requirements than conventional heat sinks. Following these many numerical, analytical, and experimental studies are done with the use of a single layer microchannel with various geometry, heat flux, and using different fluids.

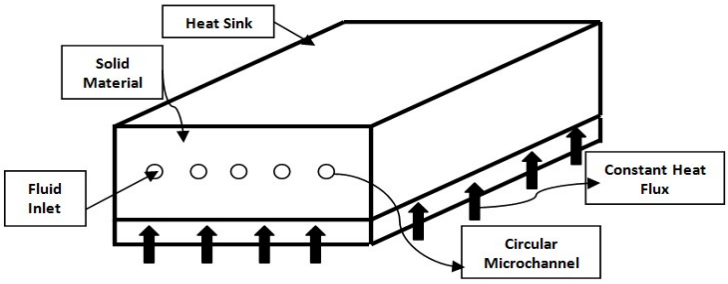

Fig 1.3 Example for Single Layer Microchannel

The example for a single layer circular microchannel is shown in Fig.1.3. The thermal and flow performance of a single-phase forced convection in circular microchannel heat sink analyzed either experimentally or numerically with different working fluid and various flow rates. The result commonly implies the heat transfer rate increased with the

mass flow rate (MFR) of the fluid. The temperature at various points and the outlet of the fluid also decline with the flow rate of the fluid.

A recent development in the microchannel flow is the concept of enhancing heat exchange with the double layer configuration. This new state of the art was first reported by Vafai and Zhu (1999) and pointed out that a double layer microchannel heat sink (DL-MCHS) requires less pressure drop and pumping power compared to the single-layered microchannel heat sink (SL-MCHS). The main purpose of implementing a double layer channel is to lower the temperature gradient along the axial direction. The dispelling heat through the microchannel is reduced with the channel hydraulic diameter and resulting in a higher heat transfer coefficient for the smaller channels. To obtain a good total heat transfer performance, the number of microchannels fabricated on a heat sink can be increased. The example for double layer circular microchannel is shown in Fig.1.4.

The double-layer concept is widely used for the increase of heat transfer in electronic equipment. The studies are done in various cross-sectional shapes and with different cooling fluids. The pressure drop is smaller than the single-layer analysis.

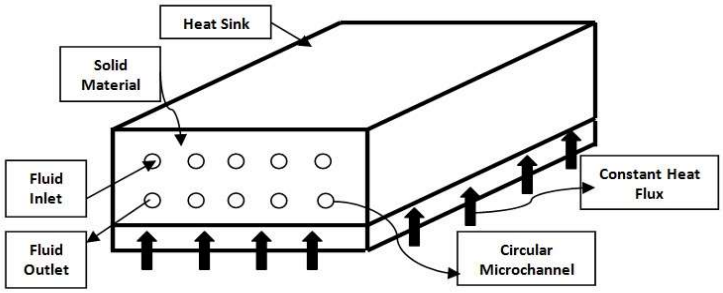

Fig 1.4 Example for Double Layer Microchannel (CF)

The results obtained with flow misdistribution through each layer with the double layer concept are limited in the literature. Numerically it can be analyzed but neither study pointed out the area of maldistribution. Limited studies are done to evaluate the heat transfer performance and pressure drop distribution of the double layer with the circular microchannel.

Nowadays, the double-layer microchannel concept does not establish very well to accurate prognosis. The inconsistencies are occurred in the experimental pressure drop values and heat transfer performances, since the inception of the microchannel studies. The heat transfer performance and friction factor values in microchannels are generally case-specific causing discrepancy with the conventional theory applicable in a similar microchannel system.

This dissimilarity in the experimental result is corrected by adopting proper numerical and analytical methods. Incorporation of the results of experimental and numerical work, usually there is a great dependency on validating the numerical result with the experimental result.

1.2 MOTIVATION FOR THE RESEARCH

The high processing speed and increased power cause significant heat generation. This extra heat has to be dissipated for a longer life of the electronic. Heat dissipation is an important aspect of thermal management. Heat dissipation from small areas is a challenge for the researchers. A heat sink is a mechanical part that is connected to an electronic device, that helps in dissipating the thus heat generated in it. Meanwhile, there are plenty of different heat sinks such as comb-profile heat sinks, finger-shaped heat sinks; miniature heat sinks, etc ready in this field, which is designed for special demands. Besides aluminium, the heat sinks are also made of good thermal conducting material like copper.

The new 9^{th} Generation Intel Core extreme edition series processor produces a Thermal Design Power (TDP) of 90 W to 95 W (*www.Intel.com*). The package size of this processor is about 37.5mm x 37.5mm. This type of processor requires high heat removal from its surface to maintain the surface temperature below the optimal operating temperature levels of 80^{o}C. Single-layer microchannels have been extensively studied. But for high heat removal in small areas multilayer channels are required.

In the present study, a detailed study of these types of heat sinks with the water as the coolant is studied extensively. The effects of flow and microchannel thermal performance are also studied in detail.

1.3 STRUCTURE OF THE THESIS

This thesis incorporates five chapters arranged logically to simplify the reader to know the perspective of the author for attaining the complete aim of the research work.

The material included in all chapters is simply explained as follows. Figure1.5 provides an overview of the structure of the thesis.

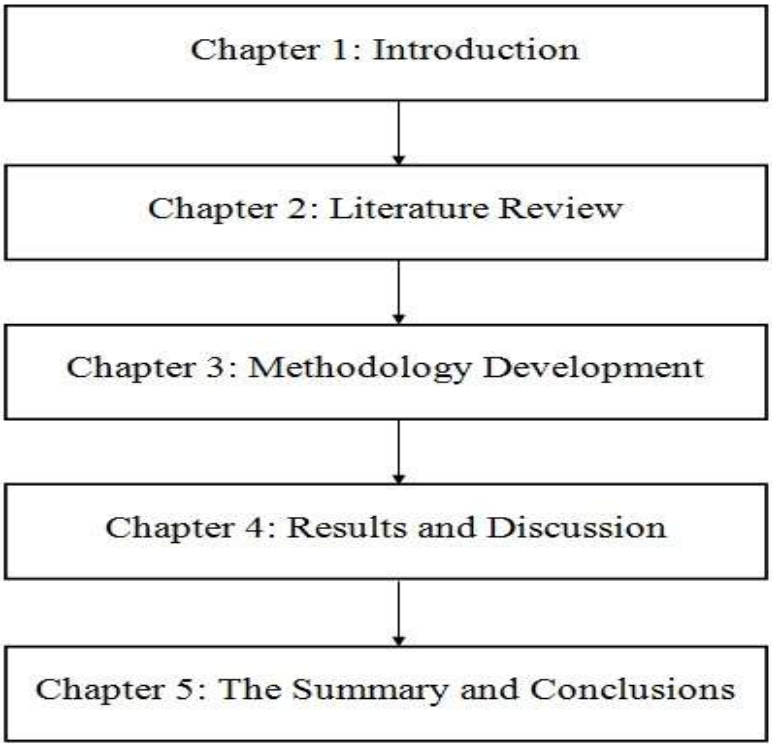

Fig 1.5 Structure of the Thesis

Chapter 1 briefly explains the introduction of the study. It also contains research motivation and the structure of the thesis in detail.

Chapter 2 explains the collective literature related to this work. The ideas of the microchannel with its history are explained in this chapter. The types of microchannel including single layer and double layer are reviewed in this chapter. This chapter also includes the research gap, research problem, research objective, research methodology, and the scope of future work.

Chapter 3 presents a complete analysis of the methodology involved in this research work. The numerical analysis used in this study and the experimental set up fabricated are explained. The laminar flow condition and turbulent flow conditions are used in the numerical analysis. The experiment is conducted with the application of the pump feed system and the gravity feed system.

Chapter 4 presents the analysis of the results obtained from both numerical and experimental work. The detailed flow and thermal analysis explained in this chapter.

Chapter 5 presents a complete summary of the study in brief. This chapter also explains the complete conclusion of the research work. At the end of this chapter contains the limitations and the future scope of this research work.

1.4 SUMMARY

An incisive analysis of the single layer and double layer microchannel heat sink and the application in the industrial area are mentioned in this chapter. The motivation for the research and the structure of the thesis is explained. A detailed review of the literature has to be done in chapter 2. The literature review is conducted in detail relating to the research gap. The literature about the single layer microchannel and double-layer microchannel are discussed in detail.

CHAPTER 2
LITERATURE REVIEW

2.1 INTRODUCTION

Use of microchannel for heat dissipation was used way back in 1981. Thereafter several researchers have studied the flow and thermal performance of microchannel. This chapter gives an overview of the research and the associated literature in a microchannel in the perspective of heat transfer dissipation. The literature is assorted for flow and heat transfer for single layer and stacked microchannels.

The literature survey is conducted by using different methods and the appropriate information and data regarding the work collected, are referred to the following paragraph.

Some of the keywords relating to the topic are as follows. "Microchannel heat transfer", "Single-phase convective heat transfer in a microchannel", "Flow parameters in the microchannel", "Single-layer microchannel", "Double-layer microchannel", "Stacked microchannel", "Flow mal-distribution in the mini-channel", "Double phase convective heat transfer", "Flow-through mini-channel", and "Microchannel heat transfer with different geometry".

A comprehensive search is completed using the general search engines with the keywords as above in single or in combined form. Using different journals of various publishers, collective papers are investigated thoroughly and the relevant papers studied in detail. The relevant works of the literature are arranged accordingly for a useful reference in the work.

The literature survey is mainly focused on a single layer and double layer microchannel heat transfer and flow performance. The following sections describe the single layer and double layer microchannel study in detail from the literature.

2.2 SINGLE LAYER MICROCHANNEL

Tuckerman and Pease (1981) instigated the heat transfer performance of a microchannel heat sink on a rectangular silicon wafer of 1 x 1 cm^2 and used for cooling purposes. The experiment was conducted with deionized water as the working fluid. The working fluid is passed out to the outlet manifold of a similar hole by maintaining a pressure of 31Psi. Heat given at the base of the heat sink is uniform. It was found that small geometric sizes have higher heat transfer characteristics and lower cooling fluid requirements than conventional heat sinks. The experimentally obtained thermal resistance was validated with the theoretically obtained data. Since then the thermal performance improvement with different geometries has been studied by many authors.

Adams *et al.* (1998) organized the work related to forced convection in circular microchannels with two hydraulic diameters 0.76 mm and 1.09 mm. The experiment was conducted using water as the coolant and compared the outcome with previous numerical results. The deviation between the experimental and the predicted Nusselt number was more significant for smaller microchannel than the others. The heat transfer enhancement was the same as with the existing literature.

Qu and Mudawar (2002) conducted the heat transfer study of 231µm wide and 713µm deep rectangular microchannel for two heat flux levels of 100 W/cm^2 (for Re from 139-1672) and 200 W/cm^2 (for Re from 385-1289). The pressure drop and the temperature distributions were matched with the numerical results. Within the tested Reynolds number range of 139-1672, laminar to turbulent change inflow was not observed. It was also noticed for large Reynolds number, the fluid outlet temperature and the heat sink temperatures decreased with the expense of the larger pressure drop.

Lee *et al.* (2002) experimentally studied heat transfer in a rectangular microchannel heat sink. The total projected channel area is 1 cm^2 and water is used as the cooling fluid. The channel width was 54 µm and height was 215 µm. The maximum local system resistance was varied from 0.10 to 0.34 ^0C /W /cm^2. The heat flux of 109 W/cm^2 was ensured throughout the experiment with 55 k Pa drop in pressure.

Kandlikar and Grande (2002) studied the thermohydraulic performance and different fabrication technology in the microchannel flow passages. The micro-fabrication technology, semiconductor like fabrication techniques, high aspect ratio lithography and modelling, and wafer bonding techniques are the different microchannel fabrication technologies discussed in this paper.

Bucci *et al.* (2003) conducted an experimental investigation on fluid flow and heat transfer of fluid in a stainless steel capillary tube of 0.172 mm, 0.290 mm and 0.520 mm diameter. The Reynolds number was varied from 200 to 6000. The heat transfer increases with the Reynolds number. At high Reynolds number, there exist significant changes in the friction factor. The experiment is conducted in the short and long tubes for the same inlet conditions. The results were obtained with the same losses for the entrance and exit.

Chen *et al.* (2004) experimentally investigated the heat transfer and friction characteristics of the fluid flow in silicon microchannel with hydraulic diameter 57 μm and 267 μm. The heat convection capabilities in the phase change and the mechanism with bubble nucleation in the single-phase flow were discussed. The phase changing process in the microchannels absorbs heat and reduces the ambient working temperature. The outcome of friction and the viscosity coefficient for the fluid in the microchannel were much significant than the macrons.

Owhaib and Palm (2004) conducted an experimental study in convective heat transfer in a circular microchannel with 1.7 mm, 1.2 mm, and 0.8 mm in diameter. In the turbulent region, the experimental results showed good agreement with the correlation.

The experimental data were compared and agreed well with the conventional theory in Hetsroni *et al.* (2005). The Poiseuille number was found to be independent of Reynolds number and the viscous energy dissipation was related to the flow parameters like hydraulic diameter, channel length, and Reynolds number. The temperature at the base of the heat sink was found to reduce with an increase in the flow rate.

Lee *et al.* (2005) organized numerical and experimental studies of heat transfer performance in a rectangular microchannel with width varying from 194 μm to 534 μm. The depth of the channel was five times larger than its width. The study also includes a

detailed analysis of heat transfer with different coolant flow rates. The range of Reynolds number selected was from 300 to 3500. The result showed that the heat transfer coefficient increased with the decreasing channel hydraulic diameter. The experimental results for the small microchannel exactly obeyed the classical theory but larger channels showed a 5% average deviation from the predicted theory.

Qui *et al.* (2007) experimentally analyzed the heat transfer characteristics in microtubes of 1.931, 1.042, 0.834 and 0.531 mm diameter with liquid nitrogen. The friction factor was compared with the conventional correlations for a range of Re 10000 – 90000. The effect of the thermal properties of the fluid liquid nitrogen is verified. The Nusselt number for the flow is analyzed and compared with the correlations and attains a higher value than the correlation data.

Li *et al.* (2007) performed their studies in both silica and stainless steel microtubes. The hydraulic diameters of silica and stainless steel micro tube were ranges from 50 μm to 100 μm and from 373 μm to 1570 μm respectively. Reynolds number was ranged from 20 to 2400. The result showed that for low Reynolds number, there was some deviation in experimental Nusselt number and the conventional result. This may be due to the axial heat conduction in the tube wall.

Sung and Mudawar (2008), experimentally and numerically investigated the hybrid microchannels with single-phase and two-phase cooling. The result showed that the correlation for Nusselt number fits with the data within a 6.1% error band.

Naphon and Khonseur (2009) experimentally analyzed the heat transfer characteristics and pressure drop in the MCHS with different configurations. The experiments were conducted with the Reynolds number ranges from 200 to1000 and the heat flux ranges from 1.8-5.4 kW/m^2. The result showed that the shape and size of the roughness irregularities of the channel had a significant effect on heat transfer.

Goldstein *et al.* (2010) reviewed extensively in two review papers the enhancement of heat transfer in single-phase flow through microchannels with different geometries. The reviewed articles are subtitled into different areas like straight wall channel and ducts,

channels having fins, also with complex geometry microchannels. The review also shows that the flow through mini channel obeys the classical correlations for the heat transfer.

Li and Wu (2010) presented a paper that contains a general criterion to classify a channel as micro, macro and, mini channels. The classification was done with different diameter of the channel, by different authors. [Mehendal *et al.* (2000)].

The effects of choking in the microchannel were analyzed by Lijo *et al.* (2012). The engineering applications in the cooling of electronic devices such as chips, semiconductors, and micro-electromechanical systems were encountered by the use of gas flow through the microchannels. The prior research works were done without considering the choking of the fluid. The high heat transfer was generated at the exit and entrance region due to the choking.

Sohel *et.al* (2013) investigated the heat transfer and thermophysical properties of three different nanofluids like Al_2O_3-water, Ti_2O_3-water, CuO-water passing through the circular copper microchannel. It was found that the CuO-water nanoparticles had better thermal enhancements at higher Reynolds numbers.

Moradi and Floryan (2013) performed an analytical study of heat transfer across the microchannel with grooves. The grooves were employed parallel to the flow direction in a rectangular microchannel. The result showed that the grooves increase the heat flow and decrease pressure loss. Furthermore, the simple grooves were replaced with sinusoidal grooves and resulted in improved system performance by about 20% to 30%.

The laminar, transient and turbulent region pressure drop and heat transfer in a single-phase flow through the microtube of diameter 0.254 mm and 0.685 mm were experimentally analyzed by Ozdemir and Kosar (2013). The experimentally found friction factor had ± 20 % deviation with existing literature and the heat transfer was within ± 30 % deviation. A fully developed hydro-dynamically and thermally developing flow were considered in this study. The results showed a high heat transfer rate in the single-phase flow at a high mass flow rate.

A detailed study of the single and two-phase microchannel cooling performance has been conducted in the review of Asadi *et al*. (2014). In single-phase, flow heat transfer and pressure drop characteristics with low Reynolds number merely obey the theoretical results and for high Reynolds number there exist some deviation in the results. It was found that the experimental measurement follows predicted thermally developing behaviours with an increase in hydraulic diameter. The successful interpretation of the two-phase frictional pressure drop is obtained by using a proper mixture viscosity correlation.

Mirmanto (2014) experimentally studied the flow boiling of de-ionized water in single-phase horizontal oxygen-free copper microchannels with 0.438mm, 0.561mm and 0.635mm hydraulic diameters. The linear pressure gradient method was used for comparison with the experimental results. The local heat transfer coefficient increased sharply in the subcooled region with quality. In this study for the high heat fluxes, the measured pressure distribution was not linear. The heat transfer coefficient decreased with the quantity of fixed mass flux and heat flux throughout the channel.

Lim *et al.* (2014) conducted a numerical study to analyze the heat transfer performance of the altering discrete two-phase flows in a microtube. To generate a plug flow pattern, the two immiscible fluids was alternately injected into the microtube. The result showed that the liquid-gas discrete flow has better heat transfer than the liquid-liquid discrete flow. The fluid temperature was more uniform due to the reduction in the fluid temperature near the wall.

Kuppusamy *et al.* (2014) analyzed numerically the performance MCHS with altering slanted passages. The results showed that the thermal resistance lowered by 76.8% and an increase in the overall performance of 146% compared with the simple MCHS with the expense of lower pressure drop. It was found that the increase of the width of the secondary passage and reduction in the angle of the slanted passage results in a better thermal enhancement.

Xia *et al.* (2015) conducted a study of both fluid flow and heat transfer in MCHS with difficult structures. The pressure drop and temperature at various locations were noticed

with experimental analysis, while the numerical analysis was used for detailed study of the complex thermal behaviour.

Xia and Chan (2015) numerically analyzed the heat transfer enhancement in rectangular microchannels. The inlet area was varied and found that heat transfer per unit effective area was greater for the case of the smaller inlet.

Sahar *et al.* (2016) conducted the pressure drop and heat transfer enhancement in a rectangular metallic microchannel. The uniform heat transfer rate was achieved at the base of the microchannel with the same flow rate among all channels of multi-channel configuration. A transition was obtained between Re 1600 – 2000, compared with the existing experiment values. The theoretical friction factor value was little larger than experimental value and in the laminar region, the deviation is insignificant.

Attalla *et al.* (2016) conducted a study on fluid flow and heat transfer of rough rectangular mini channels. The hydraulic diameter of the channel was 5.3 mm and the Reynolds number employed in this study was from 1500 to 5000 with air as the flowing fluid. The result exhibits that with an increase in Reynolds number, the Nusselt number and pressure drop also increases. The friction factor also decreases with the Reynolds number.

Li *et.al* (2016) performed an experimental and numerical study with the dimpled enhanced tube. The Reynolds number in this study was ranged from 500 to 8000 for water, and from 150 to 2000 for a glycol/water solution. The result showed that the heat transfer enhancement was 200 % excess compared with the smooth tube. Compared with traditional heat sink design, relatively high-temperature difference along the microchannel was one of the disadvantages for dimpled microchannel. In the single-layered design, the temperature rise along the channel was controlled by increasing the pressure drop across the channels.

The numerical investigation of the heat transfer in an extended surface rectangular microchannel was conducted by Yadav *et al.* (2016). This study was conducted on a plane rectangular microchannel and extended circular fins were located at three ways in the same plane namely upstream finned microchannel, downstream finned microchannel and completely finned microchannel. The result showed that the average wall surface

temperature of the bottom wall was significantly reduced by using the extended fins in the plane microchannel. The heat transfer performance was higher after using fins and maximum heat transfer obtained for the completely finned microchannel. The pressure drop penalty was higher, but this was negligible with the comparison of profit in the heat transfer.

Mahmoud and Karayiannis (2016) described the evaluation of the models and correlations predicting the flow process in the mini tubes. The main four flow patterns considered were slug, bubbly, churn and annular flow. The annular flow is obvious for increasing the heat flux.

Liu *et al.* (2017) numerically and experimentally evaluated the heat transfer performance of the T-shaped channels and Y-shaped channel heat sinks with liquid GalnSn coolant. The numerical results of the heat transfer coefficient and pressure drop were compared with the experimental data. The result showed that by increasing the number of inlets, the heat sink performance can be improved. The results then compared with water as the cooling fluid and concluded that the liquid GalnSn coolant is the best one based on heat transfer performance.

Ji *et al.* (2017) experimentally investigated the heat transfer enhancement and pressure drop in the mini channel using a combination of the nanofluid and micro fin structure. The result showed that with the increases in the fin number, the heat transfer coefficient was also increased. The heat transfer was also increased with the use of nanofluids as the working fluid.

Qu *et al.* (2017) analyzed the heat transfer performance of the micro-grooved Oscillating Heat Pipes (OHPs) experimentally. The result showed that the OHPs have higher temperature uniformity and lesser initial start-up power required than the smooth tubes. The average evaporator temperature was also significantly reduced.

Li *et al.* (2017) conducted an experimental study to investigate the refrigerant condensation heat transfer characteristics in a micro fin tube arranged horizontally. The result shows that the micro fin tubes attain 30% more pressure drop than the smooth tubes at higher mass flux regions.

The ultrasound is now used in the heat transfer enhancement [Tam *et al.* (2017)] in the field of heat transfer. The Reynolds number of the experiment varies from 600 to 3000 for different numbers of ultrasonic heads. The result found that a better heat transfer with ultrasound occurred in the laminar region.

Sajadifar *et al.* (2017) numerically investigated the fluid flow and heat transfer by forced convection of the non–Newtonian nanofluid. The effects of nanoparticles concentrations and slip coefficient on the flow characteristics were studied. The watery solution of carboxymethyl cellulose and Aluminium oxide was used as the cooling fluid. The result showed that slip velocity and temperature jump on the nanofluids were depended on the slip coefficient.

Vinoth and Kumar (2017) investigated the channel cross-section effect on the heat transfer performance of the oblique finned microchannel heat sink with water and Al_2O_3/water nanofluid of 0.25% volume fraction. The study was conducted in three types of microchannel like square, semi-circular, and trapezoidal.

The result showed that the trapezoidal cross-section has a higher heat transfer coefficient than the other two. The heat transfer can increase by increasing the concentration of nanoparticles into the base fluid. Due to the higher friction factor with the trapezoidal microchannel, the pressure drop was increased more than the semicircle and square microchannel.

Esmaili *et al.* (2018) experimentally investigated the heat transfer in the ribbed microchannel. Different inclined micro ribs with a height of 100 μm were fabricated in a microchannel with 200 μm height. The result showed that a noticeable change in the heat transfer occurred with a negligible increase in pressure drop. Also, an 80% reduction in the thermal resistance occurred by comparing it with the flat microchannel.

The numerical, experimental and analytical studies of the flow and heat transfer in the single-layer microchannel were saturated. A new design of double-layer microchannel is now obtained promising results.

2.3 DOUBLE LAYER MICROCHANNEL

This double layer configuration concept was first reported by Vafai and Zhu (1999). The result of the study showed that a double layer microchannel heat sink (DL-MCHS) need a lesser pressure drop and pumping power compared with a single-layered microchannel heat sink (SL-MCHS). The main purpose of implementing double-layer microchannel was to lower the temperature gradient along the axial direction. The main application of the new design helped to improve the cooling of electronic devices.

Wei and Joshi (2004) performed a numerical study on the stacked microchannel heat sink. The pumping power and heat removal capability of stacked MCHS were lower than the SL- MCHS. The pumping power obtained was too lower in the stacked microchannel heat sink with the same heat removal rate.

Patterson *et al.* (2004) numerically studied conjugate heat transfer in a stacked rectangular microchannel. The result found that the counter-flow analysis gave more uniform temperature distribution than parallel flow analysis. The study was conducted in three configurations of parallel flow, counter flow and serial flow. The pressure drop and different temperatures were noted for the heat transfer performance. The detailed analyze of wall temperature along the flow direction was done in all configurations.

Lei *et al.* (2006) conducted a numerical and experimental analysis on a single and double-layered square heat sink with the mini channel. The multilayered design was more efficient than a single layer design with a reduction in pressure drop. The pressure drop was decreased by increasing the number of layers of the microchannel.

Wei *et al.* (2007) performed the numerical study and experimental work relating to the heat transfer and flow performance on a microchannel heat sink integrated by many layers with the microchannel. For the constant heat removal, the new design was provided less pressure drop than the single-layer one. The result showed that a better uniform temperature profile for the flow-through CF arrangement with the adjacent layer than the PF but the parallel flow has obtained less peak temperature. The thermal performance of the new design is established with numerical and experimental measurements. The overall cooling performance ($0.09^0C/Wcm^2$) was achieved experimentally with stacked MCHS.

Martin *et al.* (2009) numerically studied the simulation-based predictive control of flow maldistribution occurs in a parallel microchannel. The result of the study showed that the bubbles or other particle matter lead to the component damage. The bubbles formed may be removed by changing the valves quickly and thus maldistribution can be reduced.

Levac *et al.* (2011) numerically explained the heat transfer enhancement in the single layer and double layer rectangular microchannel for two Reynolds numbers 116 and 1160. The result showed that the same MFR of the fluid applied in two layers was more effective than the single-layer design. The wall temperature change was increased with MFR. More uniformity was achieved for CF arrangement than the PF arrangement. The results were validated with existing experiment value.

Hung *et al.* (2012) numerically analyzed the fluid flow and heat transfer performance with optimum geometric parameters of a DLMCHS. The simplified conjugate gradient method was used for the optimization procedure. The optimum thermal resistance of 0.12 ^{0}C/W m^2 was attained for a heat sink base area of 100 mm^2 with a constant heat flux of 100 W/cm^2. The total pumping power required was found to be 0.1 W. The result showed that the higher thermal conductivity ratio substrates had achieved more heat transfer performance than the lower ratio ones. Similarly, low dynamic viscosity and high thermal conductivity of the coolant was also affected in the heat transfer performance. The DLMCHS had a 6.3% of better pressure drop than the single-layer microchannel.

Hung and Yan (2012) postulated an optimization approach to search for the optimal thermal resistance in DL-MCHS. The study was conducted in a double layer rectangular microchannel heat sink. The thermal resistance was depended on the different factors that include the type of the nanofluid, particle volume fraction, and different geometric parameters. The heat transfer obtained was more for Al_2O_3-water as nanofluid and also the thermal resistance can be reduced by varying the particle volume fraction.

Wong *et al.* (2013) investigated the heat transfer performance of a double-layered MCHS numerically with parallel flow analysis. The results were compared with counterflow analysis for different microchannel aspect ratio. The finding from this study disclosed that CF analysis had a better thermal performance at the higher Reynolds number with

high aspect ratio. The work was also extended with arranging small thickness middle rib for better heat transfer performance in all Reynolds number.

Dede and Liu (2013) numerically and experimentally investigated the effect of multi-pass branching in MCHS. The study was conducted for a broad range of flow rates with low-pressure drop and high heat fluxes. The thermal and flow parameters were studied with different flow rates range from $1070 < Re < 6370$ with ethylene-glycol/water coolant.

Thermal performance of the MCH exchanger with different working fluids (water, and Al_2O_3-water) having nanoparticles with the volume concentration of 1%, 3% and 5% were performed by Putra *et al.* (2013). The constant temperatures were set for the inlet and outlet condition. The flow rate was ranged from 100 ml/min to 300 ml/min. The overall heat transfer coefficient was increased by up to 15% in each case.

Nielsen *et al.* (2013) numerically investigated the influence of flow maldistribution on the performance of inhomogeneous parallel plate heat exchangers. The study was mainly focused on a performance parameter of the Nusselt number scaling factor. The result showed that the maldistribution of the fluid flow compared with the ideal homogeneous case. Also, high heat transfer performance was obtained in the inhomogeneous stacked parallel plates.

Lu *et al.* (2013) experimentally performed the heat transfer performance in copper-based double-layer microchannel heat exchangers. The result showed that similar heat transfer enhancement and negligible pressure drop penalty were obtained for DLMC-HS compared to SLMC-HS. The effectiveness of the double layer liquid-liquid counter-flow micro heat exchanger was also studied.

Wu *et al.* (2014) numerically conducted a parametric analysis and studied the heat transfer performance of the DLMCHS. The result showed that the coolant used and channel geometry was the main two parameters that determine the heat transfer performance. The overall thermal performance of the double-layer microchannel heat sink was increased by putting the smallest velocity in the upper layer than the lower layer.

Dai *et al.* (2014) investigated the thermal performance of a multi-port microchannel tube with a rectangular cross-section having a hydraulic diameter of 0.715 mm and a circular cross-section with a diameter of 0.86 mm. The analysis was done with both experimental and theoretical methods. The experimental study was conducted by varying the Reynolds number from 50 to 2400 with the ethanol as a working fluid. The result showed that the heat transfer coefficient was decreased by increasing the temperature of the inlet and heat flux.

Leng *et al.* (2015) numerically studied the DL-MCHS with different top layer channel truncation configuration. The better heat transfer was noticed in truncated DLMC than in the original (without truncation) one. The result also showed that an optimum position with truncation was defined by the help of the temperatures in the lower and upper outlet temperatures. Numerical simulation was done using a silicon heat sink with water as the coolant. The effectiveness of the new design was confirmed in the numerical study by employing reduced thermal resistance of the heat sink. The maximum bottom wall temperature difference was obtained in the truncated design than the original design.

Wang *et al.* (2015) numerically analyzed the heat transfer characteristics of a double-layered microchannel with porous fins instead of solid fins. The result of the study was showed that, a 45% reduction in pressure drop which results in less pumping power. The thermal resistance is increased by 15% with the same pumping power.

Dario *et al.* (2015) numerically studied the flow maldistribution of two-phase flows in multi-parallel microchannels. The study is conducted for nine parallel microchannels with an inner diameter 0.8 mm connected to a common plenum. Combined effects of the feeding tube inlet, microchannel header arrangements were studied. The result showed that the horizontal header in horizontal microchannels had an increase in flow rate.

Said *et al.* (2015) numerically studied the flow maldistribution in a microchannel. The result showed that the maldistribution is due to the development of vena-contracta at the inlet to the tube. This effect was studied with two approaches to reduce the flow maldistribution. In the first approach, the tube inlet is reduced by introducing an orifice and the flow maldistribution is reduced 12 times the original. The second approach was

done by increasing the inlet with the nozzle and the flow maldistribution was reduced 7.5 times the original.

Anbumeenakshi and Thansekhar (2016) investigated experimentally the effect of header shape and inlet configuration on flow maldistribution. The analysis was done with two different inlet flow conditions of three cross-sectional shapes of rectangular, trapezoidal and triangular geometry using deionized water as the working fluid. The result of the study showed that the vertical flow inlet configuration gives less maldistribution than the inline inlet flow configuration. At higher flow rate the rectangular cross-section header gave less maldistribution.

The flow maldistribution of inlet header configuration of the plate-fin heat exchanger was performed by Appasaheb *et al.* (2016). The study was focused on the parameters like maldistribution and velocity ratio. The result of the study showed the maldistribution was less in an improved configuration as compared with the conventional header.

Osanloo *et al.* (2016) numerically analyzed the enhancement of DLMCHS with tapered lower and upper channels. The result showed that the optimal temperature distribution was achieved with the help of thermal resistance having a convergence angle of 4^0.

Ahmed and Ahmed (2016) conducted an experimental study with triangular and rectangular aluminium DLMCHS using two nano-fluids of different volume fractions. The triangular double-layer microchannel heat sink was provided with a 27.4 % reduction in wall temperature. Temperature uniformity across the channel in triangular DLMC was 2 ^{0}C higher as compared with the rectangular double-layer microchannel heat sink. The rectangular microchannel had lesser pressure drop at lower pumping power than the triangular microchannel. The result showed that the Al_2O_3-H_2O with 0.9 % volume fraction nanofluid was providing more heat transfer than the 0.3 % volume fraction nanofluid.

Zhao *et al.* (2016) experimentally evaluated the pressure drop and friction factor of a rectangular microchannel with different shaped staggered mini-pin fins. The pin fin shapes were found to be circular, elliptical, square, diamond and triangle. The result showed that the friction factor was increased with Reynolds number, irrespective of the

shape of the fin. In the turbulent condition, the triangular pin fin geometry had attained maximum friction while the elliptical fin geometry of minimum friction factor. The contradictory of this result obtained in the laminar flow region.

Danish and Kim (2017) performed a thermal study on a double layer microchannel under the conditions of non-uniform heating with randomly arranged hot spots. The following three flow designs of counterflow, parallel flow and transverse flow were studied with three sets of heating conditions. The result showed that the less change in temperature was occurred in transverse flow configuration, while the lowest pressure drop occurred in the counterflow configuration.

Siva *et al.* (2017) investigated the flow maldistribution effect on the thermal performance of a parallel microchannel cooling system. The study was conducted by varying the different parameters like channel hydraulic diameter, channel flow configuration, and chip power. The result of the study showed that the high-pressure drop was attained with a reduced hydraulic diameter and achieves an improved channel flow maldistribution among the channels.

Zhai *et al.* (2017) numerically analyzed the temperature distribution in each layer of a double layer configuration with PF and CF arrangements. Each layer was consists of different channel geometries to decrease the pressure drop and attains good heat transfer performance. The temperature increases linearly along the flow direction in the PF arrangement. The temperature increases firstly along the flow direction and reaching a maximum and then decreases within the CF arrangement. By analyzing the transport efficiency of the thermal energy, the irreversibility of heat transfer is analyzed. More temperature uniformity attains for the counter flow with the rectangular channel in the upper layer and complex channel in the lower layer and thus used for the microelectronic cooling.

Zuo *et al.* (2018) numerically analyzed the thermal effects using an improved design CF double-channel micro combustor fueled with hydrogen. The improved counter flow design was achieved with the same temperature of the wall. The non-uniformity of the upper and right wall temperature is reduced by 23.24% and 26.79% respectively.

Wang *et al.* (2018) experimentally investigated the heat transfer efficiency of a complicated microchannel heat sink system. The silicon substrate heat sink etched with a parallel longitudinal microchannel and a copper heat spreader with microchannel electroplated in a transverse direction. The result was showed that the bottom wall temperature, a fluid outlet temperature, and a wall average temperature were decreased with the mass flow rate of the fluid. High local heat transfer efficiency was obtained with a maximum temperature difference of less than 20 ^{0}C.

Deng *et al.* (2018) numerically investigated the thermal and hydraulic performance of the DLMC-HS with different cross-section using a low velocity of 0.0625 m/s to 0.125 m/s. The result showed that the maximum wall temperature difference for circular geometry was less compared with the triangular, trapezoidal and rectangular geometry. The double-layer rectangular microchannel showed a uniform temperature distribution than others.

Jing and He (2018) numerically analyzed the thermal characteristics of staggered DLMC-HS. In this study, an offset was given in the direction of width between the upper and lower layer microchannel. The thermal resistance of this staggered DLMC-HS was increased with offset, for small vertical rib thickness. The thermal resistance was also decreased with increasing inlet velocity.

The review of the literature shows that the investigation related to the flow and thermal performance of a double layer microchannel heat sink with circular geometry is limited. The flow maldistribution study of the microchannel arranged in each layer with separate plenum cannot be seen in any of the related literature.

2.4 RESEARCH OBJECTIVES

The main focus of the research work is to evaluate numerically and experimentally the heat transfer characteristics, flow parameters and flow maldistribution of a double layer circular microchannel heat sink with different flow configurations. The objective of the present study is as follows.

1. To investigate the pressure drop, friction factor, heat transfer performance and flow mal-distribution of a double layer circular microchannel heat sink (DLCMC-

HS) numerically using water as the cooling fluid for different mass flow rates with constant heat input.

2. To experimentally investigate the flow and thermal behaviour of DLCMC-HS using deionized water for constant heat input with

    a. A pump feed system
    b. A gravity feed system

3. To experimentally investigate the flow and thermal behaviour of DLCMC-HS using De-ionized water for constant heat input for different series flow configurations.

2.5 SUMMARY

This chapter mainly focuses on the review of the literature associated with the microchannel heat transfer. The detailed literature is conducted both with the single-layer microchannel heat transfer and double-layer microchannel heat transfer. It is noted that the literature related to flow and thermal performance of double-layer circular microchannel is scarce. Therefore the objective of the present study focuses on this research gap. The next chapter discusses a detailed methodology adopted to achieve the above objectives.

CHAPTER 3
METHODOLOGY DEVELOPMENT

3.1 INTRODUCTION

The objectives of the research are achieved by conducting numerical analysis followed by experimental validation. The details of the numerical analysis and experimental setup are discussed in this chapter. A nutshell view of the methodology followed is elaborated in the Fig.3.1.

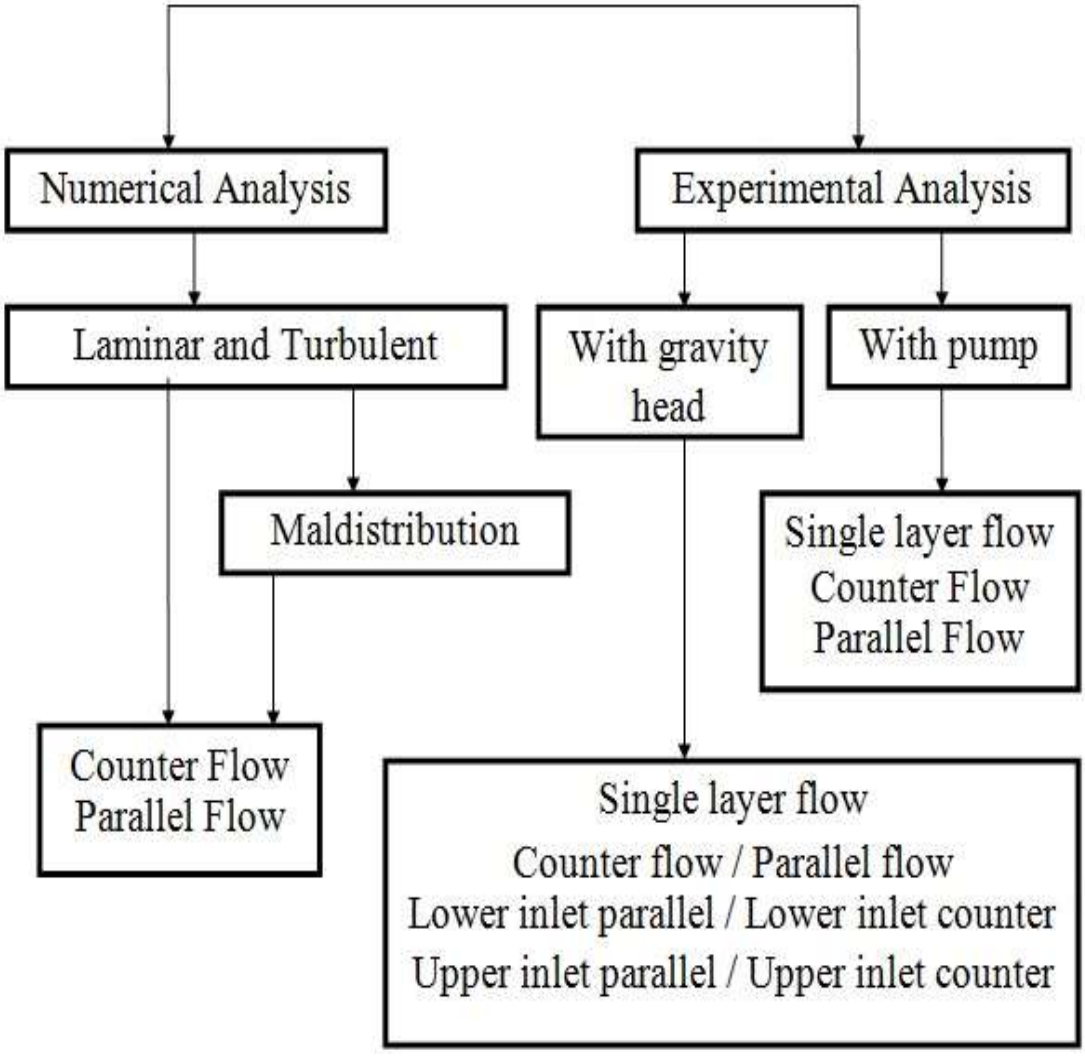

Fig 3.1 Overview of the Research Work

The experiment is conducted with (1) a pump feed system for a higher mass flow rate and (2) with a gravity feed system for a low mass flow rate.

The following are the procedure for this research work

- At first, the numerical analysis is conducted for the laminar model followed by turbulent (standard k-ω model) model. Two configurations are investigated (1) counterflow arrangement and (2) parallel flow arrangement.

- The numerical analysis is also conducted in the laminar and turbulent model for mal-distribution analysis. The analyses are done with two cases of a counterflow arrangement and a parallel flow arrangement.

- Then the experiment is conducted with a pump feed system. The analyses are done with counterflow arrangement, parallel flow arrangement in double-layer microchannel and also for single-layer arrangement.

    - ❖ The limitation of the pump feed system is that low flow rates (less than 0.0035 kg/s) cannot be achieved. Hence, gravity feed system was designed for low flow rates.

- The experimental analysis is done for counter-flow arrangement, parallel flow arrangement, and single-layer arrangement.

- Further, the experiment was also conducted with a series flow arrangement as explained later for lower inlet counter (LIC), lower inlet parallel (LIP), upper inlet counter (UIC), and upper inlet parallel (UIP) arrangements.

The detailed methodology for the numerical analysis and experimental analyses is as follows.

3.2 NUMERICAL ANALYSIS

The numerical simulation used in this research work is done with two flow conditions of laminar flow and turbulent flow. These two are explained in detail as follows.

3.2.1 LAMINAR FLOW CONDITION

The schematic of the test section used in the numerical analysis with the laminar condition is as shown in Fig.3.2 (a). The computational domain used for the numerical analysis is shown in Fig.3.2 (b).

The diameter of the microchannel is 500 µm. The advantage of symmetry consideration with the source and the heat sink is simplified the calculation time. The assumptions made are steady-state, incompressible, single-phase, laminar flow with constant properties for fluid and solid. No-slip and no jump boundary conditions are applied at the solid-fluid interface. The conservation equations used for the fluid flow and heat transfer to solving the model are as follows. The pilot study is conducted for optimizing the flow through the two layers with laminar flow conditions using this model.

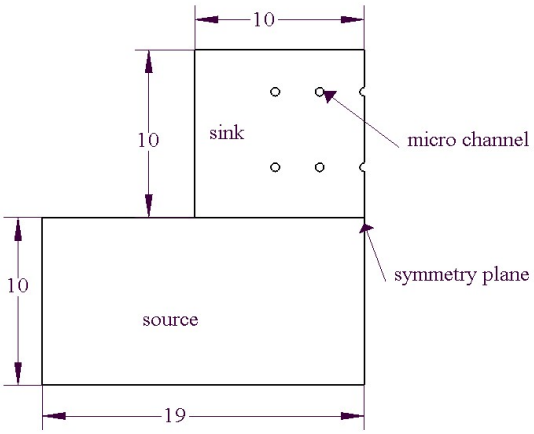

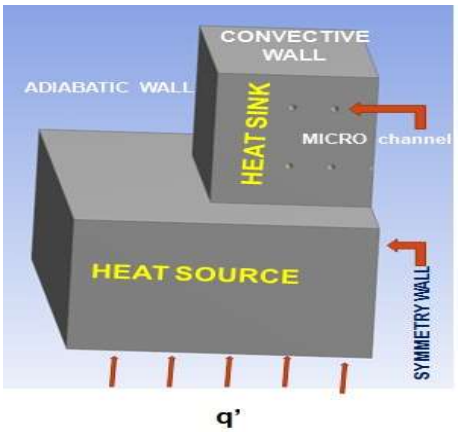

Fig 3.2 (a) Schematic of the Test Section. *Fig 3.2 (b) Computational Domain for Numerical Analysis*

The following are the governing equations

- Equation of Continuity,

$$\frac{\partial u}{\partial x} + \frac{\partial v}{\partial y} + \frac{\partial w}{\partial z} = 0 \qquad \text{(a)}$$

- Equation of Momentum,

$$\begin{aligned}
\rho\left(u\frac{\partial u}{\partial x} + v\frac{\partial u}{\partial y} + w\frac{\partial u}{\partial z}\right) &= -\frac{\partial p}{\partial x} + \mu\left(\frac{\partial^2 u}{\partial x^2} + \frac{\partial^2 u}{\partial y^2} + \frac{\partial^2 u}{\partial z^2}\right) \\
\rho\left(u\frac{\partial v}{\partial x} + v\frac{\partial v}{\partial y} + w\frac{\partial v}{\partial z}\right) &= -\frac{\partial p}{\partial y} + \mu\left(\frac{\partial^2 v}{\partial x^2} + \frac{\partial^2 v}{\partial y^2} + \frac{\partial^2 v}{\partial z^2}\right) \\
\rho\left(u\frac{\partial w}{\partial x} + v\frac{\partial w}{\partial y} + w\frac{\partial w}{\partial z}\right) &= -\frac{\partial p}{\partial z} + \mu\left(\frac{\partial^2 w}{\partial x^2} + \frac{\partial^2 w}{\partial y^2} + \frac{\partial^2 w}{\partial z^2}\right)
\end{aligned} \qquad \text{(b)}$$

- Equation of Energy for solid,

$$\left(\frac{\partial^2 T_s}{\partial x^2} + \frac{\partial^2 T_s}{\partial y^2} + \frac{\partial^2 T_s}{\partial z^2}\right) = 0 \qquad \text{(c)}$$

- Equation of Energy for fluid,

$$\rho * C_p\left(u\frac{\partial T_f}{\partial x} + v\frac{\partial T_f}{\partial y} + w\frac{\partial T_f}{\partial z}\right) = k\left(\frac{\partial^2 T_f}{\partial x^2} + \frac{\partial^2 T_f}{\partial y^2} + \frac{\partial^2 T_f}{\partial z^2}\right) \qquad \text{(d)}$$

The above governing equations are solved using commercial software Ansys Fluent. The following are the boundary conditions used for the simulation. Uniform velocity and temperature conditions are given at the channel inlet and the pressure outlet boundary condition is chosen at the channel outlet. The inlet temperature is set as 303 K. Water is used as the working fluid. The numerical analysis is conducted for the inlet velocity varying from 0.4 m/s to 0.85 m/s (The corresponding mass flow rate ranging from 0.7 x 10^{-3} kg/s to 1.6 x 10^{-3} kg/s). The residual is set as a convergence criterion for all equations is of 10^{-9}. At the bottom of the heat source block, heat flux corresponding to 100 W is applied. The heat sink top is set as convective with a convective wall heat transfer coefficient of 12 W/m^2 K. All other walls had a convective heat transfer coefficient of 8

W/m^2 K. The thermo-physical properties associated with the material and fluids are assumed to be constant and are listed in Table 3.1.

Table 3.1 Material and Fluid Properties

Item	Density ρ (kg/m^3)	Specific Heat Capacity, C_p (J/kg K)	Thermal Conductivity k (W/m K)
Copper	8954	383	387
De-ionized water	998.2	4179	0.6129

3.2.2 TURBULENT FLOW CONDITION

Fig.3.2 represents the schematic of the computational domain and actual geometry used for the numerical analysis. The advantage of symmetry consideration with the source and the heat sink is simplified the calculation time. The following assumptions are made in the analysis. Equal flow rate is given to the upper layer microchannels and lower layer microchannels throughout the study. To simplify the analysis several assumptions are made regarding the operational conditions. They are steady-state, incompressible, single-phase, turbulent flow with constant thermophysical properties for fluid and solid.

No-slip and no jump boundary conditions are applied at the solid-fluid interfaces. Based on the assumptions, the Wilcox k-ω model is (the standard k-ω model) used in the ANSYS Fluent. This model is an empirical model based on the transport equations for turbulence kinetic energy (k) and the specific dissipation rate (ω). The conservation equations for the fluid flow and heat transfer to solving the model are as follows.

- Equation of Continuity,

$$\frac{\partial \bar{u}}{\partial x} + \frac{\partial \bar{v}}{\partial y} + \frac{\partial \bar{w}}{\partial z} = 0 \qquad \text{(e)}$$

- Equation of Momentum,

$$\rho\left(u\frac{\partial \bar{u}}{\partial x}+v\frac{\partial \bar{u}}{\partial y}+w\frac{\partial \bar{u}}{\partial z}\right)=-\frac{\partial \bar{p}}{\partial x}+\mu\left(\frac{\partial^2 \bar{u}}{\partial x^2}+\frac{\partial^2 \bar{u}}{\partial y^2}+\frac{\partial^2 \bar{u}}{\partial z^2}\right)$$

$$\rho\left(u\frac{\partial \bar{v}}{\partial x}+v\frac{\partial \bar{v}}{\partial y}+w\frac{\partial \bar{v}}{\partial z}\right)=-\frac{\partial \bar{p}}{\partial y}+\mu\left(\frac{\partial^2 v}{\partial x^2}\bar{v}+\frac{\partial^2 \bar{v}}{\partial y^2}+\frac{\partial^2 \bar{v}}{\partial z^2}\right) \quad \text{(f)}$$

$$\rho\left(u\frac{\partial \bar{w}}{\partial x}+v\frac{\partial \bar{w}}{\partial y}+w\frac{\partial \bar{w}}{\partial z}\right)=-\frac{\partial \bar{p}}{\partial z}+\mu\left(\frac{\partial^2 \bar{w}}{\partial x^2}+\frac{\partial^2 \bar{w}}{\partial y^2}+\frac{\partial^2 \bar{w}}{\partial z^2}\right)$$

- Equation of Energy for solid,

$$\left(\frac{\partial^2 \bar{T}_s}{\partial x^2}+\frac{\partial^2 \bar{T}_s}{\partial y^2}+\frac{\partial^2 \bar{T}_s}{\partial z^2}\right)=0 \quad \text{(g)}$$

- Equation of Energy for fluid,

$$\rho * C_p\left(u\frac{\partial \bar{T}_f}{\partial x}+v\frac{\partial \bar{T}_f}{\partial y}+w\frac{\partial \bar{T}_f}{\partial z}\right)=k\left(\frac{\partial^2 \bar{T}_f}{\partial x^2}+\frac{\partial^2 \bar{T}_f}{\partial y^2}+\frac{\partial^2 \bar{T}_f}{\partial z^2}\right) \quad \text{(h)}$$

- Transport equations with k-ω Model

$$\frac{\partial}{\partial t}[\rho k]+\frac{\partial}{\partial x_i}[\rho k u_i]=\frac{\partial}{\partial x_j}\left[\Gamma_k\frac{\partial k}{\partial x_j}\right]+G_k-Y_k \quad \text{(i)}$$

$$\frac{\partial}{\partial t}[\rho \omega]+\frac{\partial}{\partial x_i}[\rho \omega u_i]=\frac{\partial}{\partial x_j}\left[\Gamma_\omega\frac{\partial \omega}{\partial x_j}\right]+G_\omega-Y_\omega \quad \text{(j)}$$

G_k for the generation of the turbulence kinetic energy due to mean velocity gradients and G_ω represents the generation of specific dissipation. Γ_k and Γ_ω suited for the effective diffusivity of k and ω respectively. While Y_k and Y_ω fit the dissipation of k and ω due to turbulence.

The following are the boundary conditions used for the simulation. Uniform velocity & temperature conditions are given at the channel inlet and the pressure outlet boundary condition is chosen at the channel outlet. The inlet temperature is set as 303 K. The water

is used as the working fluid. The numerical analysis is conducted for the inlet velocity varying from 0.75 m/s to 6.5 m/s (The corresponding mass flow rate is 1.5 x 10^{-3} kg/s to 14 x 10^{-3} kg/s). The convergence criterion is set for all equations at a residual of 10^{-6}. At the bottom of the heat source block, a uniform heat flux of 55401 W/m^2 (corresponding to 80 W) is applied. The heat sink top is assumed as convective with a convective heat transfer coefficient of 12 W/m^2 K. All other walls are assumed with a convective heat transfer coefficient of 8 W/m^2 K.

3.2.3 NUMERICAL SIMULATION (with mal-distribution)

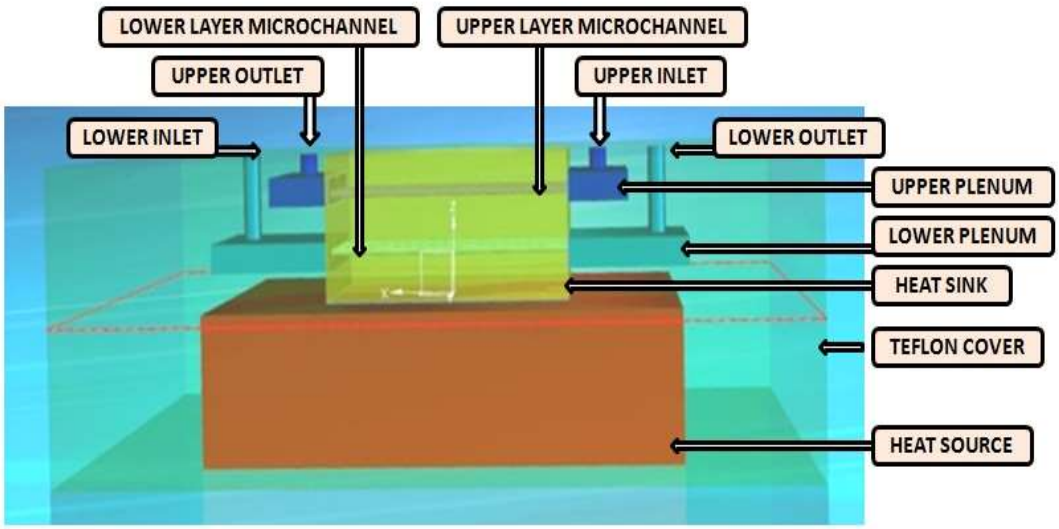

Fig 3.3 Computational Model used for Numerical Analysis

The mal-distribution study is conducted for both counterflow and parallel flow arrangements. The computational domain used for the numerical analysis for the laminar condition and turbulent flow condition (with mal-distribution) is shown in Fig.3.3.

The assumptions, governing equations and the boundary conditions made in both laminar flow and turbulent flow conditions are the same as the above. The schematic of the numerical model is shown in Fig. 3.4.

The following are the boundary conditions used for the simulation. Mass flow inlet with constant temperature conditions are given at the channel inlet and the pressure outlet boundary condition is chosen at the channel outlet. The inlet temperature is set as 303 K. Water is used as the working fluid. The numerical analysis is conducted for laminar flow conditions (CF and PF) and turbulent flow conditions (CF and PF).

The convergence criterion is set for all equations with a residual of 10^{-6}. At the bottom of the heat source block, a uniform heat generation of 1731301 W/m^3 (corresponding to 100 W) is applied. The heat sink top is assumed as convective with a convective wall heat transfer coefficient of 12 W/m^2 K.

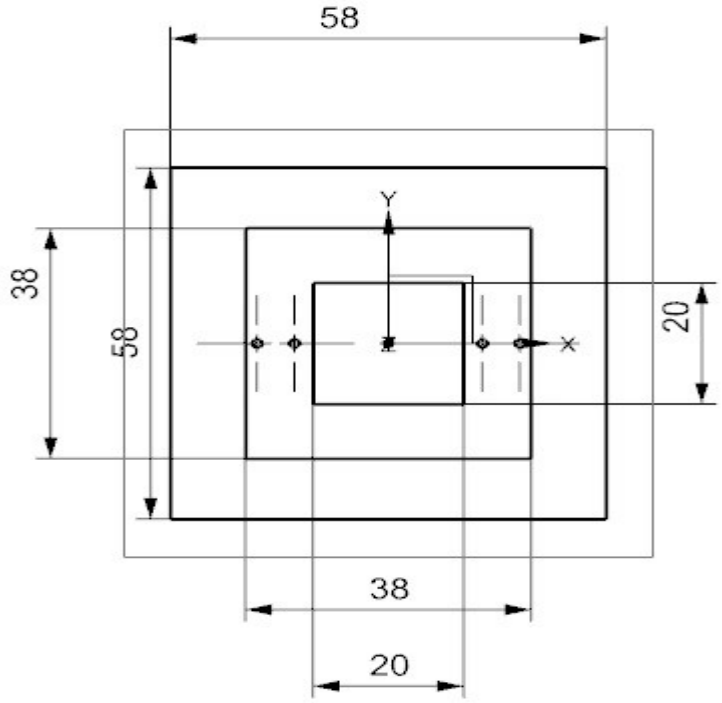

Fig 3.4 Schematic of the Computational Model used for Numerical Analysis

All other walls have a convective heat transfer coefficient of 8 W/m^2 K. The assumptions made are steady-state, incompressible, single-phase, laminar flow/turbulent flow, with constant properties for fluid and solid. No-slip and no jump boundary conditions are applied at the solid-fluid interface.

3.3 EXPERIMENTAL SETUP

As explained earlier in the chapter, to achieve low flow rates pump feed system was not sufficient. Hence two feed arrangements are studied in the present study. The experimental study in this research work is conducted for two different arrangements namely with a pump feed system and with the gravity feed system. These two methods are explained in detail as follows.

3.3.1 WITH PUMP FEED SYSTEM

The schematic flow loop of the actual experiment setup is shown in Fig.3.5.

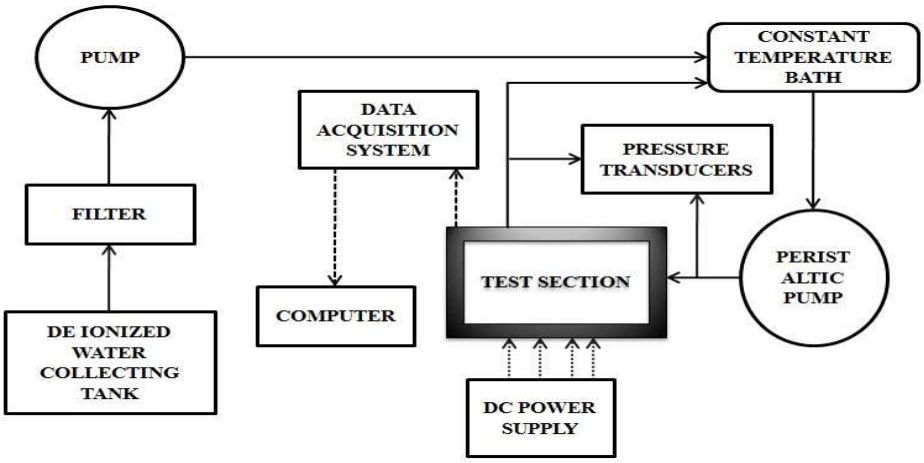

Fig 3.5 Schematic Diagram of the Experiment

It involves a collecting tank, filter, peristaltic pump, constant temperature bath, copper test section, data acquisition system (DAQ), power supply (DC), pressure transducers and a personnel computer. Figure 3.6 shows the photograph of the original experimental setup.

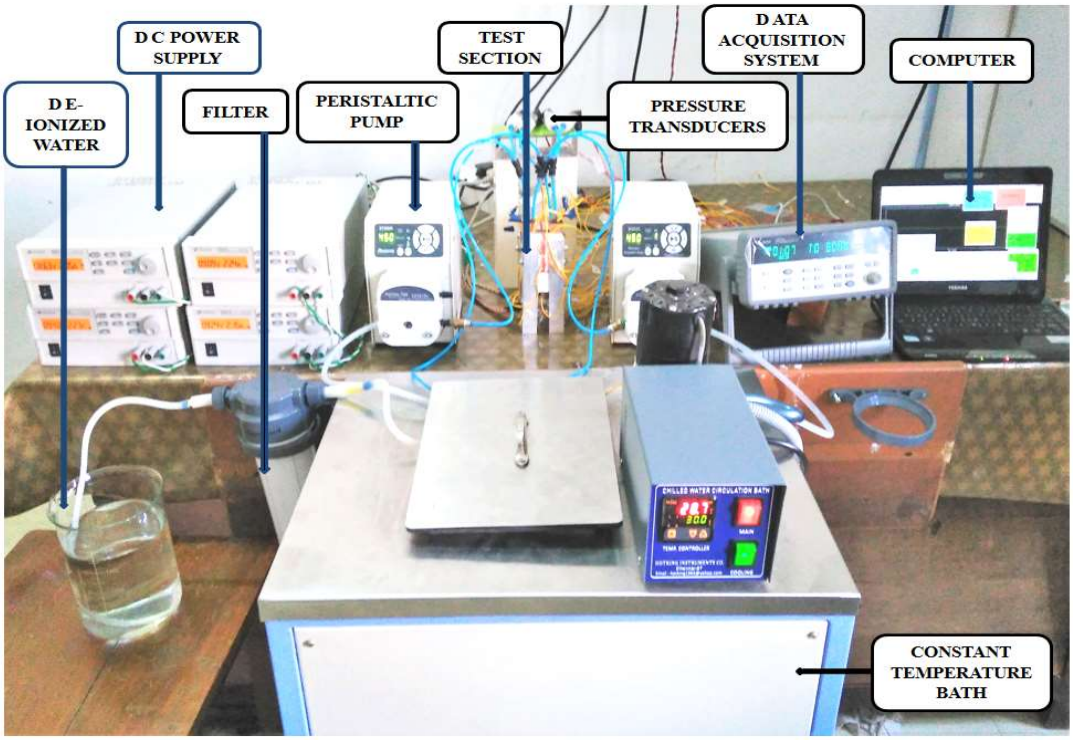

Fig 3.6 Photograph of Typical Experiment Setup

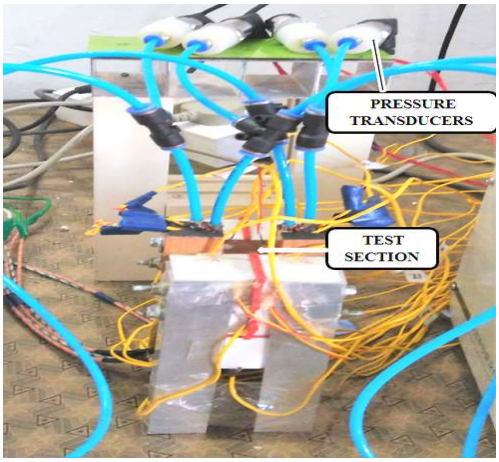

Fig 3.7 (a) Test section and Pressure Transducers

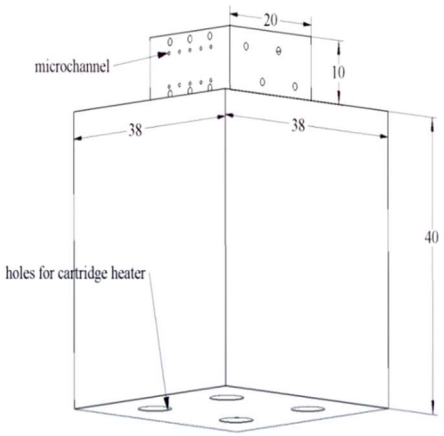

Fig 3.7 (b) Schematic of Test Section

The test section with four pressure transducer is shown in Fig. 3.7 (a). The detailed geometry of the copper block with a test section is shown in Fig.3.7 (b). De-ionized water from the deionizer (Fig.3.8 (a)) is collected in the tank and flows through the 5- micron filter (Fig. 3.8 (b)) to filter out the impurities.

Fig 3.8 (a) Direct-Q 3UV De-Ionizer

Fig 3.8(b) Filter (5 micron)

The inlet and outlet to the lower layer and upper layer plenums are connected with the aspiration needle as shown in Fig. 3.9 (a). The different connectors used are shown in Fig. 3.9 (b). The inlets to the plenum and outlet from the plenum are connected to an aspiration needle tightly with the Teflon cover.

Fig 3.9 (a) Needle

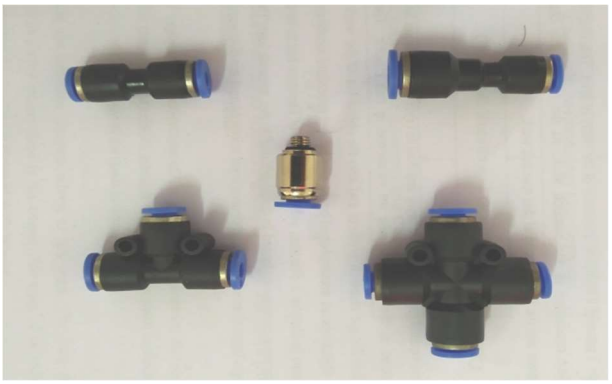

Fig 3.9 (b) Pneumatic Connectors

The filtered water is stored in a chilled water circulation bath as shown in Fig 3.10 (HOTKING INSTRUMENT make ranging -10 ^{0}C to 100 ^{0}C). This filtered de-ionized water is pumped to the copper test section. It consists of two parts namely heat sink and heat source. The copper block is covered by using Teflon insulation as shown in Fig.3.11.

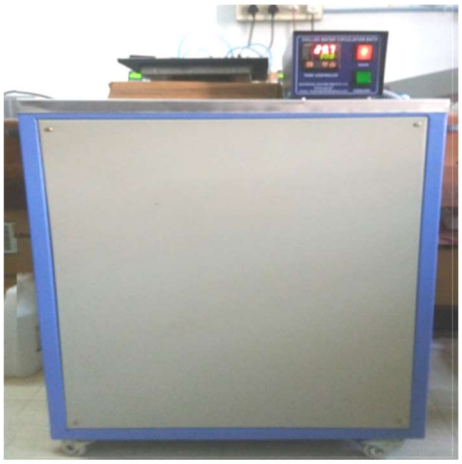

Fig 3.10 Constant Temperature Water Bath

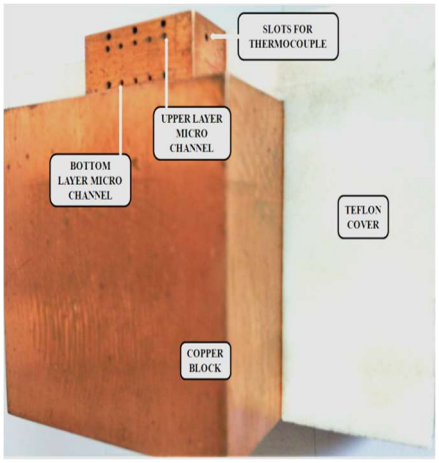

Fig 3.11 Copper Test Piece with Teflon Cover

The copper block consists of two parts namely heat sink and heat source machined in a single square copper bar. The heat sink is a square block of dimension 20 mm x 20 mm x 10mm. It consists of ten circular microchannels of 500 µm diameter and 20 mm in length.

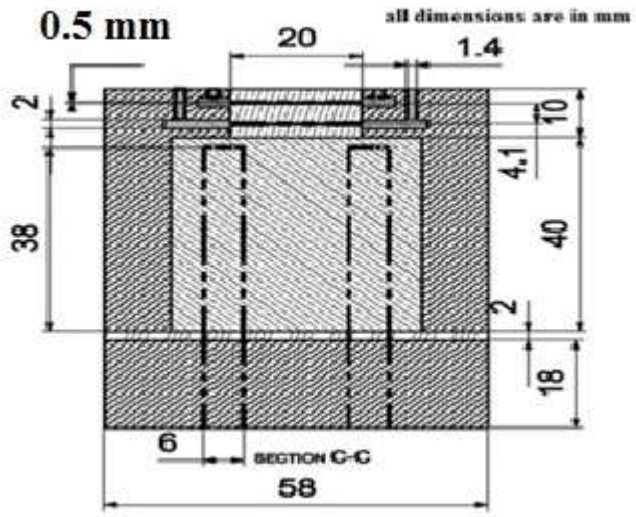

Fig 3.12 Schematic of the Test Piece with Teflon covers

The schematic of the test piece with a Teflon cover (cross-sectional view) is shown in Fig.3.12. Microchannels are machined using WIRE EDM method and are arranged in two layers, one over the other to facilitate parallel flow (PF) and counterflow (CF) arrangements. Each layer consists of five microchannels machined at 4.5 mm distance from each end and the centres are placed equidistantly. The vertical centre distance

between the two layers is 4.5 mm. The distance between the centre of the bottom layer microchannel and the top surface of the copper heat source is 2.75 mm.

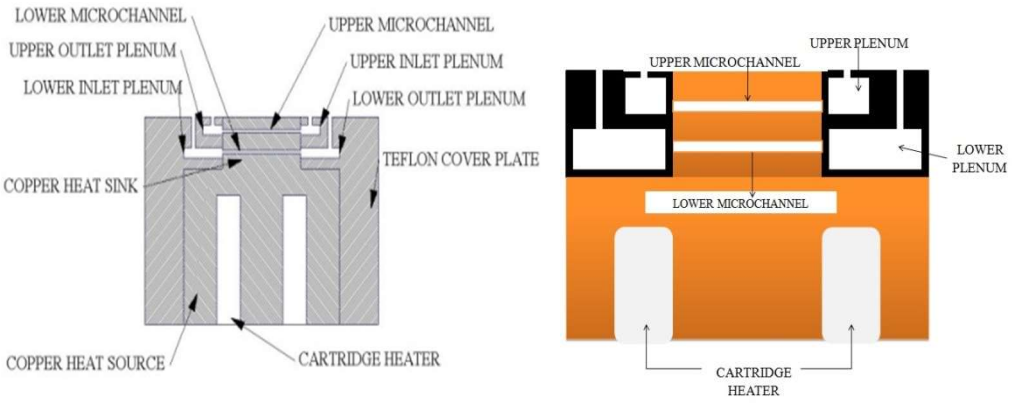

Fig 3.13 Sectional view of the Test Piece with Teflon covers.

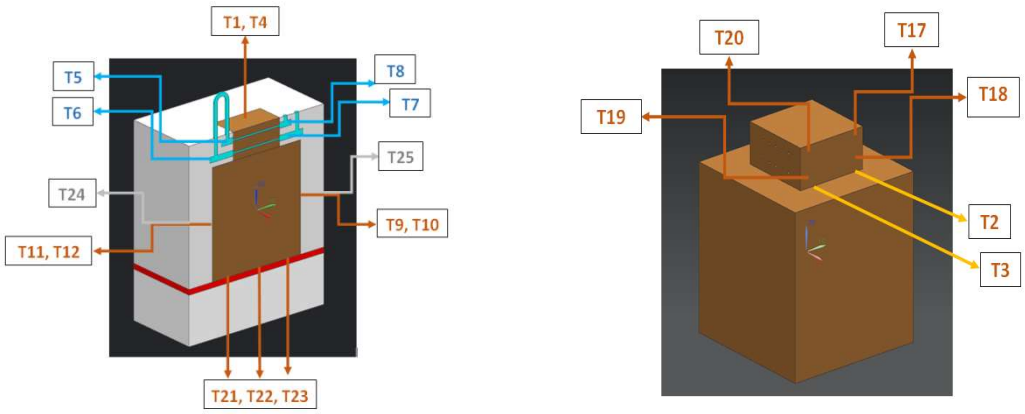

T26 – FLOAT CHAMBER WATER TEMPERATURE & T27, T29, T30 – ATMOSPHERIC TEMPERATURE

Fig 3.14 Thermocouple Positions in the Test Piece.

The Teflon insulation is given for all surfaces except top surface so as minimize the heat loss. The sectional view of the test piece connected with Teflon cover is shown in Fig. 3.13.

The thermocouple positions are marked in Fig. 3.14. Inlet and outlet plenums are cut in two Teflon blocks. A 15 mm x 2 mm x 5 mm size plenum is cut for upper channel input and output. A 15 mm x 2 mm x 10 mm size plenum is cut for lower channel input and output.

The photograph of the Teflon cover used for the experiment is shown in Fig. 3.15 and the detailed schematic view of the Teflon cover is shown in Fig. 3.16.

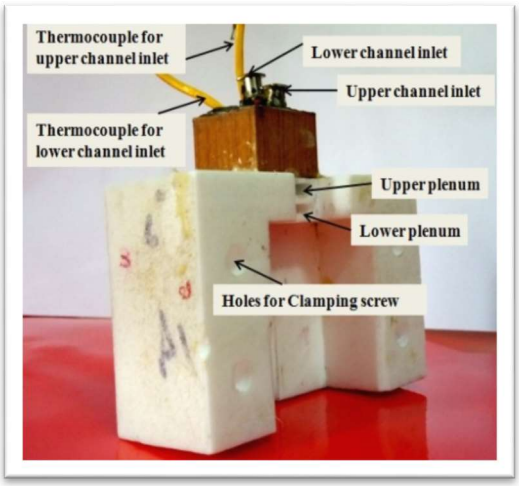

Fig 3.15 Photograph of the Teflon Cover used in the Experiment.

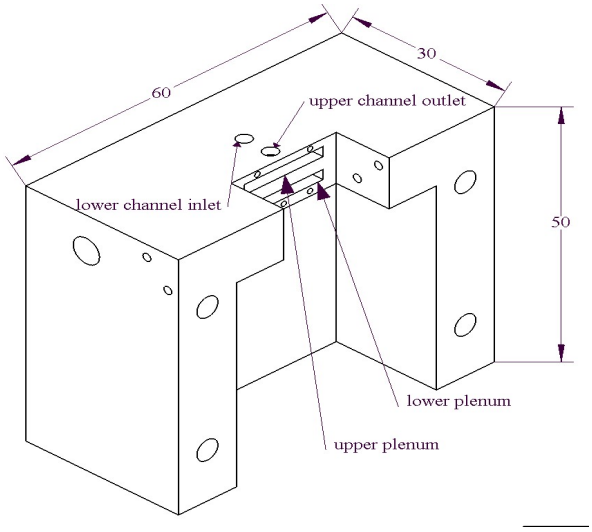

Fig 3.16 Schematic of the Teflon covers

The inlet and outlet temperatures are measured with the thermocouples bonded on the outer surface of the inspiration needles as shown in Fig. 3.17. The silicon sheet with a 1 mm thickness is also shown in this figure. These silicon sheets are used for a tight joint of the copper block and the Teflon block.

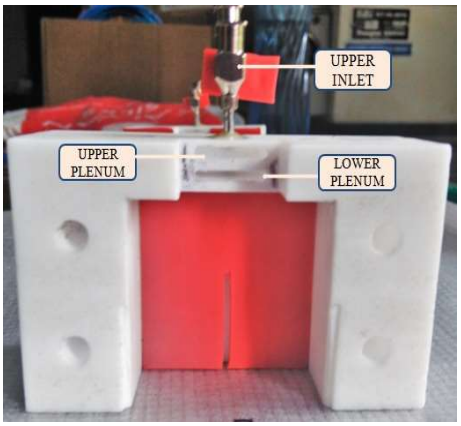

Fig 3.17 Photograph of Teflon Covers

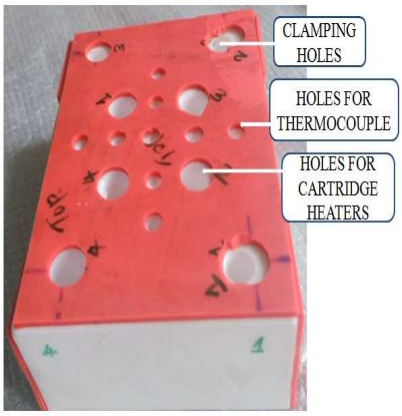

3.18 Photograph of Teflon Bottom Covers

The bottom portion of the copper block also covered with Teflon cover as shown in Fig 3.18. A 1 mm silicon sheet is used as the gasket to prevent leakage through the gap between copper and Teflon blocks.

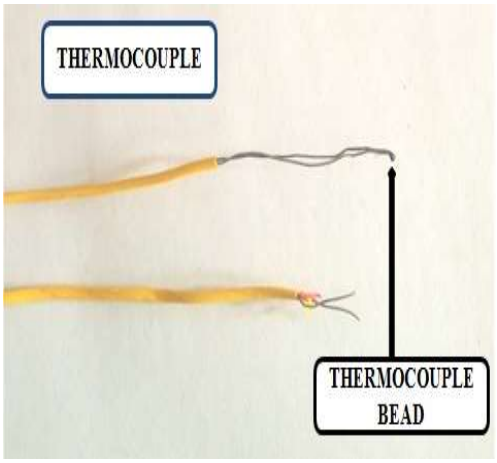

Fig 3.19 Thermocouple

Fig 3.20 Thermocouple Wire Welder

A 2 mm silicon sheet is used in all other interfaces for tight-fitting. A 2 mm grove is provided nearer the inlet and outlet to insert the thermocouples (Fig. 3.19) to measure the channel wall temperature. The thermocouple beads are made with the help of thermocouple wire welder (Fig. 3.20).

The bottom portion of the block is also covered using Teflon block with a one mm silicon sheet (Fig. 3.21). Continuous flow through the double-layered microchannel is ensured

with the help of a peristaltic pump as shown in Fig. 3.22. Two peristaltic pumps (BT600N YZ1515x Shenzhen makes range 0.035 ml/min-2280 ml/min) are used to pressurize the fluid through each layer of the microchannels.

Fig 3.21 Silicon Sheet

Fig 3.22 Peristaltic Pump

Fig 3.23 Measuring Jar

Fig 3.24 Pressure Transducer

A measuring jar (Fig. 3.23) is used to measure the discharge of fluid. The mass flow rates of fluid flow through microchannels are controlled by varying the rpm in the peristaltic pump. The de-ionized water is then returned to the chilled water circulation bath. Four pressure transducers (GEMS 3500 Series ranges 0 - 2.5 bar output of 1 - 5 Volts) are used for pressure measurement (Fig. 3.24).

The inlet and outlet pressure is measured using a pressure transducer. There are separate pressure transducers for the upper and lower channel. These pressure transducers measure the inlet and outlet pressure of the cooling fluid each layer of the microchannels. The measurement error of the pressure transducers is within 0.5% of the actual value. Throughout the experiment, the flow rate in each layer is controlled independently. Calibrated 0.8 mm diameter K-Type thermocouples are used to measure the temperature.

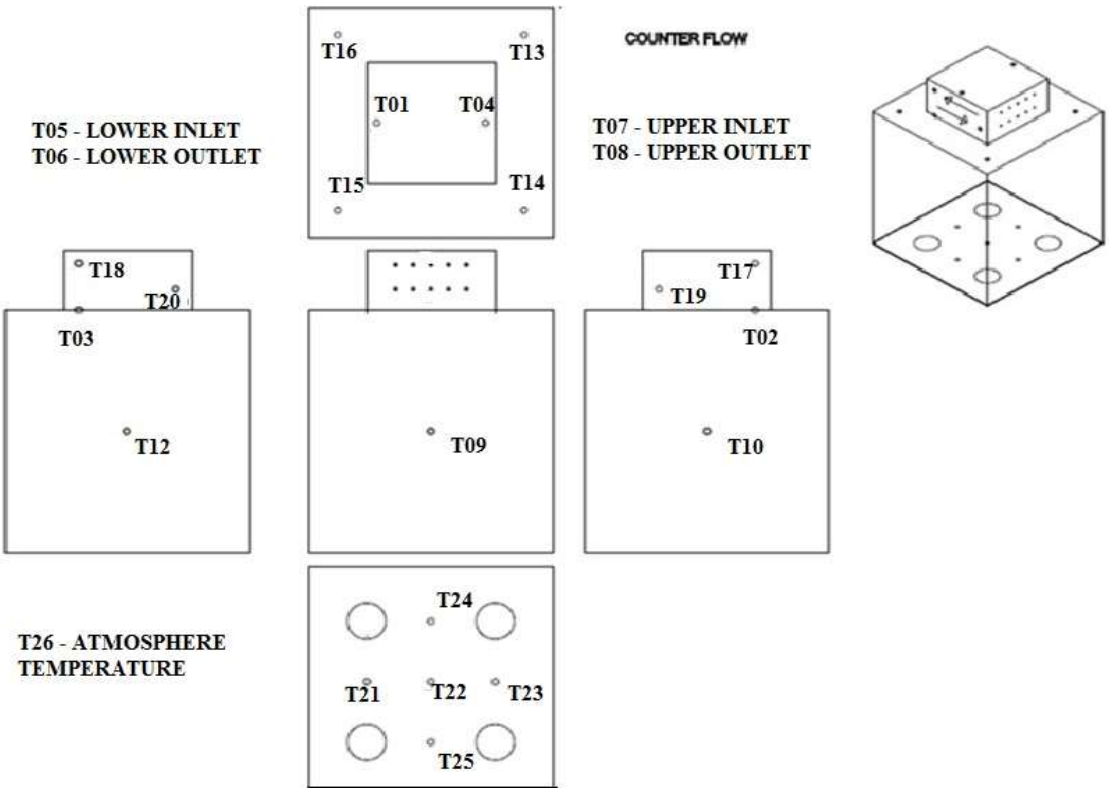

Fig 3.25 Location of Thermocouples in the Test Piece

The thermocouple connected with the copper test piece is as shown in Fig. 3.25. Total twenty-seven calibrated K- type thermocouples are connected with bead making in the thermocouple welder.

The thermocouple is fixed at different locations of the copper test piece (as shown in Fig 3.26) with the help of Araldite and copper powder mixture. The locations of the thermocouples bonded to take the temperature measurements are shown in Table 3.2.

Calibrated K Type thermocouples are fixed to measure the bottom temperature, surface temperature, fluid wall temperature, atmospheric temperature, fluid inlet temperature and outlet temperature.

Table 3.2 Location of thermocouples in the test piece

Thermocouple	Positions
T_1, T_4	top convective wall surface temperatures
T_3, T_2	Heat sink base temperature
T_5, T_6	Fluid inlet or outlet temperature (lower channel)
T_7, T_8	Fluid inlet or outlet temperature (upper channel)
T_9,T_{10},T_{11},T_{12}	heat source outer surface temperatures
T_{13},T_{14},T_{15},T_{16}	the heat source top surface temperatures
T_{17}, T_{18}	Top fluid wall temperature
T_{19}, T_{20}	Bottom fluid wall temperature
T_{21},T_{22},T_{23},T_{24} ,T_{25}	heat source base surface temperatures
T_{26}	Atmosphere temperature
T_{27}	Constant temperature bath (water temperature)

Figure 3.26 exhibits the geometry of the test section. It also shows the calibrated 0.8 mm diameter K Type thermocouple which is used to record the temperature at various points. The fluid inlet and outlet temperature is measured by using the thermocouples connected at the inlet and outlet of the plenum.

The heat source of size 38 mm x 38 mm x 40 mm is machined in the lower portion of the copper heat sink. Four 40 W cartridge heaters are used as a heat source for the microchannel heat sink (Fig. 3.27).

Four equidistant holes of 6.1mm diameter and 38 mm depth are drilled perpendicularly from the bottom to top of the copper heat source, to insert the cartridge heaters.

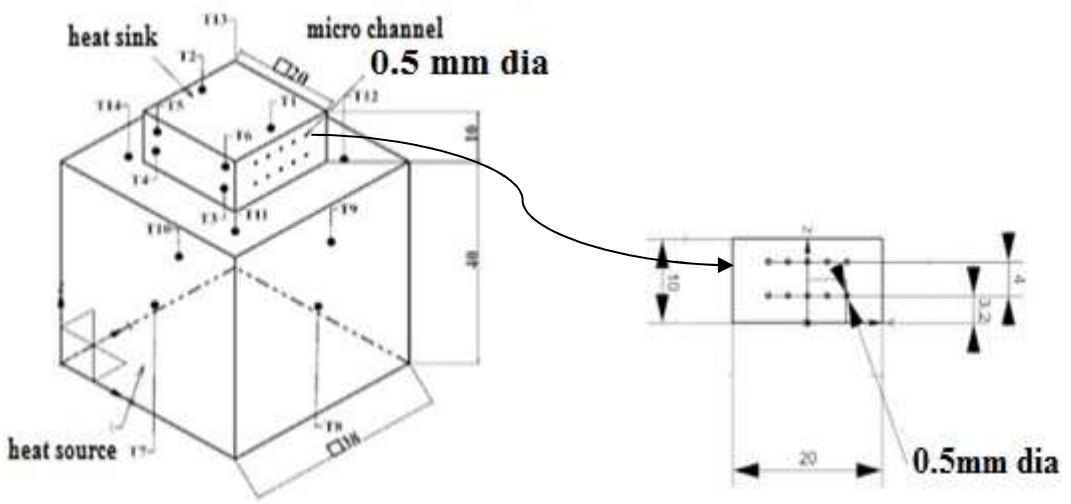

Fig 3.26 Geometry of Test Section with Thermocouple Positions

The four cartridge heaters are placed inside the copper block, which is attached to the heat sink. The cartridge heaters are then connected to the DC power supply.

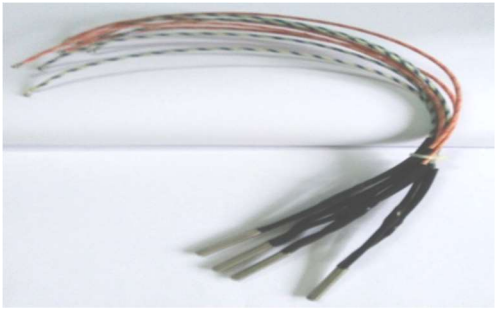

Fig 3.27 Cartridge Heaters

Fig 3.28 DC Power Supply

It is then connected to the data acquisition system and all readings are recorded to the computer. The thermal compound is pasted on the outer side of the cartridge heater to reduce the thermal contact resistance.

Four Key Sight U8001 A (0-30 V, 3 A) DC Power Supply (Fig.3.28) maintains the output of each cartridge heaters of 20W heat. Four Key Sight U8001-A, DC Power Supply (0-30 V, 3 A) maintains each cartridge heaters at 20W heat. Such that a total heat input of 80 W is ensured.

Fig 3.29 Data Acquisition Unit

Fig 3.30 Multiplexer with Thermocouple

3.3.2 WITH GRAVITY FEED SYSTEM

The schematic of the experiment work with the application of a gravity feed system is shown in Fig.3.31.

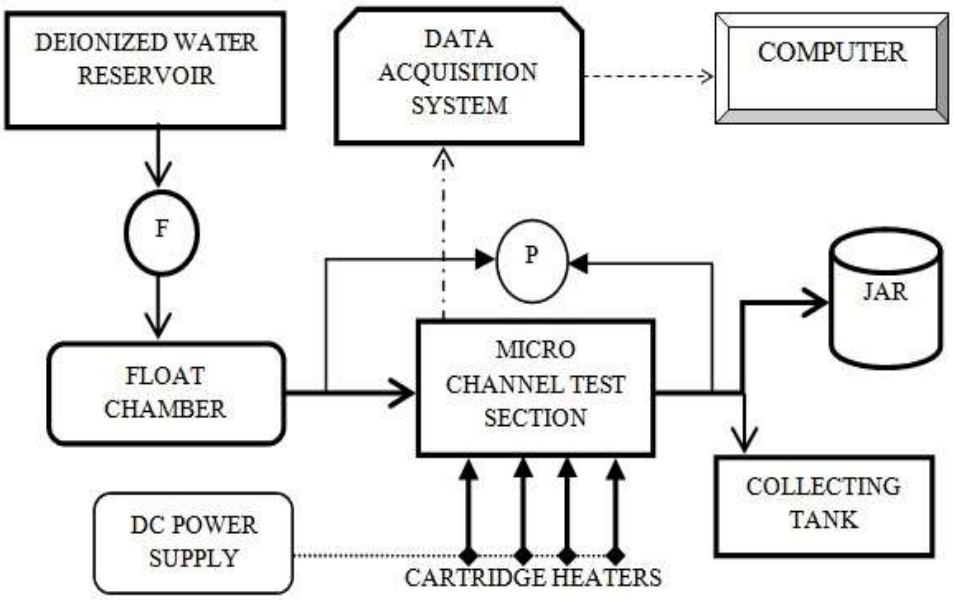

Fig 3.31 Schematic Flow Loop **(GRAVITY FEED SYSTEM)**

It consists of a collecting tank, float chamber, filter, copper test section, data acquisition system, DC power supply, U tube manometer, and a personal computer.

The pictorial representation of the experiment facility is shown in Fig. 3.32.

De-ionized water from the deionizer is collected in the reservoir and flows through a five-micron filter. The filtered water flows to the float chamber (Fig.3.33) which maintains a constant pressure head at the inlet of the fluid.

The flow of the impurities through the microchannel is restricted by the filter. This De-ionized water from the float chamber is allowed to flows through the lower channel and upper channel of the copper test section.

The exit of these channels is connected to the measuring jar. The effect of mal-distribution is not considered.

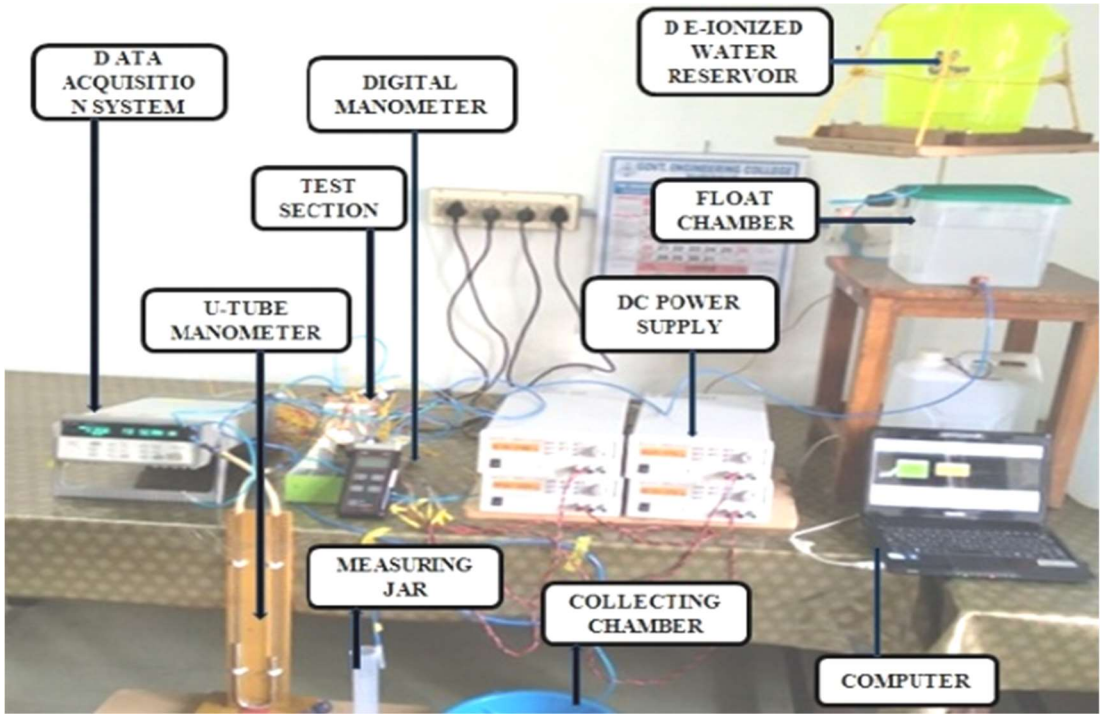

Fig 3.32 Pictorial View of Experiment Setup

The deionized water from the float chamber flows through the microchannel test section. The test section used in this study is the same as the test section used for the turbulent case.

Fig 3.33 Float Chamber with the Reservoir

The test section is manufactured in a single copper block and it consists of two parts namely heat sink and heat source. The inlets to the plenum and outlet from the plenum to both upper and lower layers are connected through the needle.

.

Fig 3.34 U- Tube Manometer

Fig 3.35 Digital Manometer

The Teflon insulation is given for all surfaces of the copper block except top surface to maintain adiabatic conditions (similar to the turbulent flow).

Unlike in the pump feed system, pressured drop along the channel is low. Hence the pressure drop in the gravity feed system is measured by a U-Tube manometer and digital manometer. The lower channel pressure drop is measured with the U-Tube manometer

(Fig.3.34) and the upper channel pressure drop is measured with a digital manometer (Fig.3.35). By changing the position of the float chamber the different continuous and constant flow rate is ensured through the microchannels.

A collecting tank with deionized water is fixed at a maximum height from the float chamber. This collecting tank is maintained the continuous flow of the fluid from the float chamber. A 100 ml measuring jar is used to measure the discharge of the fluid. Cartridge heaters are used as a heat source for the microchannel heat sink.

To reduce the thermal contact resistance, the thermal compound is pasted on the outer side of the cartridge heaters. Four Keysight U8001 A (0-30 V, 3 A) DC power Supply maintains the heat of each cartridge heaters at 25 W; Such that a total heat input of 100 W is ensured. Agilent Multiplexer Module for 34970A, with 20 channels is used to connect all the thermocouple with the data acquisition switch unit.

3.3.3 DIFFERENT SERIES FLOW ARRANGEMENT

Further series flow arrangement is studied by a gravity feed system. Here the channel outlet from one layer is fed as the inlet to the other layer to obtain four different configurations as given below in Fig. 3.36.

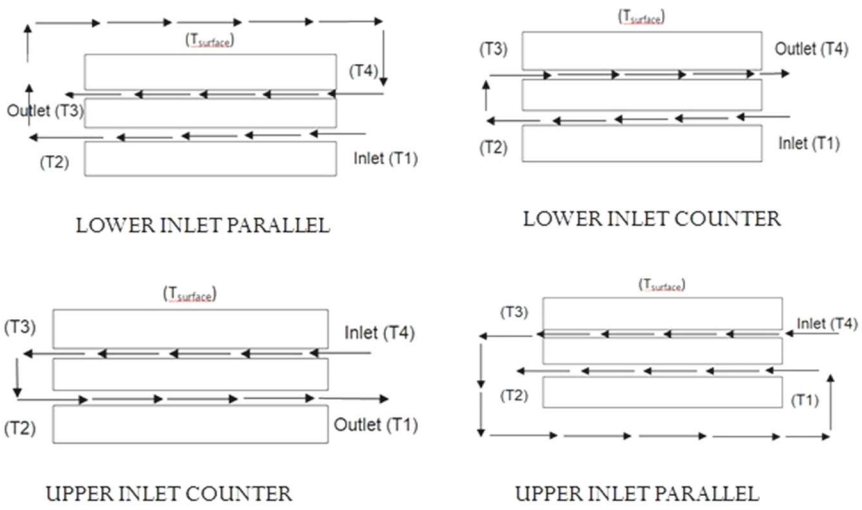

Fig 3.36 Schematic of Different Series Flow Configurations (EXPERIMENT)

All the instrumentation used for measurement is calibrated against standard values. Calibration curves are plotted for temperature and pressure measurement in appendix A.

Uncertainty in the derived quantities of friction factor, mass flow rate, and pumping power are also determined by the standard equation as discussed in the next chapter. The details of uncertainty in measurement and derived quantity are reported in appendix B.

The apparatus was allowed to run continuously for enough time to reach steady state. All the readings are taken at steady-state condition, it is assumed when the outlet temperature varied less than 0.1 ^{0}C in ten minutes. After reaching the steady-state condition temperature, pressure head, and the time taken for filling 100cc of deionized water are measured and recorded.

3.4 SUMMARY

The methodology used in this research work is explained well in this chapter. They are numerical analysis and experimental analysis. Further, this chapter describes the different components used for the experiment in detail. The detailed results and discussion explained in the next chapter.

CHAPTER 4
RESULTS AND DISCUSSION

4.1 INTRODUCTION

The results of the flow parameters, thermal performance and flow maldistribution of a double-layer stacked circular microchannel heat sink are presented and discussed in this chapter.

A parametric study is conducted numerically, for analyzing the optimized flow rate through the lower layer and upper layer of the double-layer microchannel setup. Followed by, a numerical study with turbulent flow condition for counter flow and parallel flow configuration. The results are compared with the experimentally obtained value using the pump feed system. The experimental study is also conducted with single-layer flow configuration. Then the numerical study is conducted with laminar flow condition. Low flow rates could not be achieved in the experimental study due to the setting of a minimum rpm for the pump. Therefore experiments with low flow rate are conducted using the gravity feed system. The numerical results are compared with the experimental value obtained by the application of a gravity feed system. The flow mal-distribution study is conducted numerically in both laminar flow and turbulent flow conditions. The experiment is also done with different series flow configurations using the gravity feed system. Different series flow configurations are achieved by changing the locations of inlet and outlet. The results obtained from the numerical analysis and experiment analysis are presented and discussed in this chapter.

4.2 PILOT STUDY

A pilot study relating to the optimization of the flow-through each layer is conducted at the initial stage of the research. The numerical analysis is conducted with a computational model as shown in Fig.3.2. The mesh dependence study is conducted with different mesh sizes and same velocity inlet boundary condition.

4.2.1 MESH DEPENDENCE STUDY

The mesh dependence study is carried out for an inlet velocity of 0.502 m/s with four different mesh size as shown in Table 4.1. To analyze the actual mesh size for the numerical study and to avoid iteration delay, four different meshes analyzed with different element size.

Table 4.1 Mesh dependence study

Mesh Quality	Number of Nodes	Pressure drop (Pa)	
		Lower Channel	% variation
Very coarse	1114117	560.5	---
Coarse	1633336	558.6	0.341
Fine	**2614556**	**557.5**	**0.196**
Superfine	3648785	556.6	0.161

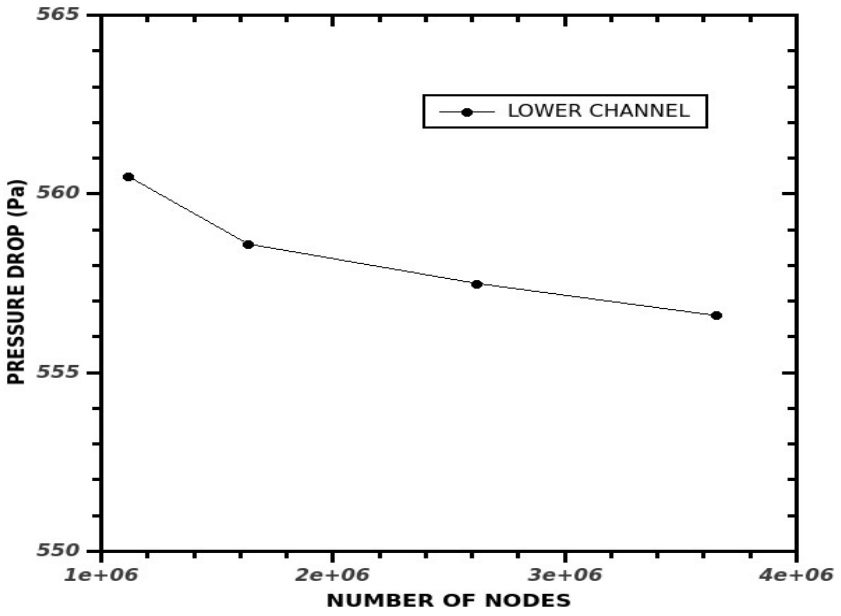

Fig 4.1 Lower Channel Pressure Drop Vs Number of Nodes

Mesh size corresponding to fine mesh is employed in this study because of the pressure drop at the lower layer microchannel between fine and superfine mesh sizes are less than

0.161%. The tolerance limit for normalized residuals for each variable was taken as less than 1.0 x 10^{-7}. From Fig. 4.1, it is clear that the lower channel pressure drop variation with the number of nodes and the measurement corresponds to the number of nodes 2614556 is taken as the present study. The fine mesh size is employed in the final simulation since less computational time is needed. The skewness of the elements used is of 0.2369.

4.2.2 OPTIMIZATION OF FLOW THROUGH THE MICROCHANNEL

The study is conducted for obtaining the optimized results for the pressure drop and average base temperatures in the microchannel heat sink. The assumptions made are steady-state, single-phase, incompressible, and laminar flow with constant properties for fluid and solid. Based on these assumptions, different analysis is done with varying the total velocity of fluid flow in the double-layered channel from 0.502 m/s to 10.045 m/s. These analyses are done using two material of copper and aluminium.

The change in total pressure drop and the average base temperature in various Reynolds number is mentioned in Table 4.2. The optimized flow through each layer is summarized from the table below. The three sets of combinations are analyzed with the same total velocity by varying the velocity in the upper layer channel and lower layer channel. It is understood that the optimized value of the total pressure drop is obtained when applying the same velocity in both the upper and lower layer channel.

The less average base temperature is also obtained when the same velocity is taken in both upper and lower channel as compared with different velocity is taken in the lower and upper channel. For different materials like copper and aluminium, the same trend is observed. The copper attains lesser average base temperature than the aluminium.

The pilot study was conducted using the same geometry with different material properties of Aluminium and Copper. The boundary conditions in each case are the same. So the pressure drop values are nearly the same. But in the values of average base temperature has considerable deviation. The values are less when using the same flow rate through each upper and lower layer. The result obtained from this table is to finalize the flow rate with both upper and lower layer microchannel.

After getting these results, the research work in the double-layered circular microchannel study is conducted by applying approximately the same velocity in both the upper and lower channel. The microchannels are made in the copper-based material.

Table 4.2. Pressure drop and Average Base Temperature Analysis of the Double Layer Microchannel in Cu and Al with Different Reynolds Number in Lower and Upper Channel (Parallel Flow)

REYNOLDS NUMBER (Re)			TOTAL PRESSURE DROP (Pa)		AVERAGE BASE TEMPERATURE (K)		TOTAL VELOCITY
UPPER CHANNEL	LOWER CHANNEL	TOTAL	Cu	Al	Cu	Al	m/s
75	25	**100**	1628	1628	423.83	426.78	**0.502**
50	**50**		**1618**	**1618**	**415.86**	**418.15**	
25	75		1628	1629	423.1	425.09	
200	100	**300**	5145	5144	364.41	366.98	**1.506**
150	**150**		**5104**	**5105**	**362.96**	**365.3**	
100	200		5146	5146	364	366.23	
350	150	**500**	9075	9076	351.5	354.15	**2.511**
250	**250**		**8916**	**8916**	**350.02**	**352.42**	
150	350		9077	9077	351.06	353.28	
600	200	**800**	15843	15844	342.87	345.56	**4.018**
400	**400**		**15231**	**15231**	**342.29**	**343.45**	
200	600		15845	15847	341.03	344.52	
800	400	**1200**	25281	25310	335.48	338.06	**6.027**
600	**600**		**24719**	**24721**	**334.85**	**337.22**	
400	800		25285	25285	335.13	337.41	
400	1600	**2000**	51130	51130	329.54	331.71	**10.045**
1000	**1000**		**46957**	**46957**	**328.41**	**330.79**	
800	1200		47416	47415	328.85	330.84	

4.3 TURBULENT FLOW AND USING PUMP FEED SYSTEM

The numerical analysis with the symmetry model is done using the turbulent flow condition. The inlet velocity of the lower channel and upper channel are varied to analyze the different sets of combination.

The study is conducted with the parallel flow and counterflow configurations.

4.3.1 MESH DEPENDENCE STUDY

The mesh dependence study is conducted using an inlet velocity of 1.67 m/s with four different mesh sizes as shown in Table 4.3.

To analyze the optimized mesh size, four different mesh qualities are analyzed. Mesh size corresponding to fine mesh is employed for the future study because of the variation of the outlet temperature at the lower layer microchannel between fine and superfine mesh qualities are less than 0.0027%.

Table 4.3 Mesh dependence study

Mesh Quality	Number of Nodes	Outlet Temperature(K)	
		Lower Channel	% variation
Very coarse	1002297	308.836	---
Coarse	2071409	308.814	0.0071
Fine	4756507	308.806	0.0025
Superfine	8876049	308.782	0.0027

The minimum reductions in normalized residuals for each variable are taken as 1.0×10^{-5}. From the Fig.4.2, it is clear that the lower channel outlet temperature variation with the number of nodes and the measurements corresponds to the number of nodes 4756507 is taken for the future study.

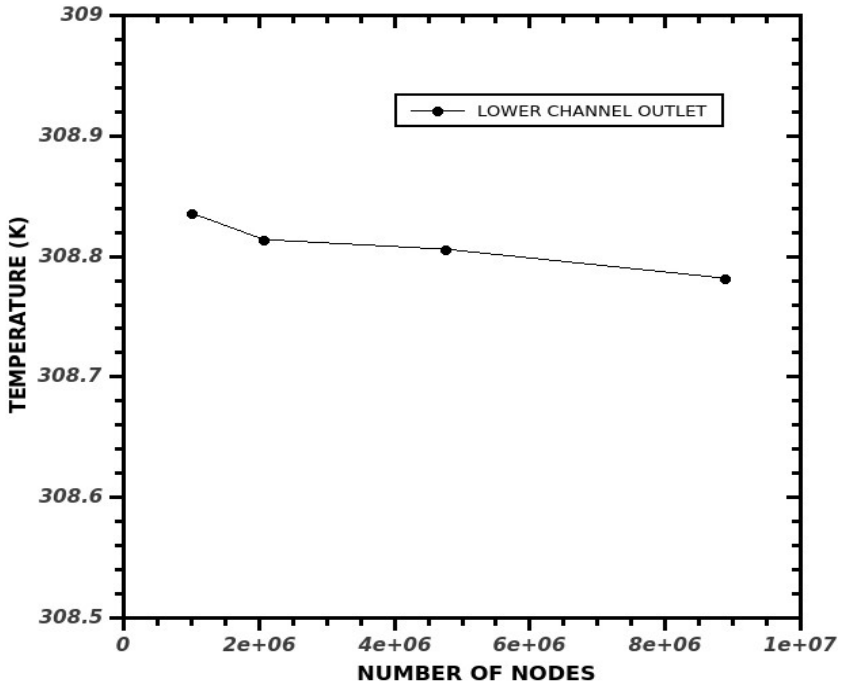

Fig 4.2 Lower Channel Outlet Temperature Vs Number of Nodes

The fine mesh size is employed in the final simulation since less computational time is needed.

4.3.2 TEST OF ENERGY BALANCE FOR VALIDATION

Energy balance test is conducted with the numerical analysis by taking the same flow in the lower layer and upper layer of the double-layered circular microchannel.

Here the lower channel (LC) velocity and upper channel (UC) velocity are taken as 12.054 m/s for the analysis. From Table 4.4, it is clear that the input heat energy is transferred to the conduction through the fluid and convection through the convective surface.

The 3LC, 4LC, 5LC are the lower channel microchannel numbers and 6UC, 7UC, 8UC are the upper channel microchannel numbers in the symmetry model is shown in Table 4.4.

Table 4.4 Energy balance test

MICROCHANNEL	TEMPERATURE (K)			DENSITY	SP.HEAT	VELOCITY	ENERGY
	INLET (T_i)	OUTLET (T_o)	To-Ti	ρ (kg/m^3)	C_p (J/kgK)	u (m/s)	$\dot{m}\ C_p\Delta T$ (Watts)
3 LC	303	303.89	0.895	998.2	4182	12.054	4.42
4 LC	303	303.86	0.864	998.2	4182	12.054	8.53
5 LC	303	303.91	0.912	998.2	4182	12.054	8.99
6 UC	303	303.74	0.748	998.2	4182	12.054	7.38
7 UC	303	303.70	0.702	998.2	4182	12.054	6.92
8 UC	303	303.74	0.745	998.2	4182	12.054	3.674
Conduction energy							39.92
Convective energy = $h*A_2*\Delta T$ h is the convective heat transfer coefficient (12 W/m^{2}K) A_2 is the surface area of the convective wall (0.0002 m^2) ΔT is the difference in temperature between the convective wall surface and atmosphere (29)							0.0696
Total energy							39.99
Total input energy							40 W

The schematic of the flow configurations used in the turbulent flow conditions for experiment analysis is shown in Fig.4.3.

The numerical and experimental analysis is conducted to analyze the fluid flow and heat transfer characteristics of a DLCMC-HS. Numerical analysis is carried out with different inlet velocities, with the standard k-ω model used in the ANSYS Fluent software. The y+ value obtained in this numerical analysis is less than 5. The effect of parallel flow and counter flow arrangements on the heat transfer and flow parameters is performed for a

constant heat input of 80 W. The total mass flow rate of the lower channel and the upper channel is taken for plotting all comparison curves.

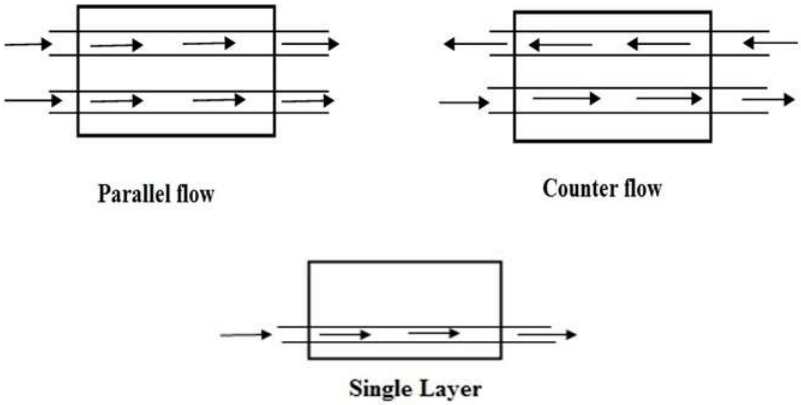

Fig 4.3 Flow Configuration for Experiment Study

Figure 4.4 depicts the variation of total pressure drop with the total mass flow rate through the double-layered circular microchannel for different flow arrangements like the counterflow, and parallel flow. The experiment is also conducted by allowing flow through the lower layer only, namely single-layer flow.

Discharge of the coolant through the outlet of each layer of the microchannel is

$$Q = \frac{A_1 * h_1}{t} \tag{1}$$

where A_1 is the cross-sectional area of the collecting vessel (in m^2) with diameter d_1 (in m), h_1 is the height of water collected (in m) of the water collected in the collecting vessel and t is the time taken (in seconds) for collecting de-ionized water.

The fluid average velocity in (m/s) is,

$$u = \frac{Q}{A} \tag{2}$$

where A is the cross-sectional area of the microchannel with diameter d.

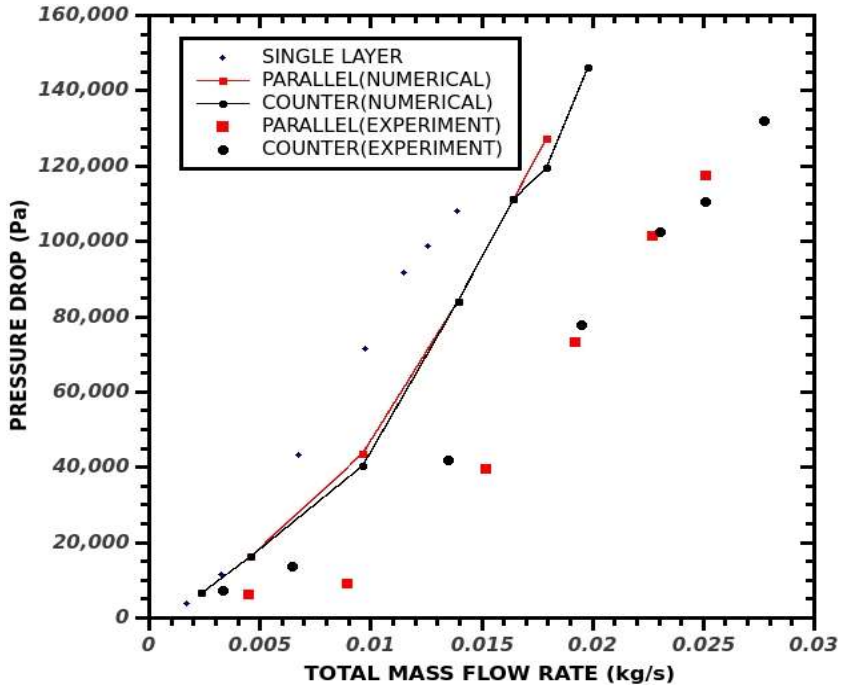

Fig 4.4 Pressure Drop Vs the Total Mass Flow Rate

The mass flow rate through the microchannel is

$$\dot{m} = \rho * A * u \tag{3}$$

where ṁ is the mass flow rate of the fluid (kg/s),

ρ is the density of the flowing fluid in kg/m^3.

The total pressure drop (ΔP_f) in Pascal is calculated using equation (4).

$$\Delta P_f = \Delta P_{fL} + \Delta P_{fU} \tag{4}$$

The pressure drop of the lower layer channel is (ΔP_{fL})

$$\Delta P_{fL} = P_{Li} - P_{Lo} \tag{5}$$

where P_{Li} is the pressure at lower channel inlet in Pascal and P_{Lo} is the pressure at lower channel outlet in Pascal.

The pressure drop of the upper channel is (ΔP_{fU}),

$$\Delta P_{fU} = P_{Ui} - P_{Uo} \tag{6}$$

where P_{Ui} is the pressure at upper channel inlet in Pascal and P_{Uo} is the pressure at upper channel outlet in Pascal.

Figure 4.4 indicates that, the variation of pressure drop with the mass flow rate (MFR). An expected similar trend is observed for both numerical and experimental results. The pressure drop increases with mass flow rate and a slight deviation occurred in the high MFR. The small deviation in the experimental value from the numerical pressure drop may be due to the entrance and exit losses at channel inlet and outlet respectively.

The variation in the experimental and numerical result may be due to the microchannel diameter tolerance in the experiment. The total pressure drop of the single layer is more than the double-layer with total MFR. In single-layer flow analysis, pressure drop rapidly increases after the mass flow rate of 0.0014 kg/s. The sudden increase in pressure drop may due to the sudden contraction and expansion at the microchannel inlet and outlet.

Change in the friction factor with the MFR is as shown in Fig.4.5. The friction factor is calculated using equation (7).

$$\text{Friction factor} \quad f = \frac{2 * \Delta P_f * d}{\rho * L * u^2} \tag{7}$$

where L is the length of the microchannel in meter(m).

The friction factor is found to decrease with the mass flow rate as expected. Numerical analysis of the CF and PF arrangements has exhibited a similar trend. The experimentally calculated friction factor is found to be similar to the numerical results. The slope of the curve also decreases with the mass flow rate as expected. Comparing the numerical analysis of CF and PF arrangement with experimental data, with a similar trend is observed.

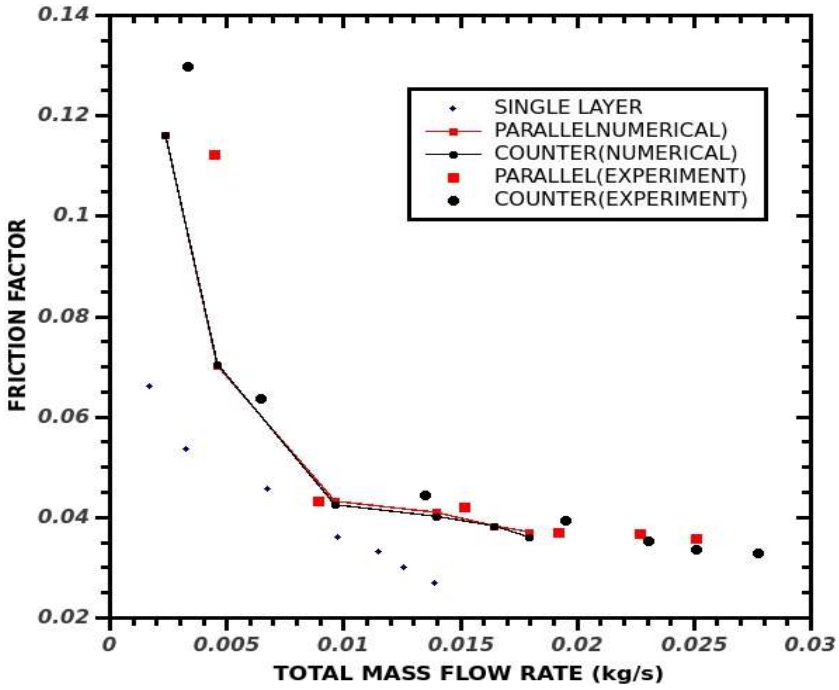

Fig 4.5 Friction Factor Vs the Total Mass Flow Rate

In the experimental analysis, for CF and PF arrangement the friction factor decreases with mass flow rate and a large deviation between these arrangements is noticed at a lower mass flow rate. A maximum of 1.6 % to 10.7 % change is noted between the experimental and numerical values. At higher discharge, the percentage change is very small. This indicates the smoothness of the circular microchannels.

Comparing the entire experimental friction factor with the numerical result obtained from Fig.4.5, an acceptable range of ±12% deviation is obtained. The friction factor in the experimental analysis is higher for CF arrangement compared to PF arrangement at low mass flow rates. While increasing the mass flow rate, friction factor decreases and the difference become almost negligible. The classical theory of fluid flow also follows the same trend.

Figure 4.6 exhibits the variation of the pumping power with the total mass flow rates through the double-layered circular microchannel.

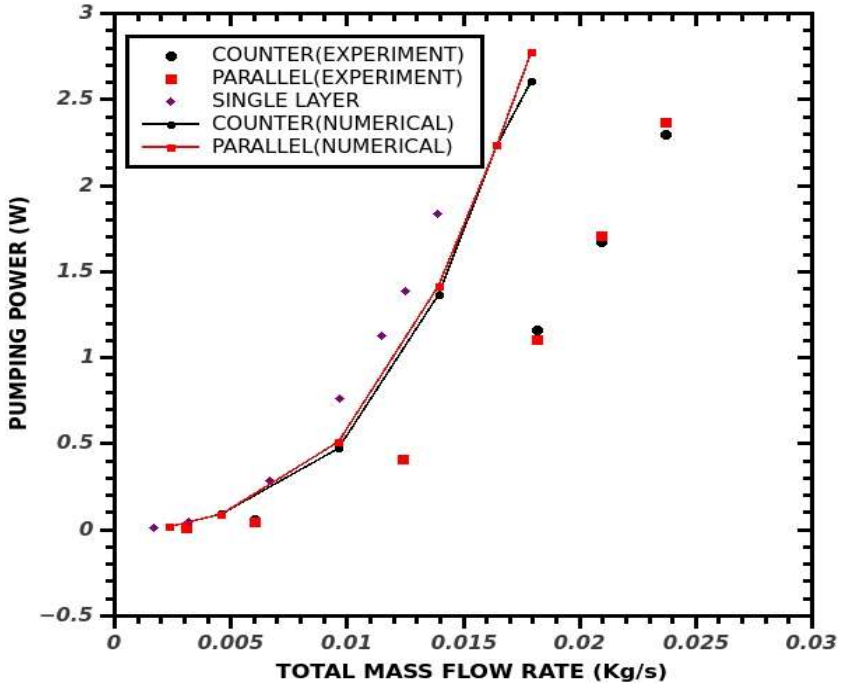

Fig 4.6 Pumping Power Vs the Total Mass Flow Rate

The pumping power is also related to the pressure drop and the discharge of the fluid through the microchannel.

The Pumping Power (in W) is calculated using

$$P = Q * \Delta P_f \tag{8}$$

In the numerical analysis of PF and CF arrangement, the deviation is negligible. With an increase in the coolant flow rate, the pumping power is also increased. Comparing with the single-layer flow the double layer has less pumping power. The numerical results and experimental values are scattered with a deviation may be due to the diameter tolerance in the experimental work. The total pumping power required is less than 3 W for the higher MFR in the double layer arrangement.

The variation of fluid outlet temperature with the mass flow rate is plotted in Fig.4.7. The outlet temperature obtained from the numerical analysis and experimental study decreases with the mass flow rate in both PF and CF analysis.

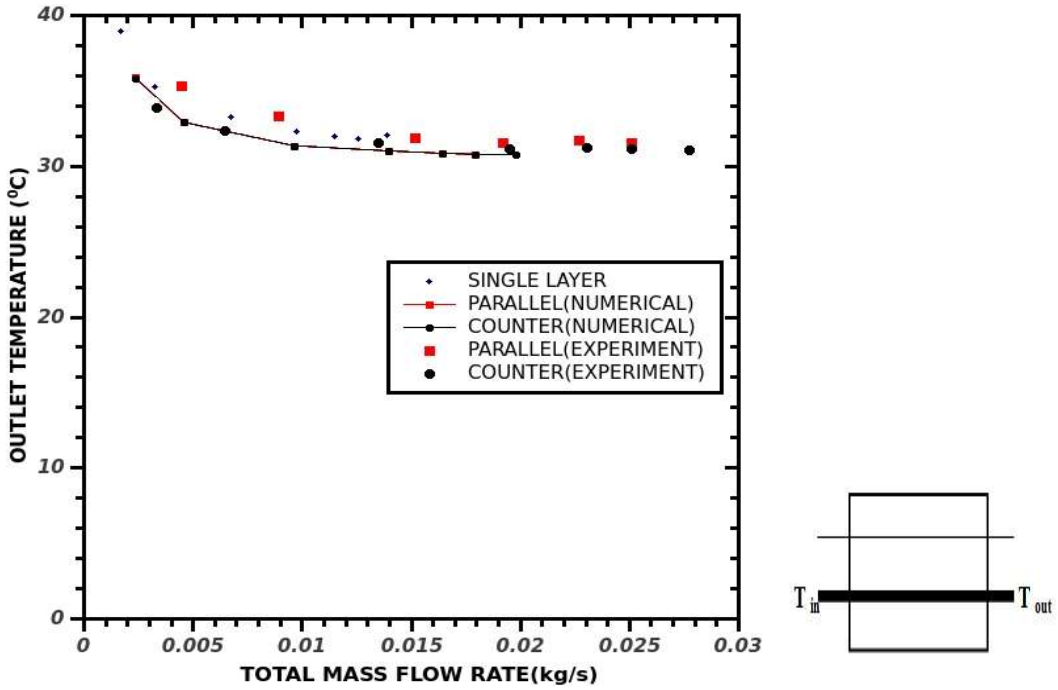

Fig 4.7 Outlet Temperature Vs the Total Mass Flow Rate

In the numerical analysis due to the same inlet condition and constant heat input of 80 W, a similar trend is observed for both CF and PF arrangements. The outlet temperature of the CF arrangement is slightly lower than the PF arrangement. The inlet temperature is 30^0C. A 2 ^{0}C change occurs in the lower mass flow rate. Here the maximum temperature is less than 38 ^{0}C. This temperature is lower than the allowable working temperature of the electronic competent of 60 ^{0}C. Due to this temperature, the fluid viscosity may increase. This results in a large pressure loss. This may the reason for the large fluctuation of flow observed at the lower mass flow rate.

A good agreement is observed for the numerical and experimental results, especially at high flow rates. While the cooling fluid entered in each layer from the same side and leaves the fluid from the opposite side of the microchannel, the fluid outlet temperature in parallel flow arrangement is higher than the counter flow arrangement.

The variation of the convective top wall surface temperature in the PF, CF and SL flow arrangement with the total mass flow rate is plotted in Fig.4.8. Experimentally the temperatures at the two points on the (T_1 and T_4) convective wall are measured and the average of this reading is plotted. In the numerical analysis for both PF and CF

arrangement, the convective wall surface temperature decreases with the mass flow rate correspondingly.

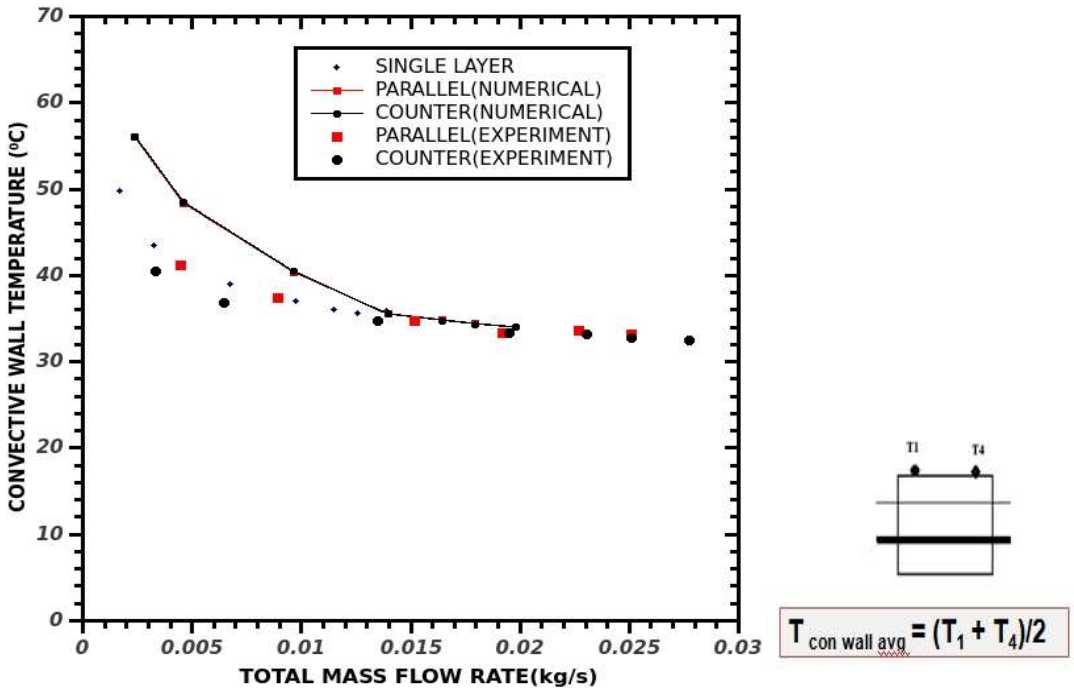

Fig 4.8 Convective Wall Surface Temperature with the Total Mass Flow Rate

At low mass flow rate the convective wall surface temperature is nearly 58 ^{0}C and gradually decreases with the mass flow rate and at the higher mass flow rate, it is nearly 32 ^{0}C. This temperature is less than the actual operating temperature (60 ^{0}C) of the electronic equipment.

The experimental result of the top convective wall temperature also decreases with the mass flow rate. The counter flow arrangement has less temperature than the parallel flow arrangement in all mass flow rates. This temperature ranges from 32 ^{0}C to 42 ^{0}C, which gives better surrounding temperature inside the cabin of the electronic devices. As the flow rate increases the minimum temperature and maximum temperature decreases both in the counter and parallel flow of the fluid. This temperature is more than the normal surrounding temperature.

As compared with the parallel flow and counter flow analysis an average change in the convective wall temperature is about 1 % to 5 %. The temperature is increased from the

inlet and become uniform after 10 % of the flow in the axial direction due to uniform heating for the counter-flow analysis and the parallel flow analysis. These excess temperatures circulate inside the cabin of the electronic equipment. For the parallel flow and counter flow analysis, the same trend is found and there is no more deviation between them.

The flow through the lower channel only (single layer) has higher values of the convective wall temperature than the double layer concept in the experimental analysis. At low mass flow rate, the convective wall temperature in the double layer is nearly 42 ^{0}C and gradually decreases with the mass flow rate. At the higher mass flow rate, it is nearly 32 ^{0}C. For the single-layer flow, it is 50 ^{0}C and 37 ^{0}C respectively, meaning an average 5 ^{0}C to 8 ^{0}C changes is noticed. An 8 % to 11 % change in convective wall temperature is noticed between single layer and double layer arrangements. So that the double layer concept is better for heat transfer enhancement instead of a single layer one.

The variation of wall average temperature in CF, PF and SL arrangements with the mass flow rate are shown in Fig.4.9. The wall average temperature is calculated using Equation (9).

The wall average temperature (T_{wa}) in ^{0}C is calculated using,

$$T_{wa} = \frac{T_{wi}+T_{wo}}{2} \quad (9)$$

Where, T_{wi} is the inlet wall side temperature in (^{0}C) and T_{wo} is the outlet wall side temperature in (^{0}C).

The fluid wall average temperature decreases with the mass flow rate for the constant inlet temperature and the input power. The fluid wall average temperature values in the numerical results of parallel flow and counter flow arrangement are coinciding with the same mass flow rate. This may be due to the same inlet conditions.

The experimental results showed a slight deviation from the numerical results. Maximum of 21 % deviation is occurs at low mass flow rates. The experimental values are higher than the numerical values after a mass flow rate of 0.018 kg/s.

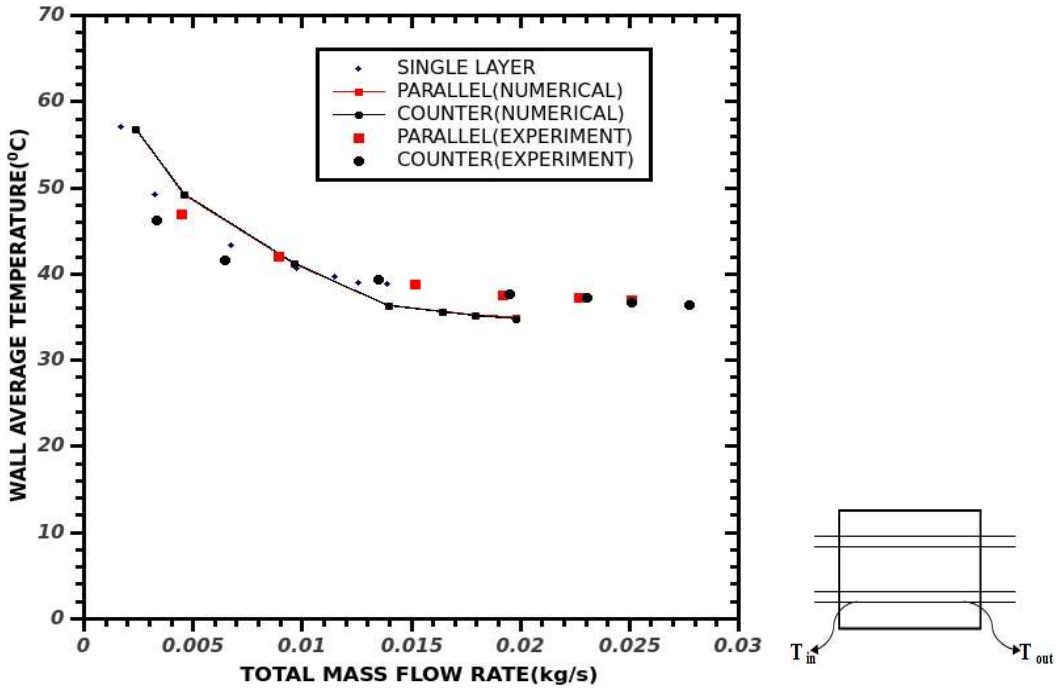

Fig 4.9 Wall Average Temperature Vs the Total Mass Flow Rate

Variation of the heat sink base temperature with the mass flow rate is plotted in Fig.4.10. The temperature decreases gradually in all the configurations. The maximum temperature obtained at the base of the heat sink is found to be below 60 ^{0}C. This temperature is well below the allowable maximum temperature of electronic devices.

The lower channel is at a distance of 2.5 mm from the base of the heat sink. Therefore, the temperature just below the channel is also a clear indication of the heat sink base temperature.

Experimentally the temperature is measured in two locations (T_2 and T_3) and the average of these reading is taken. Numerically it shows that the temperature variation is not linear. The variation in the numerical and experimental values may be due to this reason.

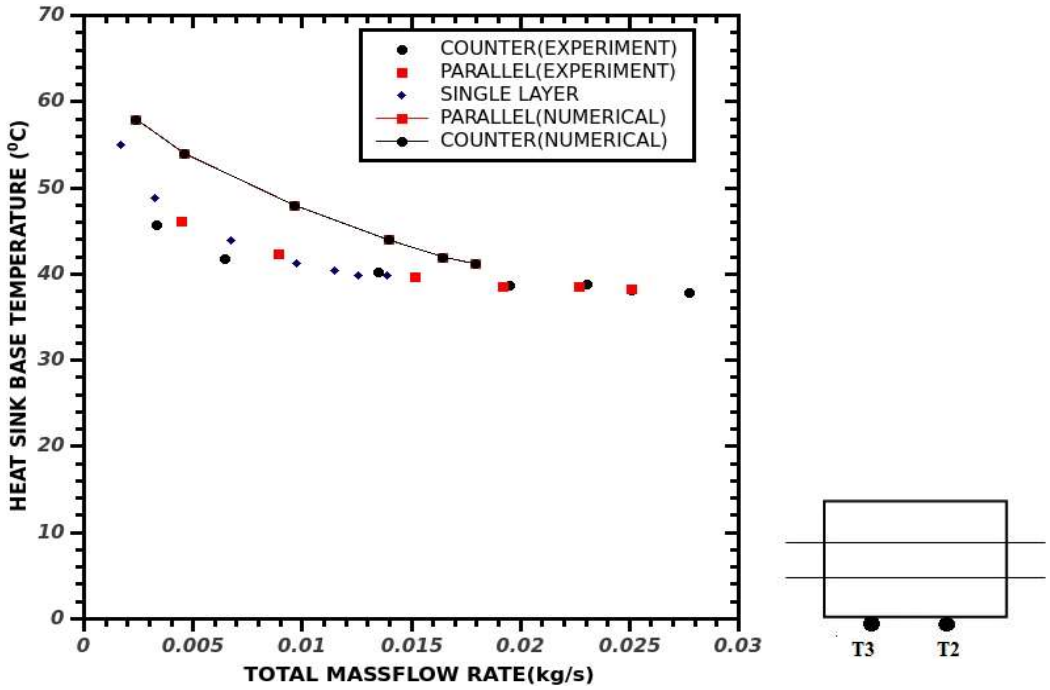

Fig 4.10 Heat Sink Base Temperature Vs the Total Mass Flow Rate

The heat loss from the Teflon surface is calculated by measuring the temperature across the Teflon surface.

The heat loss through the Teflon insulation is estimated using Fourier's law of heat conduction. The temperatures T_7, T_8, T_9, and T_{10} are the temperatures of the outer surface of the heat source.

The Teflon outer surface is also noted and calculated the heat loss. The maximum heat loss is found to be less than 12 % of the input power. Due to this heat loss which may affect the reduction in the heat sink base temperature compared with the numerical analysis.

Temperature contours with different cases are plotted in Fig.4.11 to Fig.4.15. Comparing these figures with the Fig.4.10 the heat sink base temperature of the numerical analysis is higher than the experiment results.

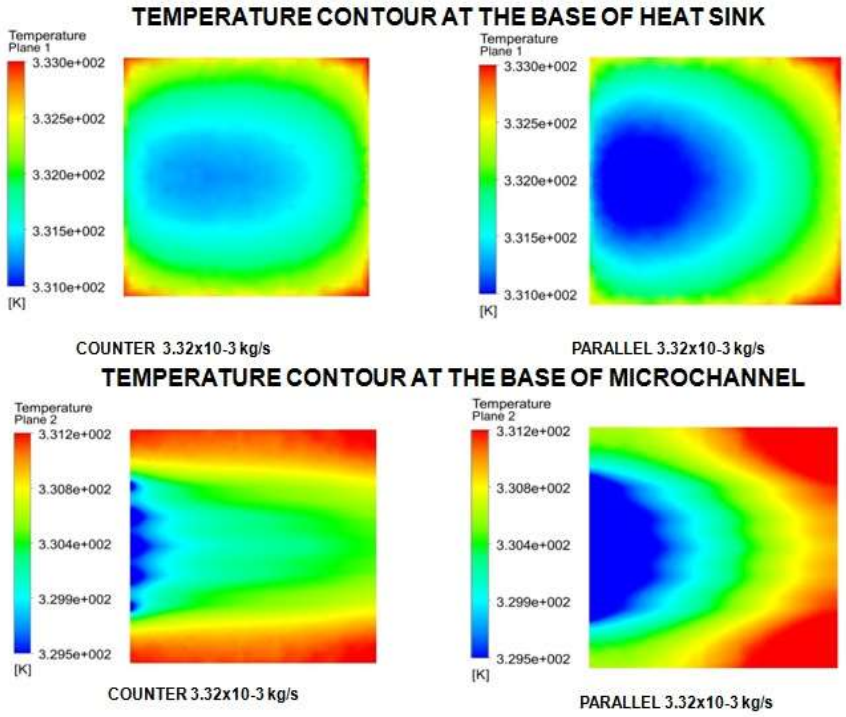

Fig 4.11 Temperature Plot (Case 1)

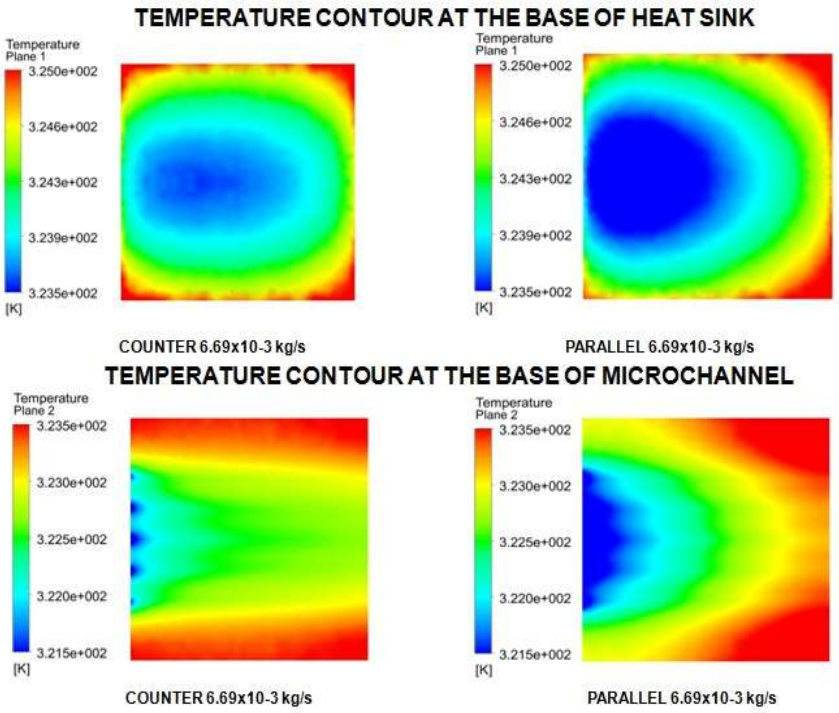

Fig 4.12 Temperature Plot (Case 2)

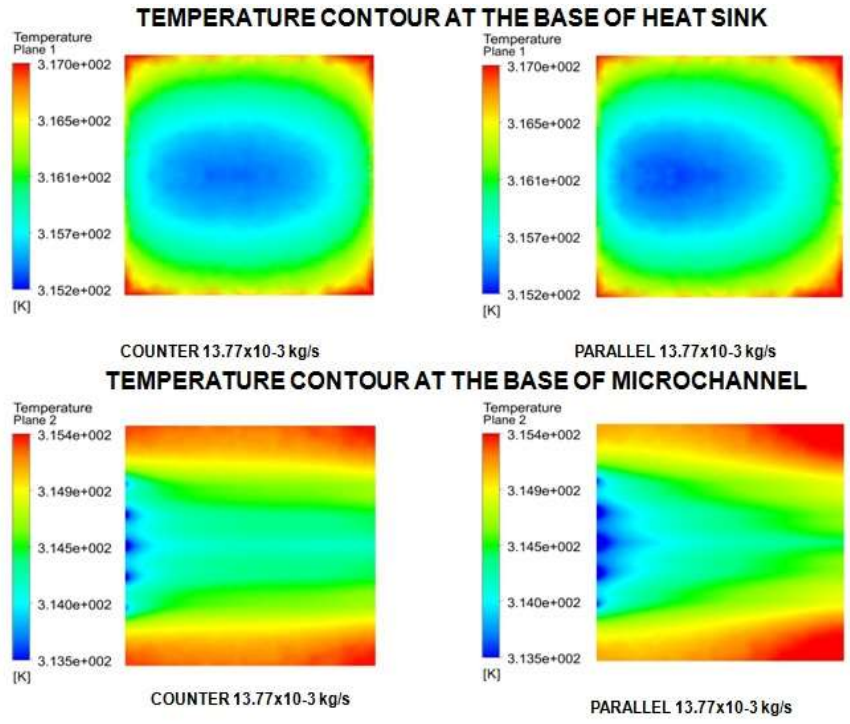

Fig 4.13 Temperature Plot (Case 3)

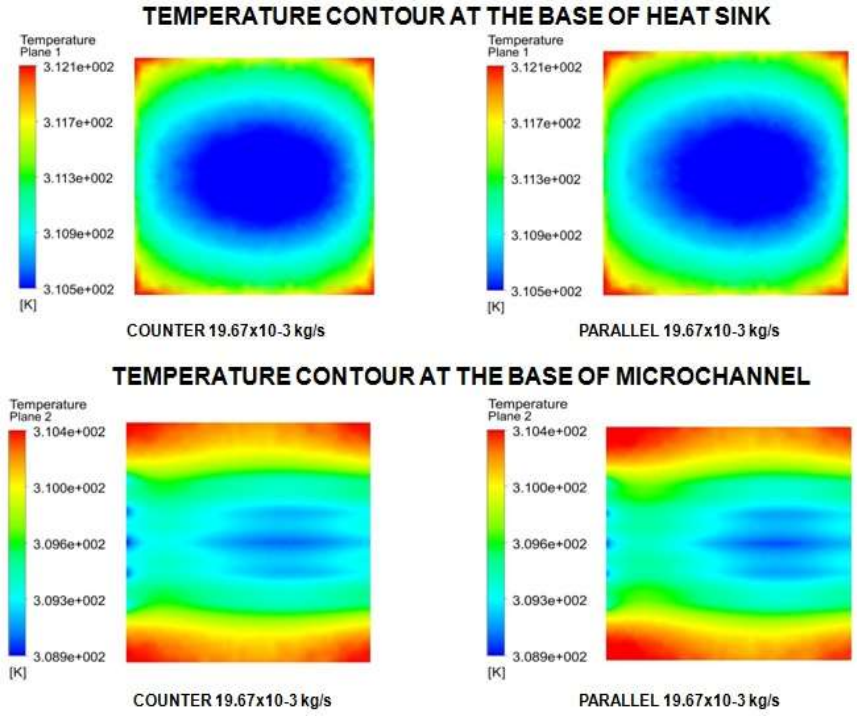

Fig 4.14 Temperature Plot (Case 4)

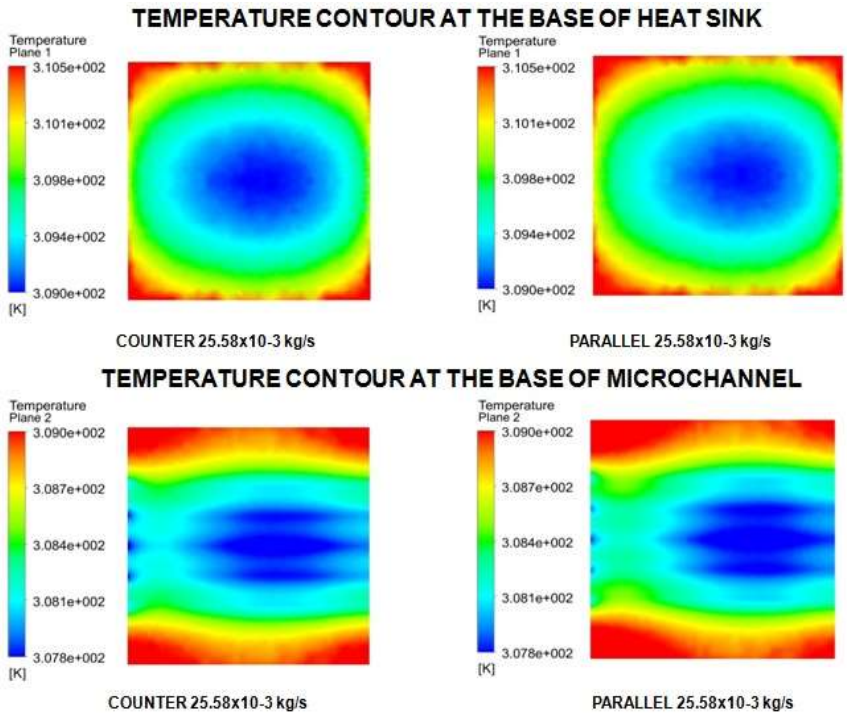

Fig 4.15 Temperature Plot (Case 5)

Further, the temperature uniformity is found more for the counter-flow arrangement than the parallel flow and single-layer flow arrangement. This is confirmed by plotting the temperature contours at two different planes of the five different cases in Fig.4.11 to Fig.4 15. For the same MFR of the fluid, uniformity of temperature under the chip in CF arrangement follows more effective than PF design. The double-layer design gets improved temperature uniformity at the base of the heat sink. Thus counter-flow and parallel flow arrangements show better performance than the single layer. This underlines the solidity of the electronic devices

Figure 4.16 exhibits the variation of maximum wall temperature difference with the total mass flow rate. This temperature difference is the difference between the maximum temperature and minimum temperature at the wall surface.

The wall temperature difference (T_{wd}) is calculated using Equation (10)

$$T_{wd} = (T_{w0} - T_{wi}) \tag{10}$$

where T_{wi} is the inlet wall surface temperature and T_{wo} is the outlet wall surface temperatures.

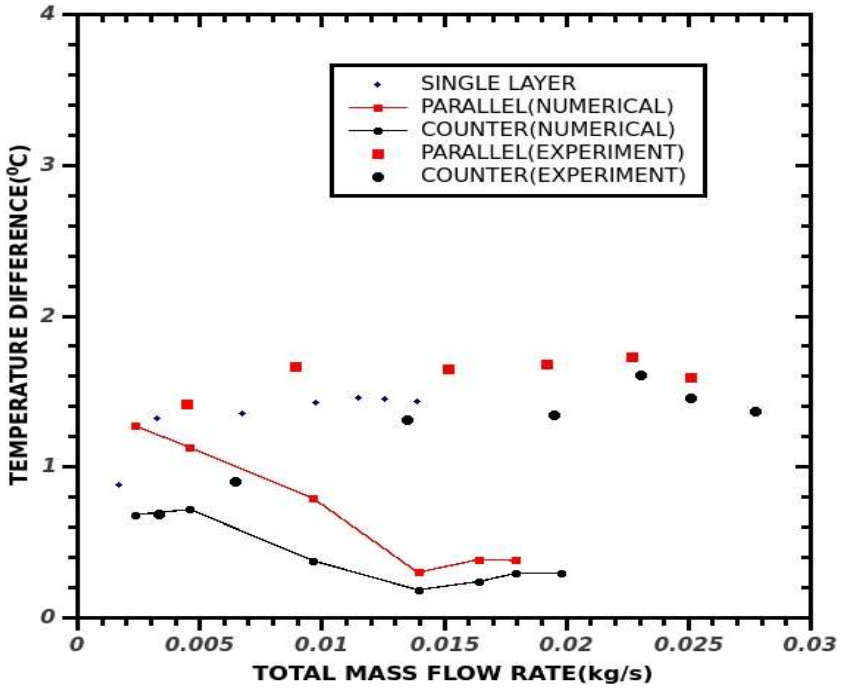

Fig 4.16 Wall Temperature Difference with the Total Mass Flow Rate

The experimental and numerical values have considerable deviations in the temperature difference in Fig. 4.16 may be due to the point at which the experimentally measured. It is 1mm to 2 mm apart from the wall.

The result shows that for both numerical and experiment analyses, the fluid wall temperature difference of the counter flow analysis are less than the PF analysis. The thermal stress is directly proportional to the thermal strain. Also, the thermal strain is equal to the product of the coefficient of expansion and the difference in temperature. Therefore the thermal stress is proportional to the difference in temperature and less thermal stress is found in the counter flow analysis.

The overall thermal performance is explained on the base of these different temperature curves. From these performances, this experimental study is suited for the practical application in the electronic cooling with the given pumping power. While in the numerical analysis the variation follows the same trend both in the parallel flow and

counter flow analysis. This advantages the solidity of electronic devices. This temperature is well below the allowable maximum temperature of electronic devices. Therefore the results show that the counter-flow arrangement is always better in a double layer configuration.

4.4 LAMINAR FLOW AND USING GRAVITY FEED SYSTEM

The numerical study is also conducted with the laminar flow condition. The results from the numerical study are validated with the results obtained by the experiment. The experiment is conducted with a gravity feed system for low mass flow rates.

4.4.1 MESH DEPENDENCE STUDY

The mesh dependence study is carried out for an inlet velocity of 0.428 m/s with four different mesh sizes as shown in Table 4.5.

The mesh size corresponding to the fine mesh is employed for further study because of the outlet temperature at the lower layer microchannel between fine and superfine mesh sizes is less than 0.188 %. The minimum reductions in normalized residuals for each variable are taken as less than 1.0×10^{-7}.

Table 4.5 Mesh dependence study

Mesh Quality	Number of Nodes	Outlet Temperature(^{0}C)	% Change
Very coarse	1244281	54.611	---
Coarse	2248328	54.304	0.565
Fine	**3050685**	**54.202**	**0.188**
Superfine	4355677	54.101	0.186

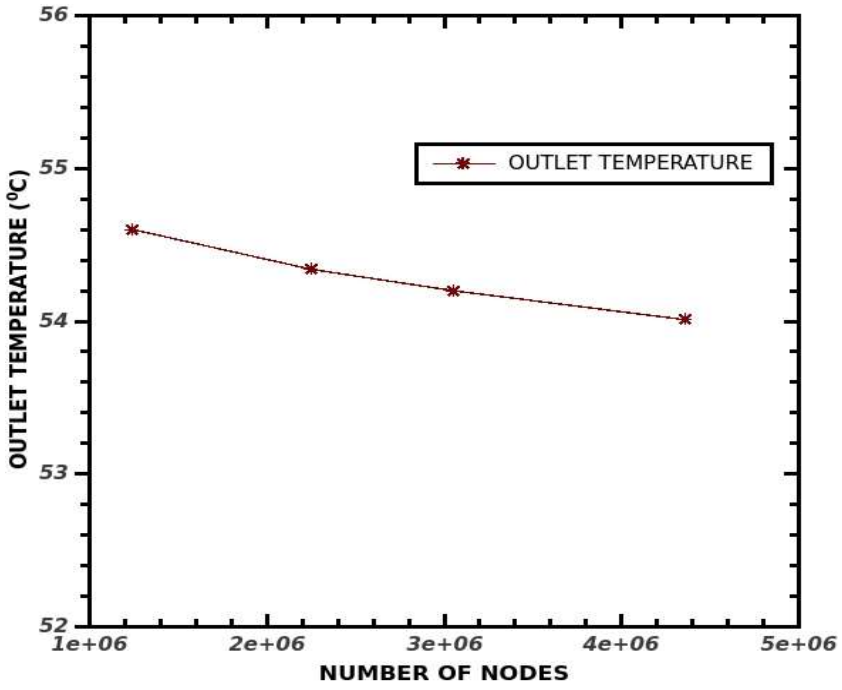

Fig 4.17 Lower Channel Outlet Temperature Vs Number of Nodes

From the Fig.4.17, it is clear that the lower channel outlet temperature variation with the number of nodes and the measurement corresponds to the number of nodes 3050685 is taken for the future study. The fine mesh size is employed in the final simulation since less computational time is needed.

The experiment is conducted for three different flow configurations as shown in Fig.4.18. They are (1) Single layer flow (2) Parallel Flow and (3) Counter Flow.

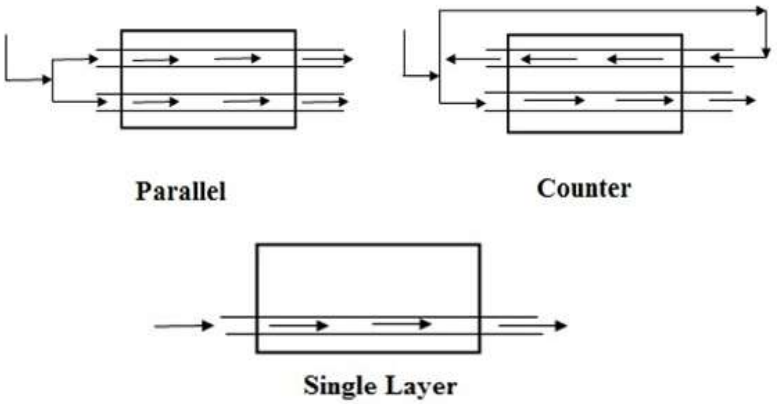

Fig 4.18 Schematic of the Flow Pattern for the Experimental Analysis

The constant heat input given to the heat sink is 100 W. The apparatus is allowed to run continuously for sufficient time to reach the steady-state. All the readings are taken at steady-state condition; it is assumed that the outlet temperature varies with less than 0.1^0C in ten minutes. After reaching the steady-state condition temperature, pressure head, and the time taken for filling 100cc of water are measured and recorded.

The velocity of the fluid flow through each layer is controlled by varying the vertical position of the float chamber. The discharge of the fluid through the lower layer and the upper layer is separately calculated using equation (11) by measuring the time taken (t) in seconds for collecting 100 ml of fluid.

Discharge of the fluid in m^3/s

$$Q = \frac{0.0001}{t} \tag{11}$$

Average velocity and mass flow rate of the fluid at the outlet are calculated using Equation (2) and (3)

Figure 4.19 shows exclusively the variation of pressure drop with a total mass flow rate in the double-layered circular microchannel for (1) Single layer flow (2) Parallel Flow and (3) Counter Flow arrangements. The numerical and experimental results are plotted with the total mass flow rate. The total pressure drop is calculated using Equation (4).

It is observed that the pressure drop of the single layer is more than the double-layer flow arrangements. The numerical pressure drop of the counter flow and parallel flow are compared with the experimental pressure drop. The pressure drop varies with the mass flow rate. The variation between the experimental results and the numerical values are well in the acceptable range.

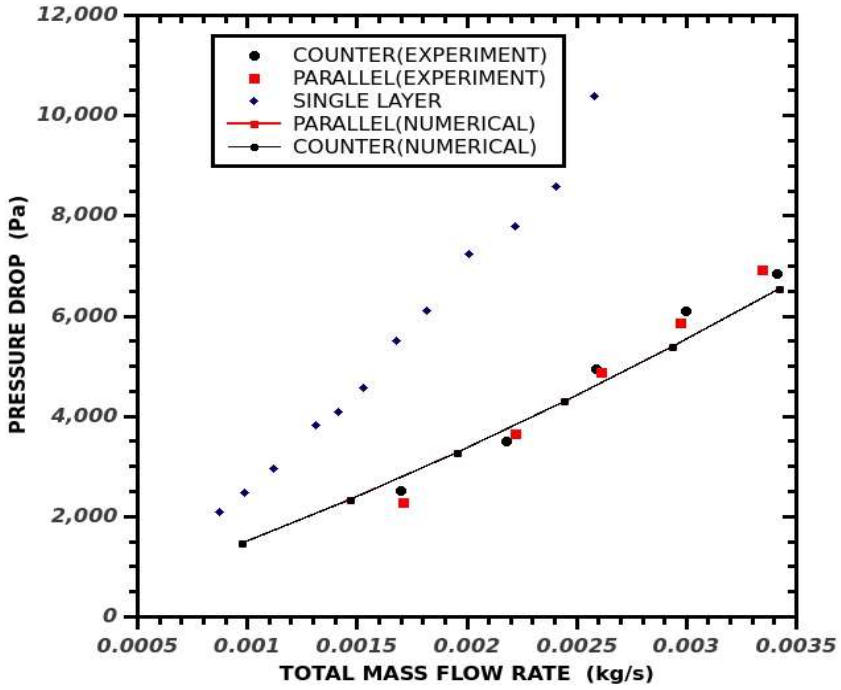

Fig 4.19 Total Pressure Drop with the Total Mass Flow Rate

The variation of pressure drop per unit length with the total mass flow rate is plotted in Fig.4.20. The pressure drop per unit length increases with the total mass flow rate. The uncertainty for the experimental results also plotted in this Fig.4.20. The uncertainty of pressure drop is calculated using equation (12) and plotted.

$$\frac{\Delta p}{P_f} = \left(\left(\frac{\Delta h}{h}\right)^2\right)^{\frac{1}{2}} \tag{12}$$

where 'h' is the difference in pressure head

Actual pressure drop is,

$$\Delta P_{actual} = \Delta P_f \pm (\Delta p) \tag{13}$$

It is observed that the pressure drop is found to be similar as expected for the same mass flow rate. This indicates that both the upper and the lower channel are identical in geometry. Similar variation is observed for both counter flow and parallel flow arrangements.

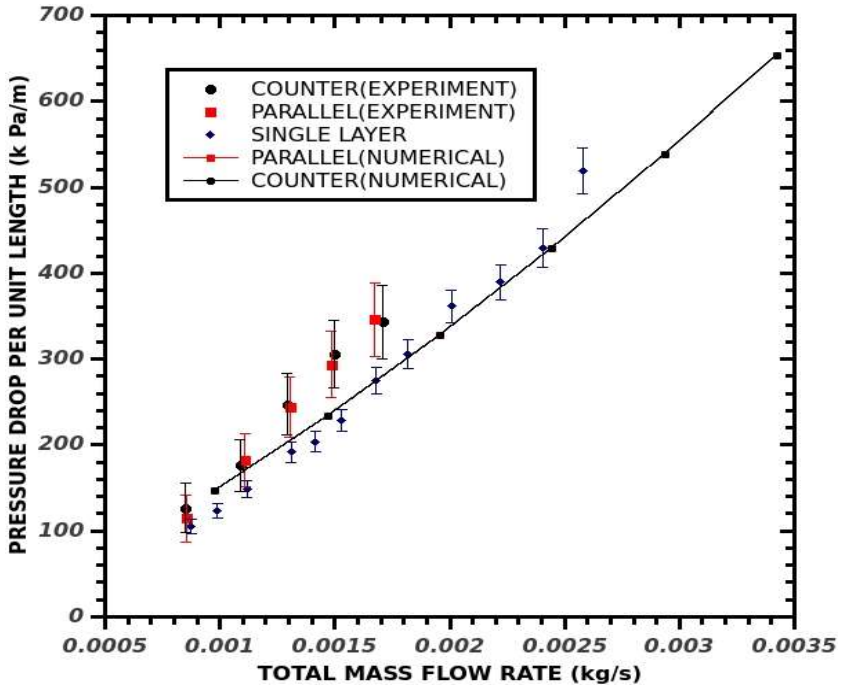

Fig 4.20 Pressure Drop per Unit Length with the Total Mass Flow Rate

This indicates that the flow behaviour in the upper and the lower layers are identical. The total pressure drop per unit length in the experimental double-layer microchannel varies from 100 k Pa to 350 k Pa.

The friction factor is calculated using equation (7) and its variation with mass flow rate is shown in Fig.4.21. The uncertainty in the experimental results is also plotted in this figure.

The experimental friction factor decreases with the total mass flow rate. The fiction factor for the experimental study varies between 0.25 and 0.35. This also indicates the channel smoothness. The counter flow and parallel flow has the same trend as that of single-layer flow configuration.

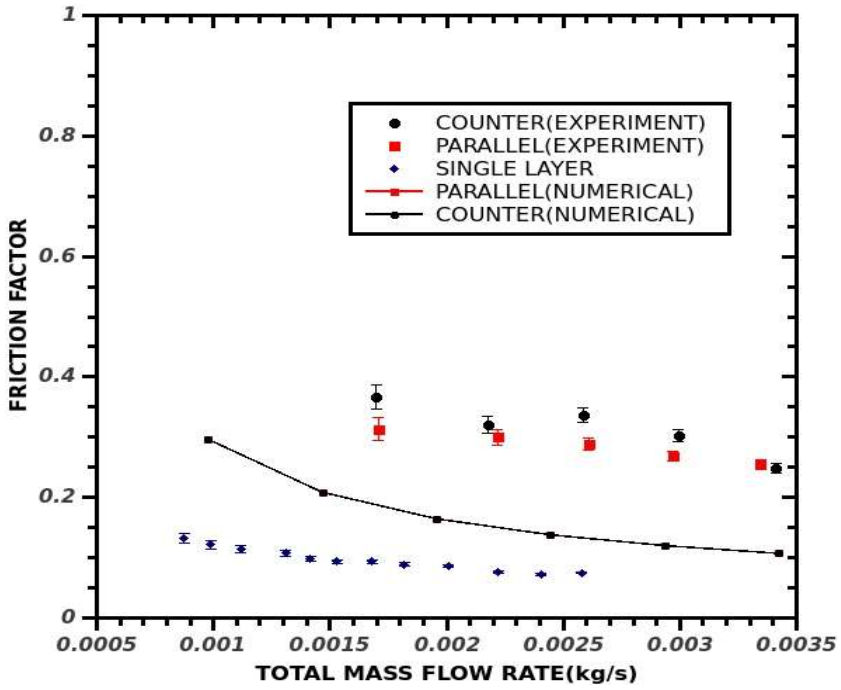

Fig 4.21 Friction Factor with the Total Mass Flow Rate

The uncertainty in the friction factor is calculated using the equation (14).
Uncertainty of the friction factor is,

$$\frac{\Delta f}{f} = \left(\left(\frac{\Delta p}{P}\right)^2 + \left(\frac{\Delta l}{l}\right)^2 + \left(\frac{\Delta d}{d}\right)^2 + \left(\frac{2\Delta u}{u}\right)^2\right)^{1/2} \tag{14}$$

$$\frac{\Delta u}{u} = \left(\left(\frac{\Delta \dot{U}}{\dot{U}}\right)^2 + \left(\frac{2\Delta d}{d}\right)^2\right)^{1/2} \tag{15}$$

$$\frac{\Delta \dot{U}}{\dot{U}} = \left(\left(\frac{\Delta U}{U}\right)^2 + \left(\frac{\Delta t}{t}\right)^2\right)^{1/2} \tag{16}$$

Where ΔU is least count of measuring jar and U is the total volume of measuring jar.

Figure 4.22 shows the variation of the pumping power with total mass flow rate for the single-layer flow, CF and PF arrangements. The pumping power is calculated using equation (8). It is clear that with an increase in the mass flow rate of the fluid, the pumping power also increases.

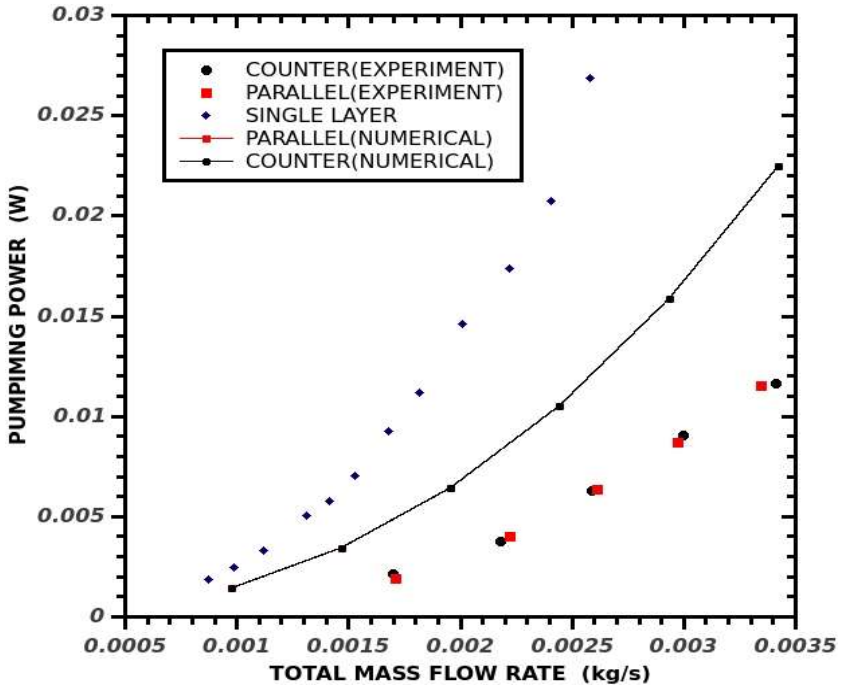

Fig 4.22 Pumping Power with the Total Mass Flow Rate

The pumping power for CF and PF arrangements are found to be similar as expected. The pumping power required for a single layer configuration is higher than the double-layer configuration. The maximum pumping power required for the double-layer configuration is less than 0.015 W.

The variation of fluid outlet temperature with the total mass flow rate is plotted in Fig.4.23.

This decreases with the increase of the mass flow rate. The fluid outlet temperature for double-layer flow configuration is in between 35 ^{0}C to 40 ^{0}C. The experimental value is less than the numerical value. This is because of the heat loss occurred in the experiment.

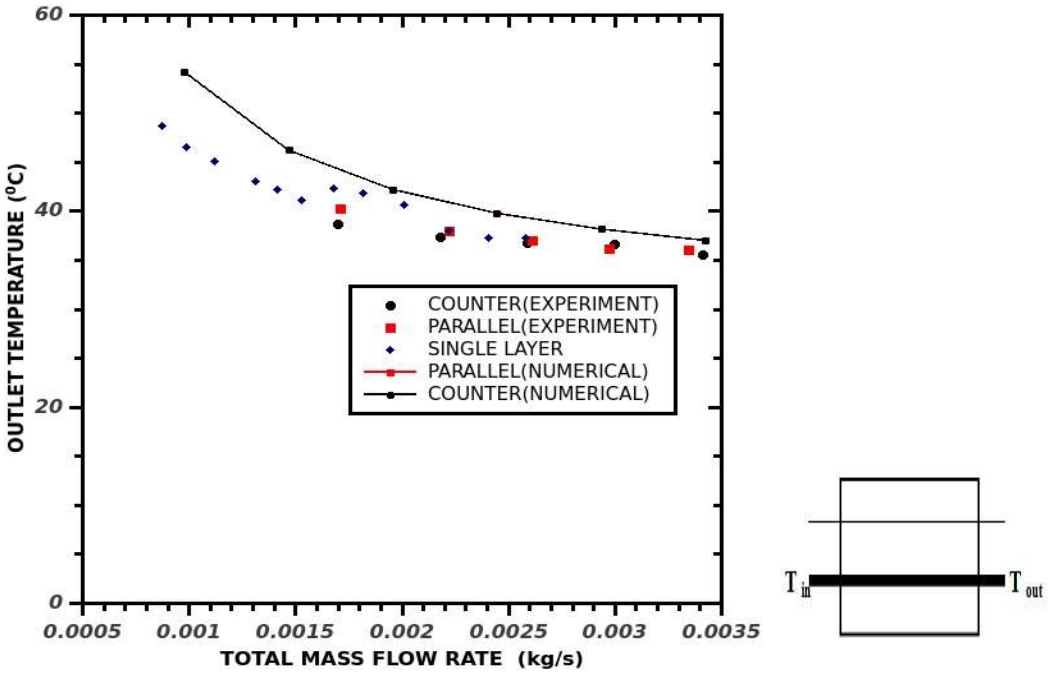

Fig 4.23 Outlet Temperature with the Total Mass Flow Rate

Figure 4.24 shows the relation between change in convective wall surface temperatures for both numerical and experimental analysis with the total mass flow rate in the PF and CF arrangement.

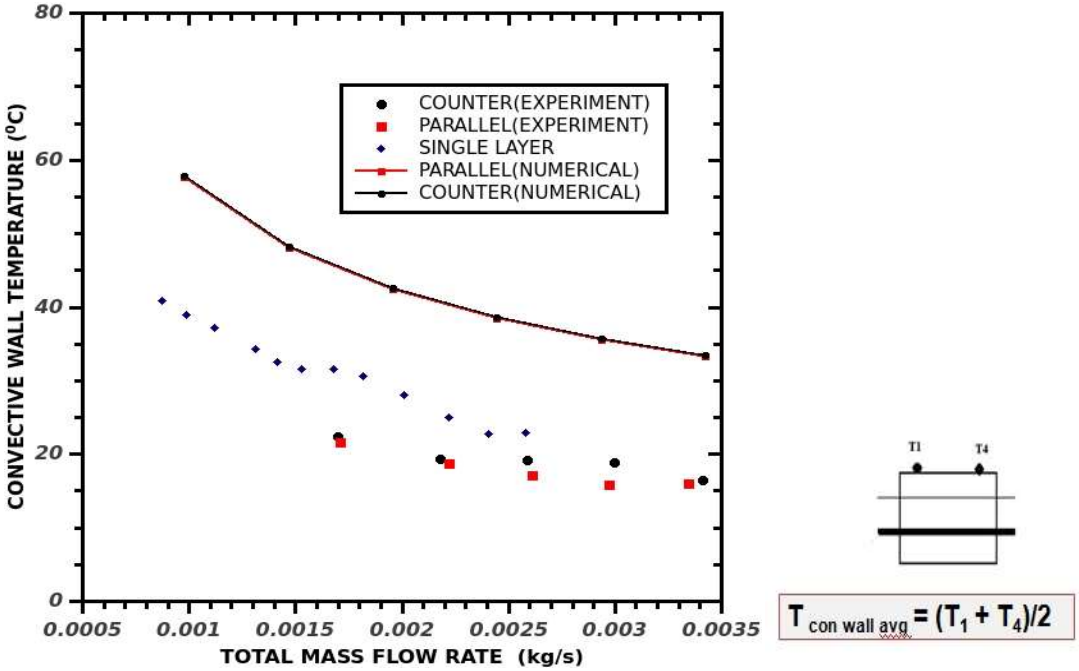

Fig 4.24 Convective Wall Temperature with the Total Mass Flow Rate

The counter flow and parallel flow arrangement have the same trend with negligible deviation. At a low flow rate, the convective wall surface temperature in the double-layer is nearly 52^0C and gradually decreases with Reynolds number and at the higher Reynolds number, it reaches 45^0C.

In the numerical analysis, the convective wall temperature is found to be similar in counter-flow and parallel flow arrangements. Higher convective wall temperature results in higher cabin air temperatures.

Variation of the average wall temperature with total mass flow rate for single-layer flow, counter flow and parallel flow arrangement is shown in Fig.4.25. For both parallel flow and counter flow arrangements the numerical predictions have almost the same values due to the same boundary conditions.

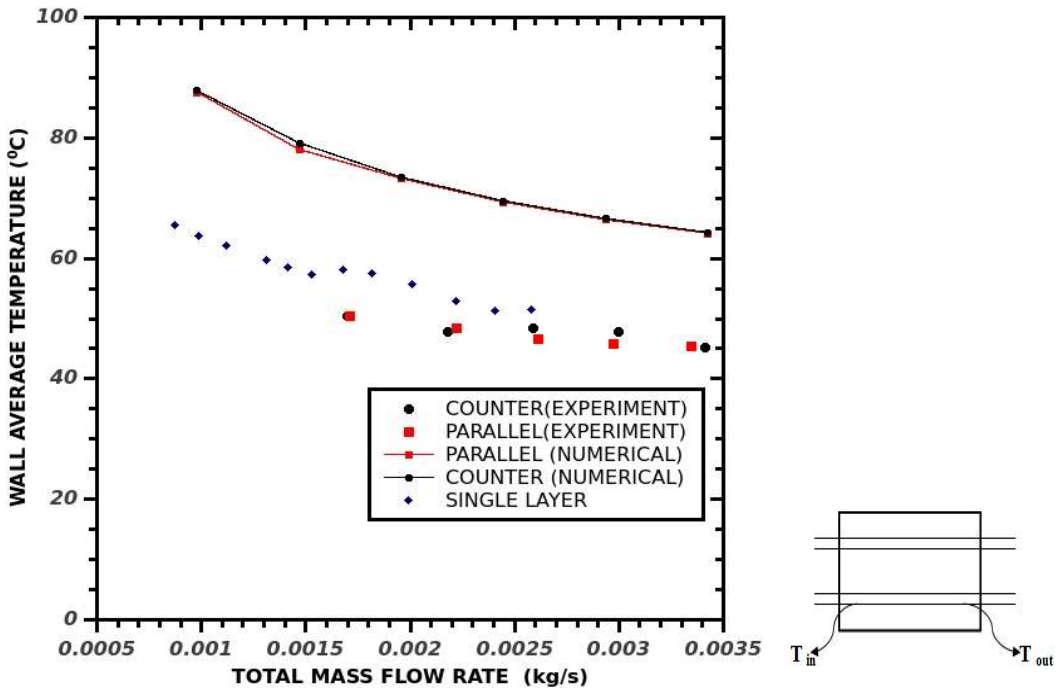

Fig 4.25 Wall Average Temperature with the Total Mass Flow Rate

The average wall temperature is calculated using Equation (9)

The average wall temperature for CF and PF is found to decrease from 51^{0}C to 44 ^{0}C with mass flow rate. The numerical values are higher than the experimental analysis may be due to the boundary conditions.

Figure 4.26 shows the variation of the heat sink base temperature with total mass flow rate for single-layer flow, counter flow and parallel flow arrangements. The experimental results are compared with the numerical results. The temperature decreases gradually in all flow configurations.

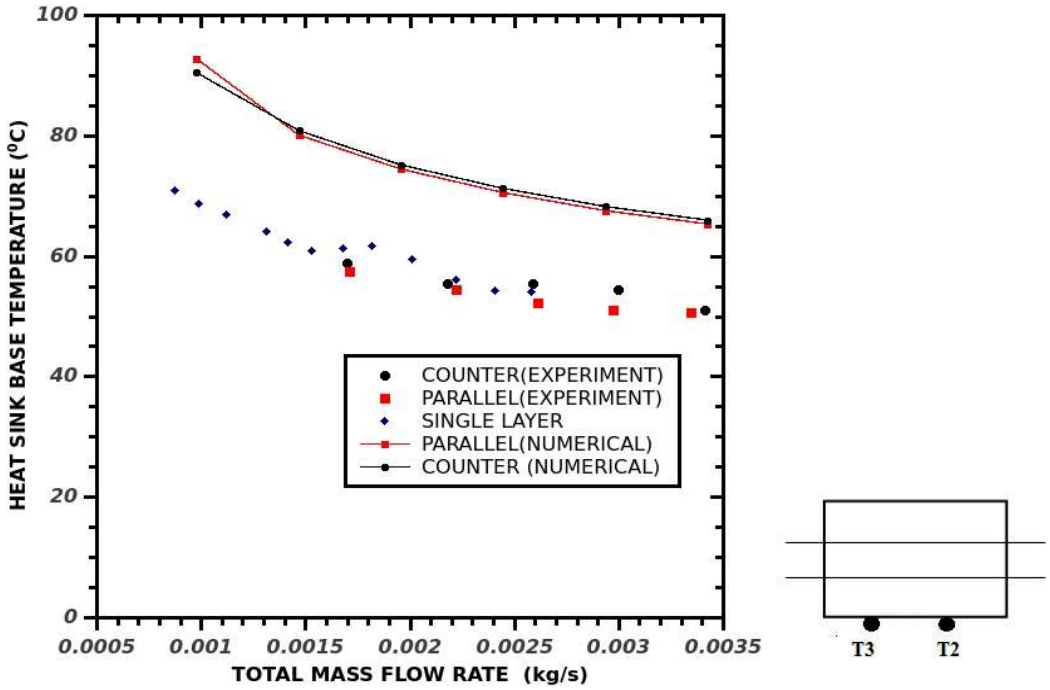

Fig 4.26 Heat Sink Base Temperature with the Total Mass Flow Rate

The maximum temperature obtained at the base of the heat sink in the double-layer design is found to be below 60 ^{0}C. This temperature is well below the allowable maximum temperature of electronic devices. While the single-layer configuration, the temperature obtained is higher than the double-layer configuration.

In the numerical analysis, the heat sink base temperature decreases with the total mass flow rate. The variation follows the same trend both in the parallel flow and counter flow analysis. The same trend occurs in both parallel flow and counterflow arrangements.

The temperature contours of different cases are plotted in Fig.4.27 to Fig.4.32. By comparing these figures with Fig.4.26, the heat sink base temperature of the numerical analysis is higher than the experimental results. The deviation in the experimental results may be due to heat loss. The overall thermal performance is explained on the base of these different temperature curves.

Further, the temperature uniformity is found that the parallel flow arrangement had better uniformity than counterflow. This is confirmed by plotting the temperature contours at two different planes of the six different cases in Fig. 27 to Fig.32.

The temperature contour at the base of the microchannel shows the less temperature spread in the parallel flow arrangement. For the same mass flow rate of the fluid, uniformity of temperature under the chip in parallel flow arrangement is more effective than counter flow design. This also advantages the solidity of electronic devices.

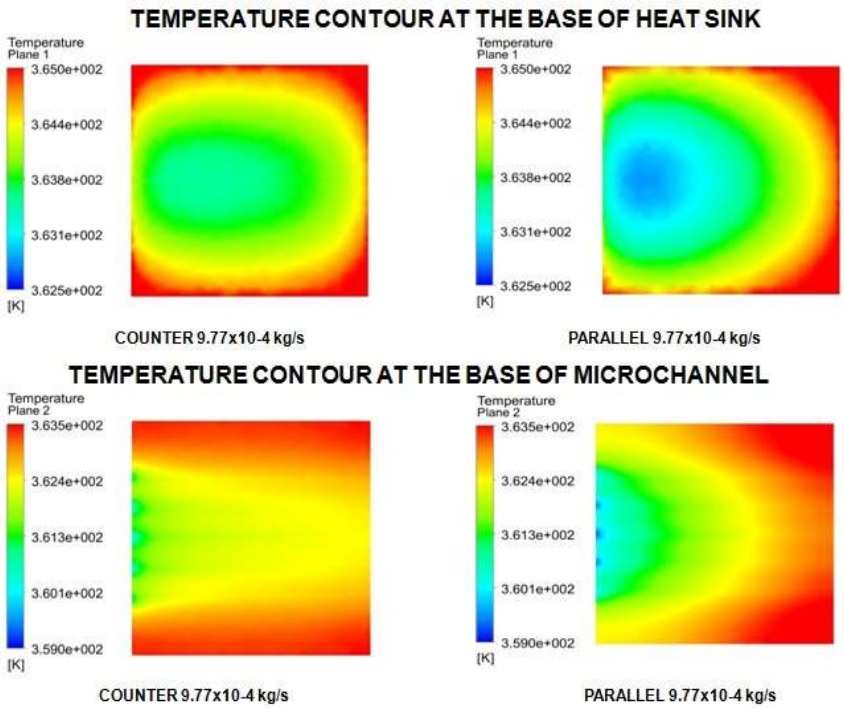

Fig 4.27 Temperature Contour (Case 1)

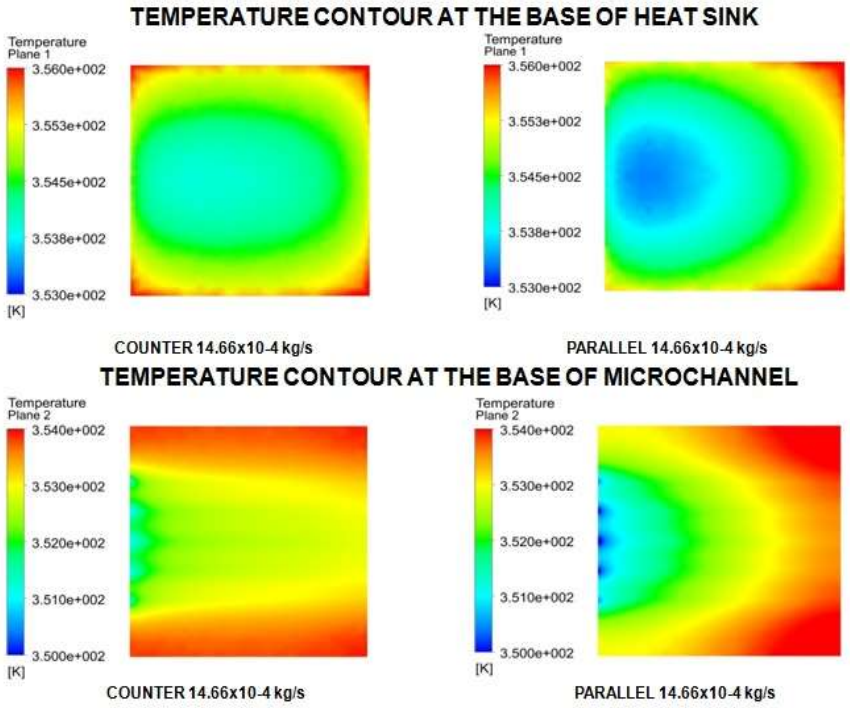

Fig 4.28 Temperature Contour (Case 2)

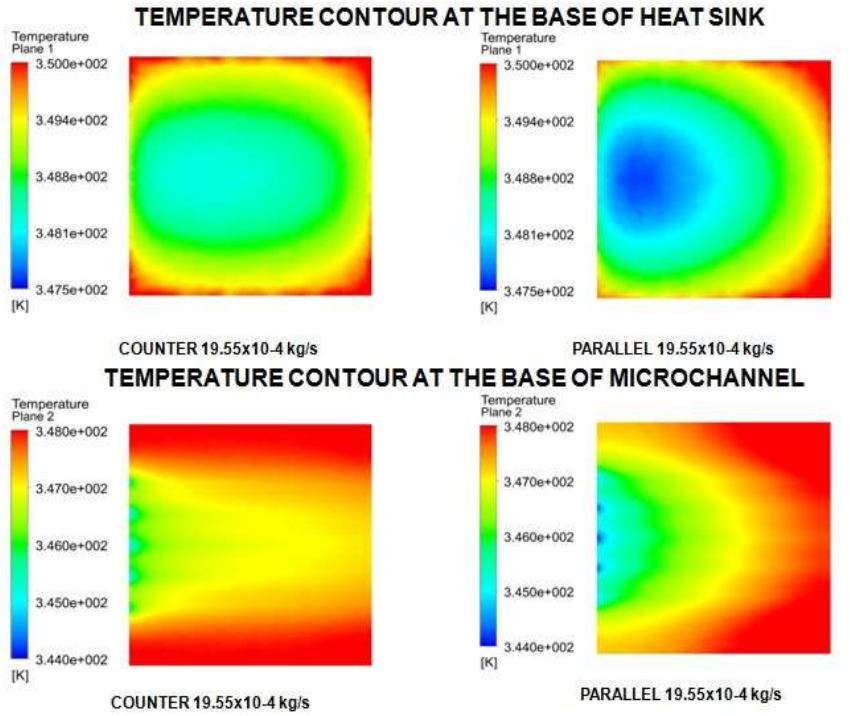

Fig 4.29 Temperature Contour (Case 3)

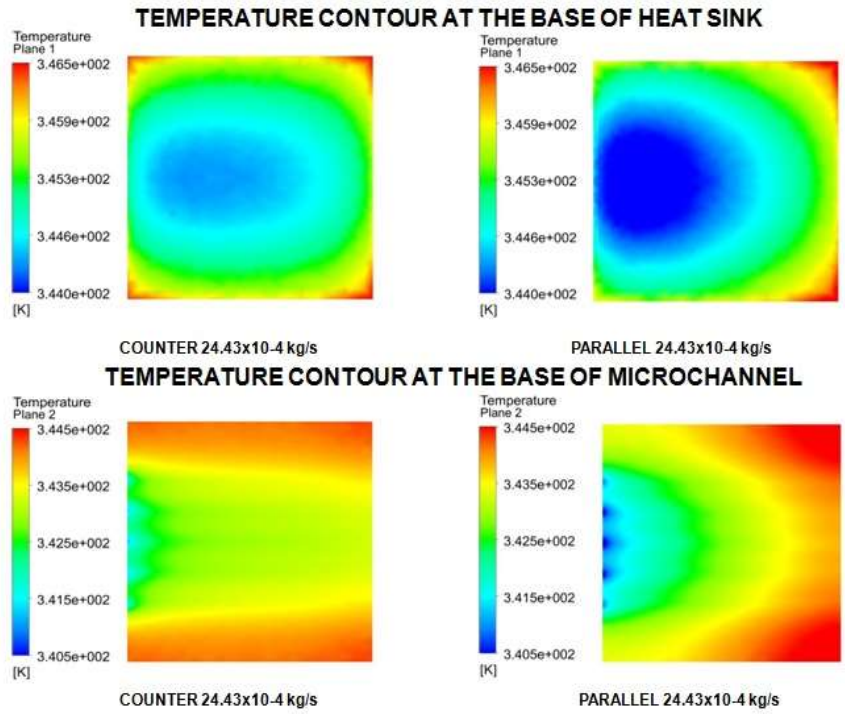

Fig 4.30 Temperature Contour (Case 4)

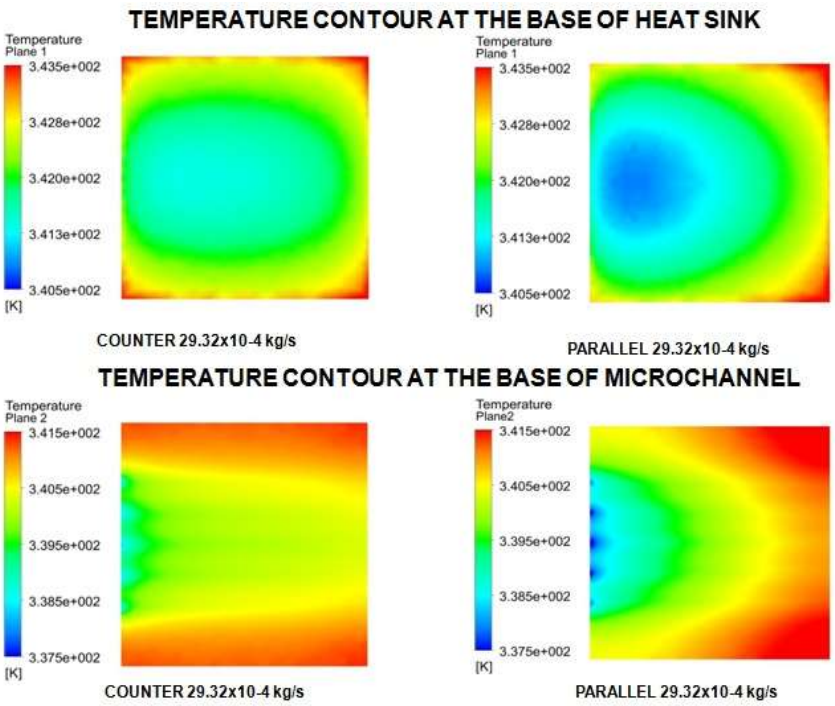

Fig 4.31 Temperature Contour (Case 5)

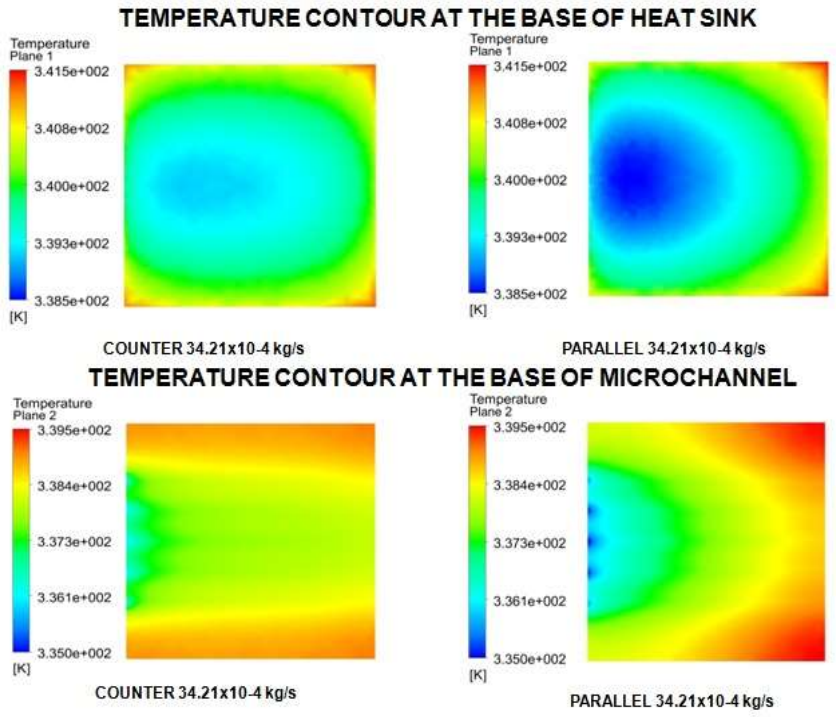

Fig 4.32 Temperature Contour (Case 6)

Figure 4.33 shows the variation of the fluid wall temperature difference (calculated by using Equation (10)) between the inlet and outlet temperature with a total mass flow rate in single layer flow, CF and PF arrangements. Lower the temperature difference, more the temperature uniformity and vice versa.

For reducing thermal stress in the microchannels, temperature uniformity plays an important role. Temperature uniformity is the variation of wall temperature along the length of the channel.

Therefore this result indicates that nearly the same temperature uniformity obtained in both counter flow and parallel flow arrangements. There is no deviation in the results between the CF and PF arrangement. Here also the thermal stress is proportional to the temperature difference.

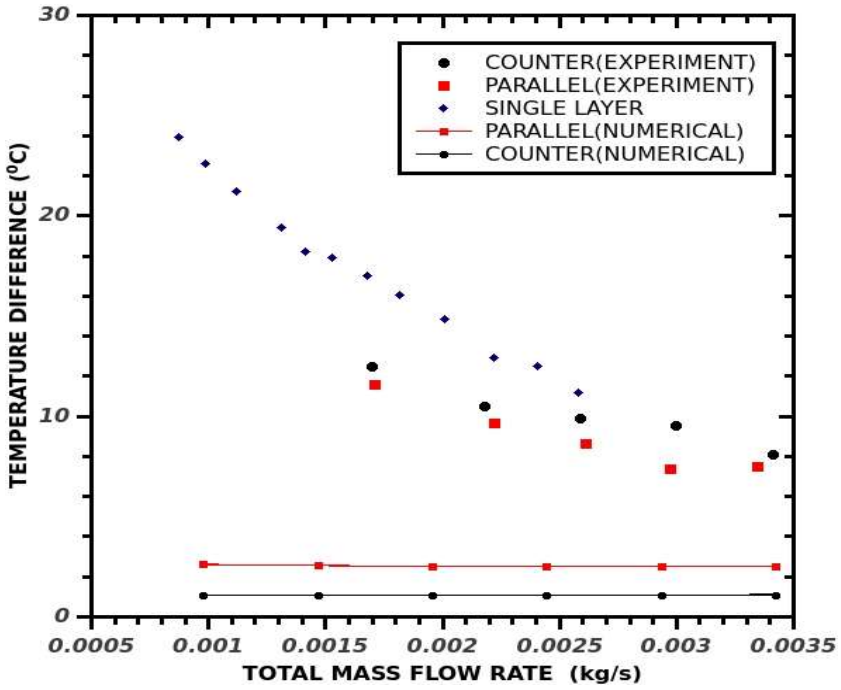

Fig 4.33 Wall Temperature Difference with the Total Mass Flow Rate

From Fig.4.33, it is clear that the experimental value of fluid wall temperature difference is nearly the same for the parallel flow arrangement and counter flow arrangement for all mass flow rates. Also, the double-layer flow configurations have more temperature uniformity than the single-layer flow configurations. This indicates that even though the average temperature of the heat sink base remains the same for CF and PF, temperature uniformity is higher for the parallel flow configuration. This temperature is below the operational temperature of the electronic devices.

The temperature uniformity across the chip is affected by the flow rate combinations through the channel. The parallel flow has attained more uniform temperature uniformity than the counterflow configurations.

4.5 THE FLOW MAL DISTRIBUTION STUDY

The maldistribution study is conducted to analyze the flow rate variation through the lower layer microchannel and upper layer microchannel. The numerical model used for the flow maldistribution with the schematic of the flow loop is shown in Fig.3.2.

4.5.1 MESH DEPENDENCE STUDY

The grid independence study is carried out for an inlet velocity of 3.14 m/s with four different mesh sizes as shown in Table 4.6. For the fine meshing, four different meshes analyzed with a different number of nodes.

Table 4.6 Mesh dependence study

Mesh quality	Number of nodes	Outlet temperature		Deviation (%)	
		lower (^{0}c)	upper (^{0}c)	lower	upper
Very coarse	1342596	44.74	31.78	-	-
Coarse	1754570	33.09	31.49	26.039	0.912
Fine	**1826247**	**32.02**	**31.46**	**3.233**	**0.095**
Superfine	2048573	32.01	31.43	0.0315	0.095

Mesh size corresponding to fine mesh is employed in this study because of the outlet temperature at the lower layer microchannel and the upper microchannel between third and fourth mesh sizes are less than 3.2 %. The problems are solved with the minimum reduction in normalized residuals for each variable at less than 1.0×10^{-4}.

From the Fig.4.34, it is clear that the lower channel outlet temperature variation with the number of nodes and the measurement corresponds to the number of nodes 1826247 is taken as the future study. The fine mesh size is employed in the final simulation since less computational time is needed.

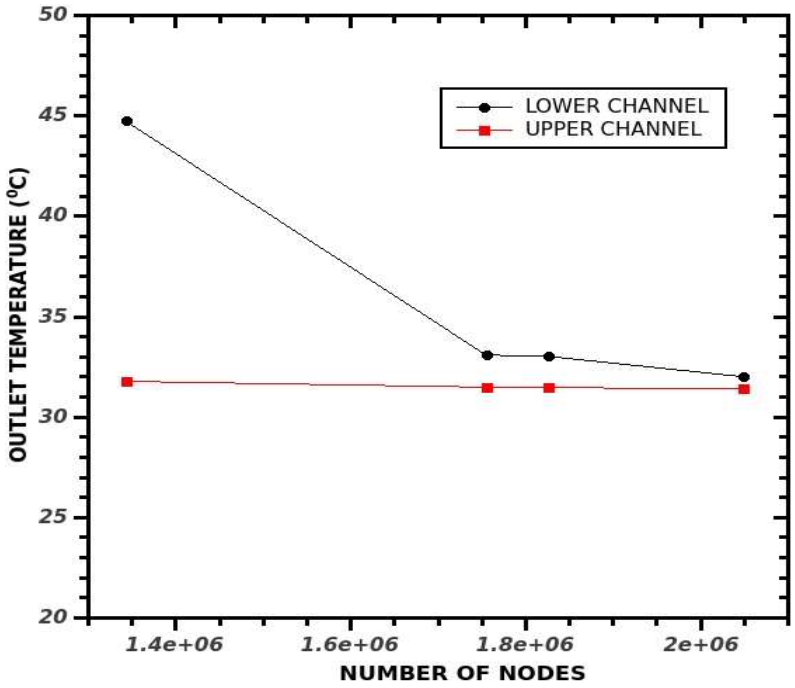

Fig 4.34 Outlet Temperature Vs Number of Nodes

The flow maldistribution study is conducted in two different flow rates with the parallel flow and counterflow configurations.

4.5.2 TURBULENT FLOW CONDITION

The maldistribution study is conducted in turbulent flow condition for counter flow and laminar flow configuration. For that, the inlet velocity of each channel in the lower layer and upper layer are noted. The mass flow rate through each microchannel is calculated.

4.5.2.1 COUNTER FLOW

Table 4.7 shows the percentage change in the mass flow rate of each channel in the lower layer and upper layer for the counter-flow with turbulent flow condition. The percentage change of the mass flow rate through each channel is plotted in Fig.4.35.

Table 4.7 % Mass Flow Rate through the Lower and Upper Channel

Channel	Velocity UMC m/s	Velocity LMC m/s	ṁ LMC kg/s	% Flow rate in Each Channel	ṁ UMC kg/s	% Deviation
1	6.33	6.27	0.00241	19.90	0.00243	19.30
2	6.44	6.302	0.00242	20.00	0.00247	19.60
3	7.32	6.33	0.00243	20.10	0.00281	22.30
4	6.44	6.3	0.00242	20.00	0.00247	19.60
5	6.33	6.28	0.00241	19.90	0.00243	19.30
			0.01209		0.01261	

Figure 4.35 depicts that the middle channel in both the lower layer and the upper layer has a small increase in the mass flow rate compared with other channels. Nearly the same mass flow rate flows through each channel in the lower layer.

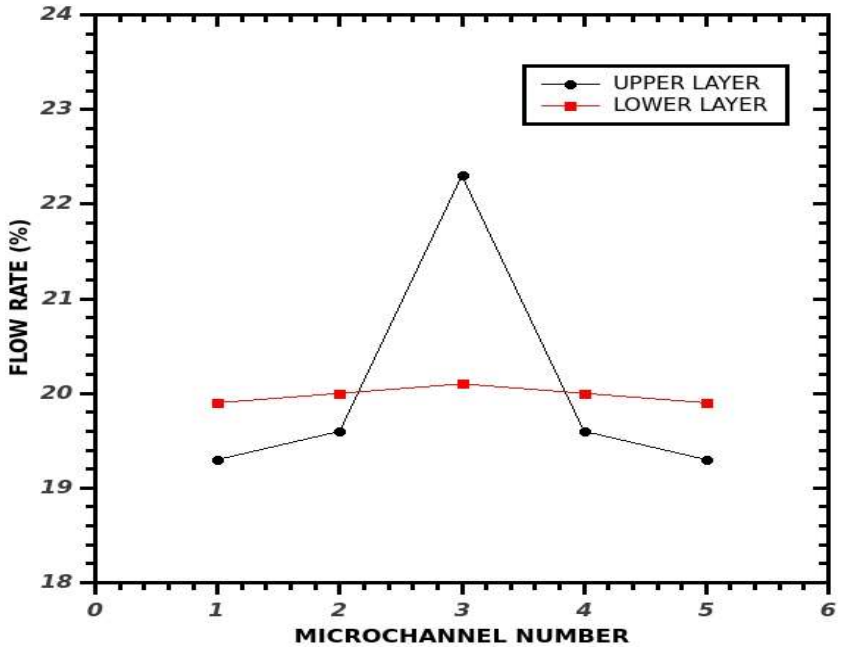

Fig 4.35 Flow Rate Vs Microchannel Number (CF)

At higher mass flow rate the maldistribution in the upper layer channel is significant. The size of the plenum in the lower layer and the upper layer are different. This may be an effect for the maldistribution in the channels.

4.5.2.2 PARALLEL FLOW

Table 4.8 shows the percentage deviation of the mass flow rate of the lower channel and upper channel for the parallel flow with turbulent flow condition.

Table 4.8 % Mass Flow Rate through the Lower and Upper Channel

Channel	Velocity UMC m/s	Velocity LMC m/s	ṁ LMC kg/s	% Flow rate in Each Channel	ṁ UMC kg/s	% Deviation
1	5.22	6.34	0.00243	20.00	0.002000	18.40
2	5.82	6.35	0.00244	20.00	0.002230	20.06
3	6.11	6.38	0.00245	20.10	0.002350	20.16
4	5.86	6.35	0.00244	20.00	0.002250	20.07
5	5.3	6.34	0.00243	20.00	0.002040	18.70
			0.0122		0.01087	

The percentage deviation of the mass flow rate through each channel is plotted in Fig.4.36.

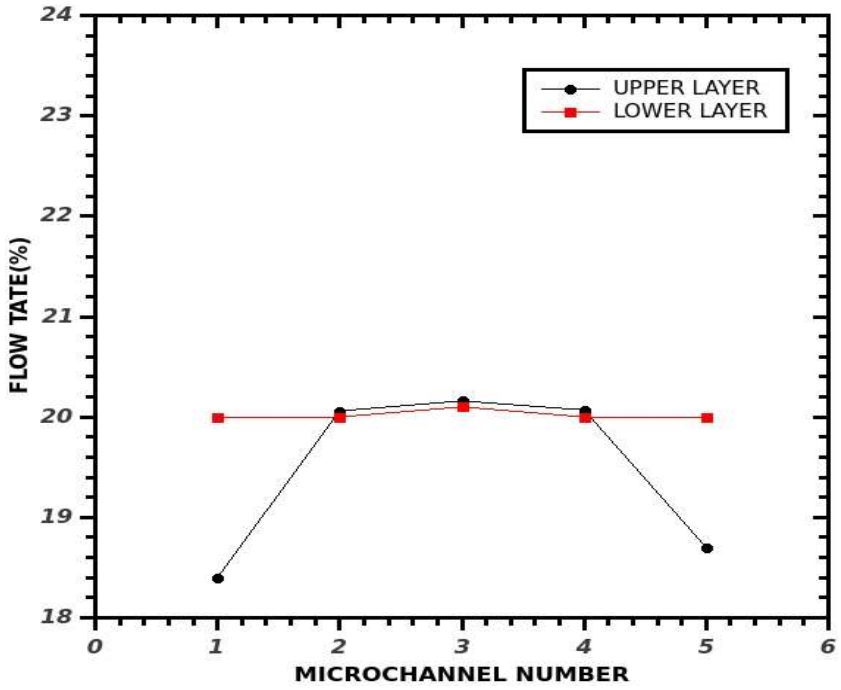

Fig 4.36 Flow Rate Vs Microchannel Number (PF)

The Fig.4.36 depicts the end channels in the upper layer has a small decrease in the mass flow rate compared with the middle channel. Nearly the same mass flow rate flows through each channel in the lower layer.

4.5.3 LAMINAR FLOW CONDITION

The maldistribution study is conducted with a laminar flow condition for counter flow and parallel flow configurations. The mass flow rate through each microchannel of the lower layer and the upper layer is calculated.

4.5.3.1 COUNTER FLOW

Table 4.9 shows the percentage deviation of the mass flow rate of the lower channel and upper channel for the counter-flow with low mass flow rate. The percentage deviation of the mass flow rate through each channel is plotted in Fig.4.37.

Table 4.9 % Mass Flow Rate through the Lower and Upper Channel

Channel	Velocity UMC m/s	Velocity LMC m/s	ṁ LMC kg/s	% Flow rate in Each Channel	ṁ UMC kg/s	% Deviation
1	0.7188	0.6493	0.000249	20.01	0.000276019	19.83
2	0.7274	0.6536	0.000251	20.14	0.000279322	20.07
3	0.7303	0.6464	0.000248	19.916	0.000280435	20.14
4	0.7246	0.646	0.000248	19.91	0.000278246	19.99
5	0.7245	0.6503	0.00025	20.04	0.000278208	19.98
			0.001246		0.00139223	

The negligible deviation is noted in the mass flow rate through each channel of the lower layer and upper layer.

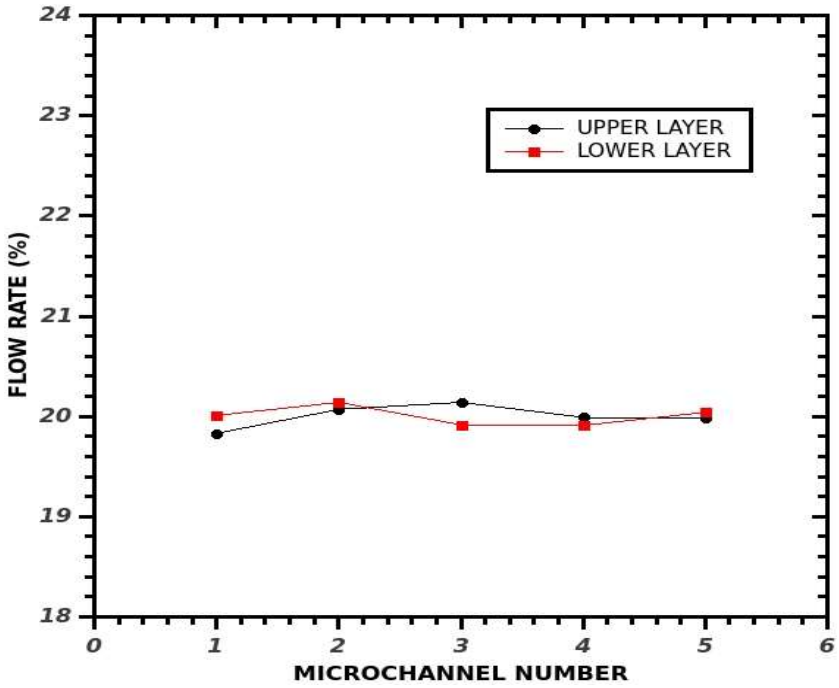

Fig 4.37 Flow Rate Vs Microchannel Number (CF)

At lower mass flow rate the maldistribution in the upper layer and lower layer channel is insignificant. The size of the plenum in the lower layer and the upper layer are different. This may be an effect for the maldistribution in the channels.

4.5.3.2 PARALLEL FLOW

Table 4.10 % Mass Flow Rate through the Lower and Upper Channel

Channel	Velocity UMC m/s	Velocity LMC m/s	ṁ LMC kg/s	% Flow rate in Each Channel	ṁ UMC kg/s	% Deviation
1	0.7168	0.6659	0.000255706	20.01	0.000275251	19.95
2	0.718	0.67029	0.000257391	20.14	0.000275712	19.98
3	0.7182	0.6628	0.000254515	19.91	0.000275789	19.99
4	0.7191	0.6624	0.000254362	19.90	0.000276134	20.01
5	0.721	0.6669	0.00025609	20.04	0.000276864	20.07
			0.001278063		0.00137975	

Table 4.10 shows the percentage deviation of the mass flow rate of the lower channel and upper channel for the counter-flow with low mass flow rate. The percentage deviation of the mass flow rate through each channel is plotted in Fig.4.38.

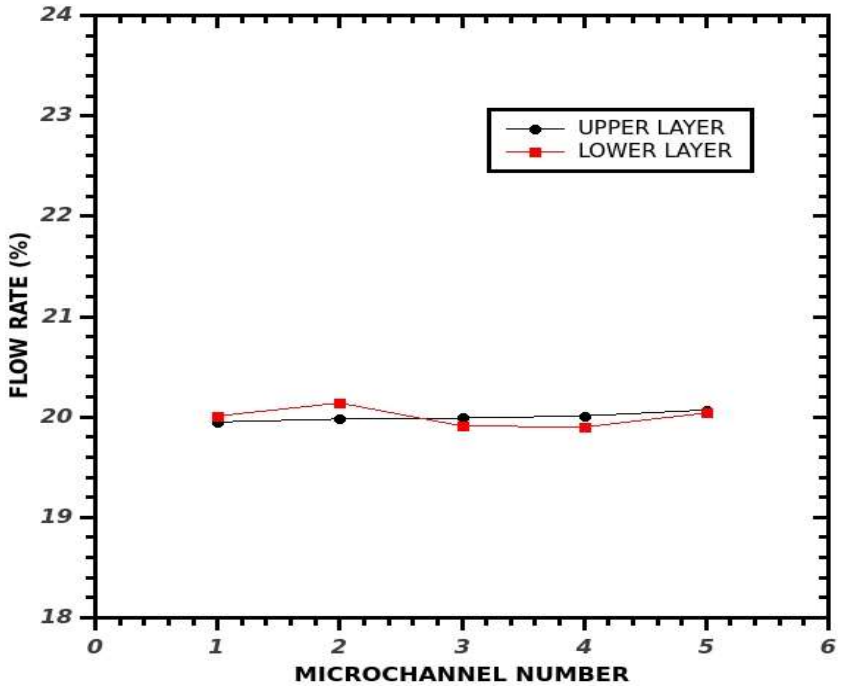

Fig 4.38 Flow Rate Vs Microchannel Number (PF)

Figure 4.38 depicts the percentage change in the mass flow rate of each channel in the lower layer and upper layer. A negligible deviation in mass flow rate through each channel has occurred in the lower and upper layers.

The significance of graphs 4.35, 4.36, 4.37 and 4.38 are to analyze the flow through each microchannel (lower layer and upper layer) in the turbulent and laminar flow conditions.

4.6 EXPERIMENTS WITH GRAVITY FEED SYSTEM

The experiment is conducted in a different continuous flow arrangement through the lower and upper layer channels. The low mass flow rate is attained with the application of the gravity feed system.

4.6.1 DIFFERENT SERIES FLOW CONFIGURATIONS

The experiment is conducted in four different flow configurations as shown in Fig.4.39. The following are the flow configurations. 1. Series flow Lower inlet Counter (LIC) 2. Series flow Lower inlet Parallel (LIP) 3. Series flow Upper inlet Counter (UIC) and 4. Series flow Upper inlet Parallel (UIP). The heat input to the heat sink is set as 100W. The mass flow rate of the fluid is controlled by varying the vertical position of the float chamber.

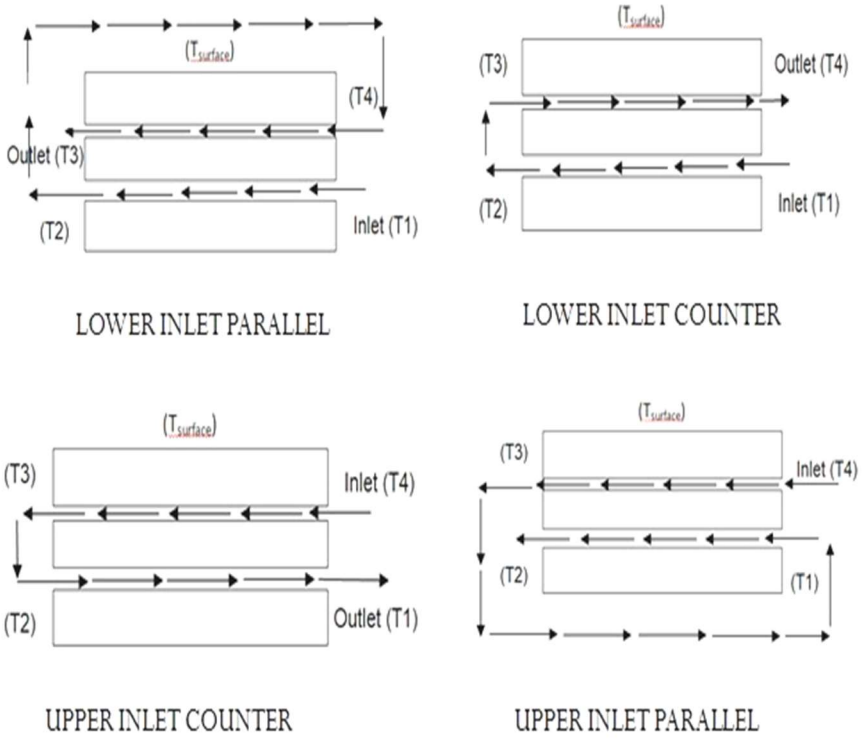

Fig 4.39 Schematic of Different Series Flow Configurations (EXPERIMENT)

The variation of the pressure drop with mass flow rate is shown in Fig.4.40. As expected the pressure drop is increased with the mass flow rate in all four flow configurations. The upper inlet parallel flow configurations have less pressure drop as compared to the other three.

The pressure drop per unit length with the mass flow rate is plotted in Fig.4.41. The pressure drop per unit length increases with the mass flow rate. For all four configurations, the pressure drop per unit length is within the uncertainty limit.

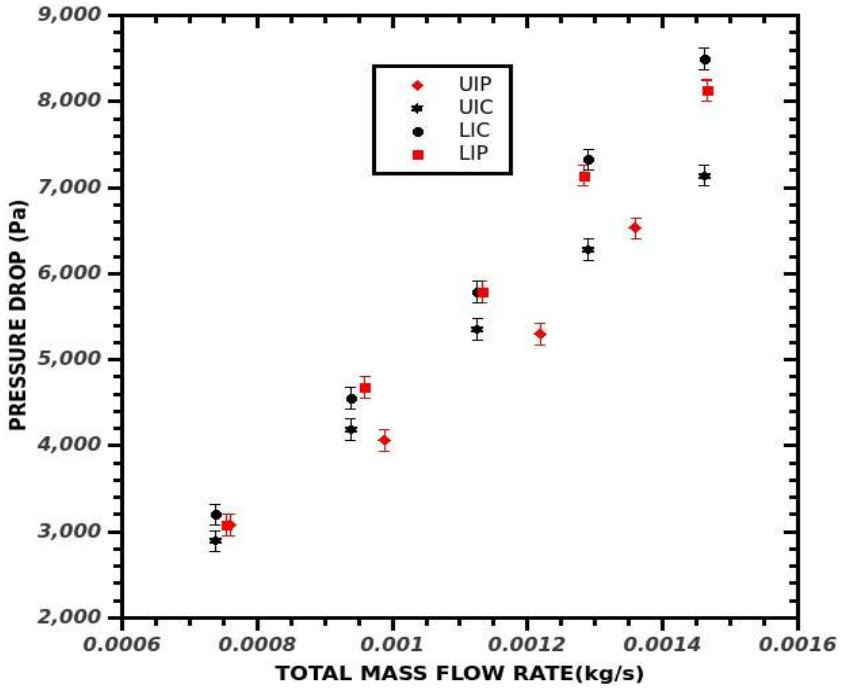

Fig 4.40 Pressure Drop with the Total Mass Flow Rate

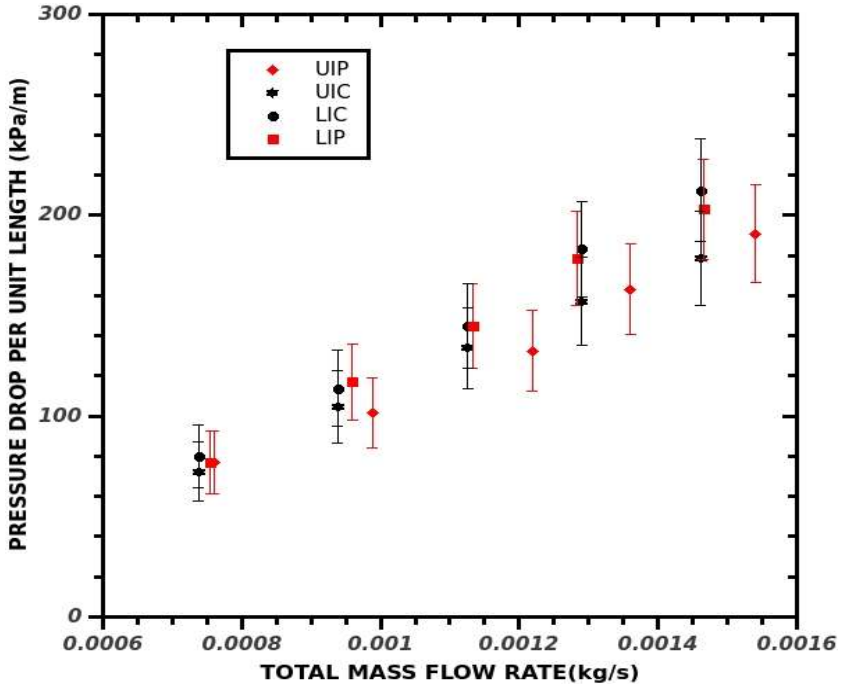

Fig 4.41 Pressure Drop per Unit Length with the Total Mass Flow Rate

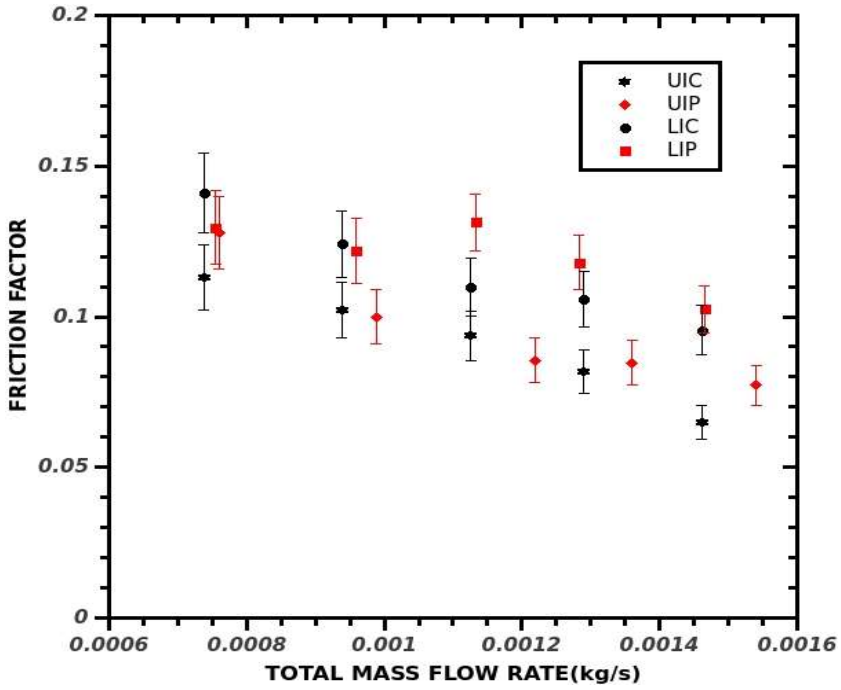

Fig 4.42 Friction Factor with the Total Mass Flow Rate

The variation of the friction factor with mass flow rate is shown in Fig.4.42. As expected the friction factor is decreases with the mass flow rate in all four flow configurations.

The friction factor is very less in between 0.01 and 0.013 for all configurations. The upper inlet parallel and upper inlet counter flow configurations have less friction factor as compared to the lower inlet parallel and lower inlet counterflow configurations.

The variation of the pumping power with the mass flow rate is plotted in Fig.4.43. The pumping power required increases with the mass flow rate. The maximum pumping power required for the higher mass flow rate is less than 0.012 W.

The pumping power for LIP, LIC, UIC and UIP flow arrangements are found to be similar as expected. The upper inlet parallel flow configuration has required minimum pumping power compared with other flow configurations. The higher mass flow rate introduces more prominent entrance effects into the liquid flow. Due to this reason, the pressure drop increases faster at high mass flow rates. The same trend is seen in the pumping power at high mass flow rates.

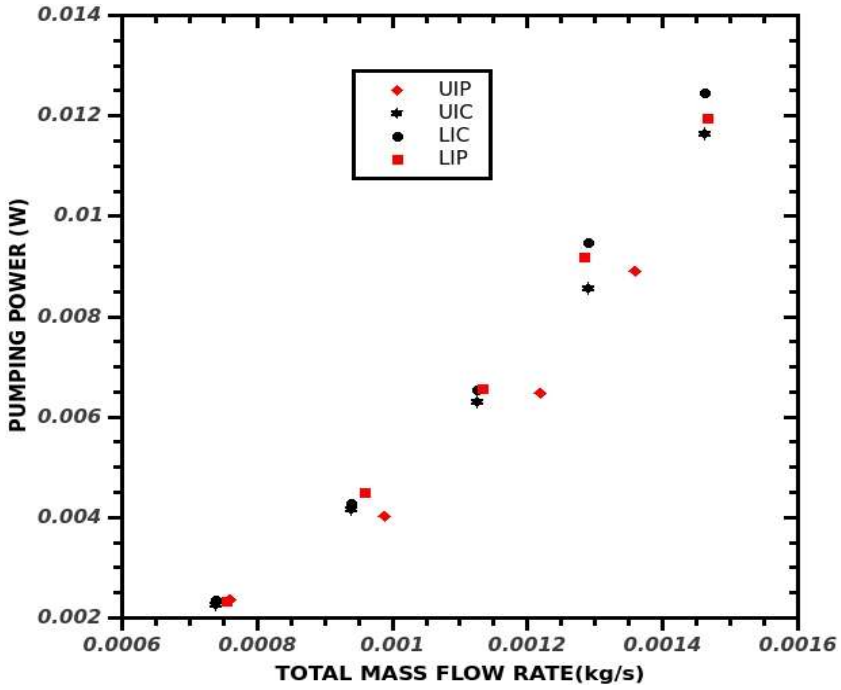

Fig 4.43 Pumping power with the Total Mass Flow Rate

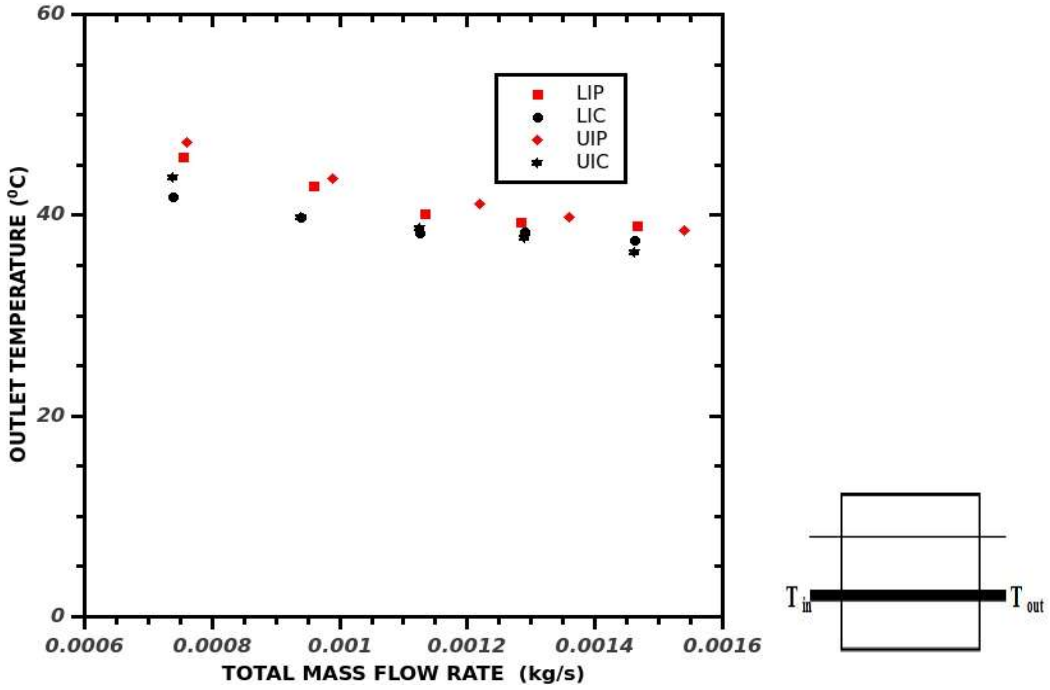

Fig 4.44 Outlet Temperature with the Total Mass Flow Rate

The variations of outlet temperature with the mass flow rate in all four configurations are shown in Fig.4.44. The counter flow configuration has less fluid outlet temperature than

the parallel flow configurations. The working fluid absorbs the heat corresponds to this temperature.

The variation of the fluid wall average temperature with the mass flow rate is plotted for LIP, LIC, UIC and UIP flow arrangements are shown in Fig.4.45. The wall average temperature decreases with the mass flow rate for the constant inlet temperature and the input power.

The fluid wall average temperature values range from 47 ^{0}C to 55 ^{0}C in the flow ranges to 0.0007 to 0.0011 kg/s. An 8 ^{0}C deviation is noted at a low mass flow rate and, while increasing the mass flow rate to 0.0011 kg/s the deviation is less than 3 ^{0}C. This is indicated that the increase in the mass flow rate to another maximum level does not affect the fluid wall average temperature. This implies that while increasing the mass flow rate a steady temperature is obtained.

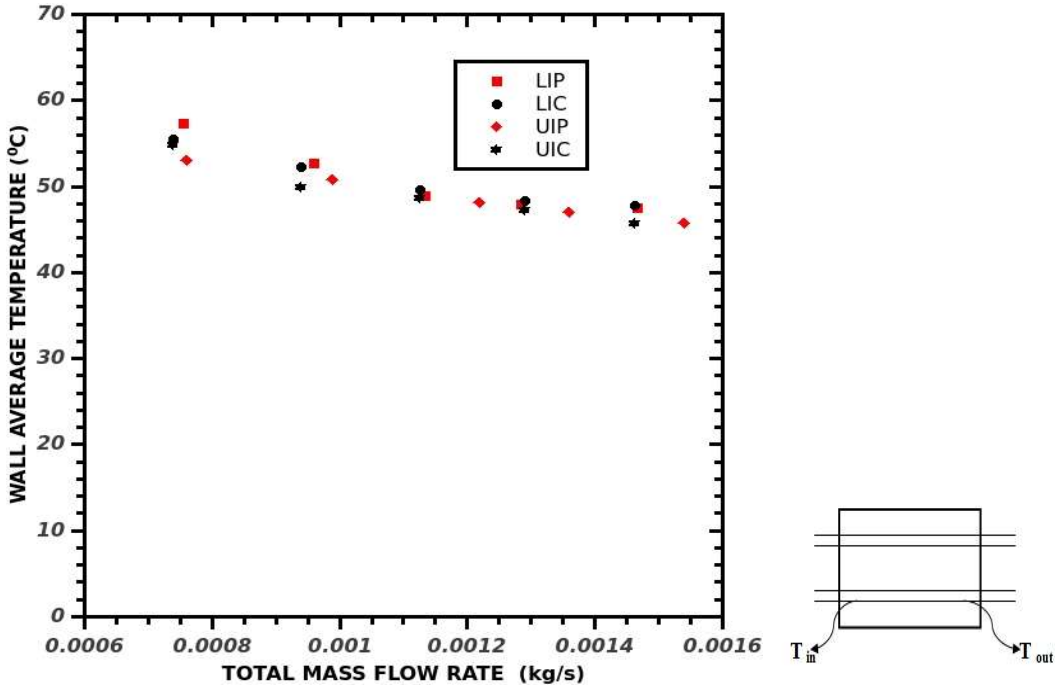

Fig 4.45 Wall Average Temperature with the Total Mass Flow Rate

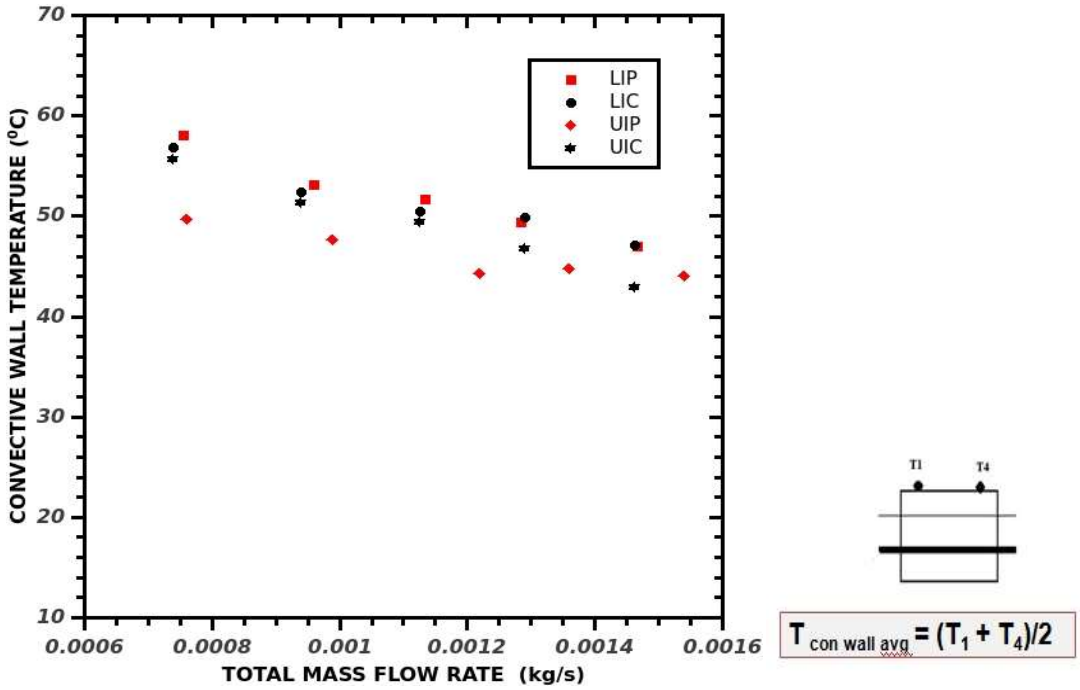

Fig 4.46 Convective Wall Temperature with the Total Mass Flow Rate

The variation of the increase in convective top wall surface temperature with the total mass flow rate is plotted in Fig.4.46. For all configurations, the convective wall surface temperature decreases with the mass flow rate similarly.

At low mass flow rate, the increase of convective wall surface temperature is nearly 28 ^{0}C and gradually decreases with the mass flow rate and at the higher mass flow rate, it is nearly 13 ^{0}C. This is less than the actual operating temperature (60 ^{0}C) of the electronic equipment. As the flow rate increases the minimum temperature and maximum temperature decreases in LIP, LIC, UIC and UIP flow arrangements. These excess temperatures circulate inside the cabin of the electronic equipment.

Figure 4.47 shows the variation of the heat sink base temperature with total mass flow rate for LIP, LIC, UIC and UIP flow arrangements. The heat sink base temperature decreases with the mass flow rate in all four configurations. The maximum temperature obtained at the base of the heat sink in the double-layer design is found to be below 68 ^{0}C. The UIC flow configuration has less heat sink temperature as compared with other there configurations.

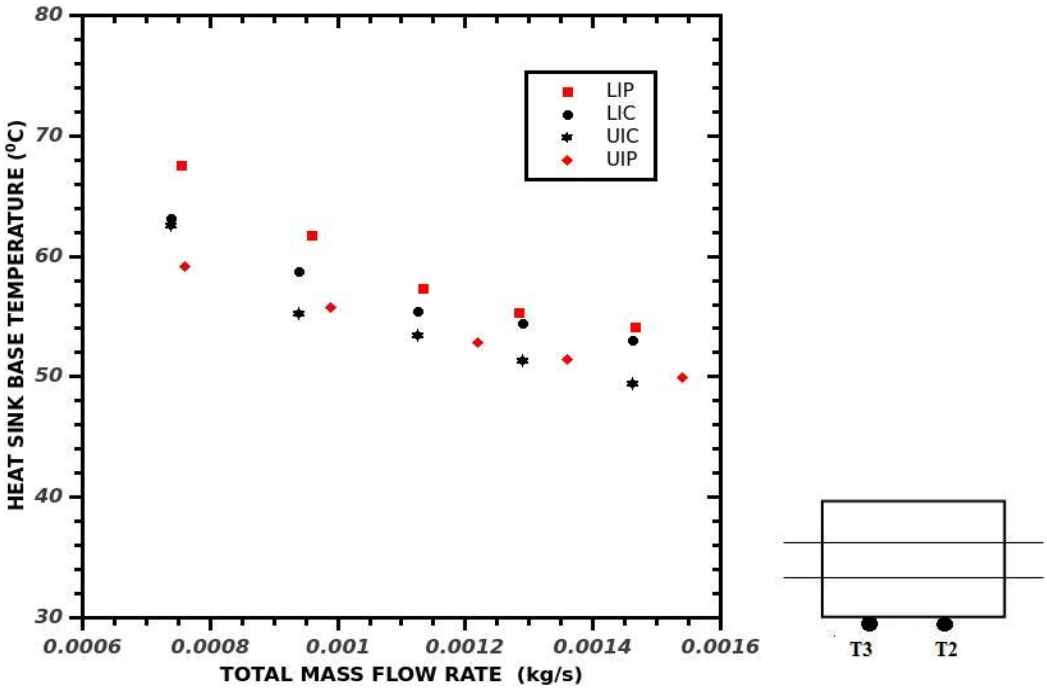

Fig 4.47 Heat Sink Base Temperature with the Total Mass Flow Rate

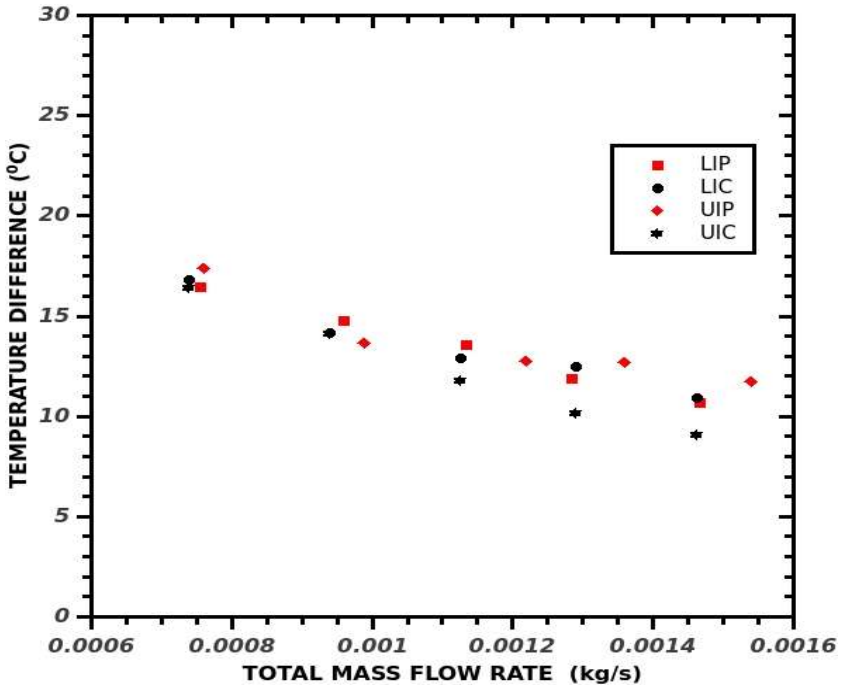

Fig 4.48 Wall Temperature Difference with the Total Mass Flow Rate

Figure 4.48 shows the variation of the fluid wall temperature difference with total mass flow rate for LIP, LIC, UIC and UIP flow arrangements. The fluid wall temperature difference is decreases with the mass flow rate in all four configurations. The maximum

temperature difference is obtained for low mass flow rate. This denotes the temperature uniformity at the base of the heat sink. The UIC flow configuration has less heat sink temperature as compared with other there configurations.

The variation of heat sink base temperature and pressure drop with mass flow rate for LIP, LIC, UIC and UIP flow arrangements are shown in Fig.4.49 to Fig.4.52.

The mass flow rate for a constant heat sink temperature of 55 ^{0}C is marked in each graph.

The mass flow rate of the fluid to maintain the 55^{0}C temperature is 0.00103 kg/s (UIC), 0.00105 kg/s (UIP), 0.0012 kg/s (LIC), 0.00132 kg/s (LIP) with corresponding pressure drop of 4.3 k Pa, 4.4 k Pa, 6.5 k Pa, and 7.4 k Pa respectively.

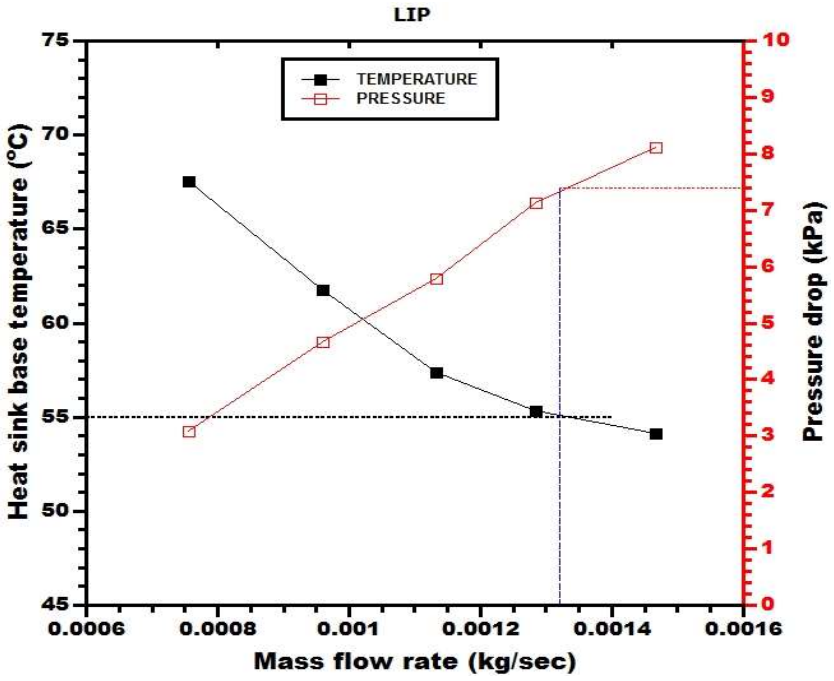

Fig 4.49 Variation of Heat Sink Base Temperature and Pressure Drop with the Mass Flow Rate (LIP)

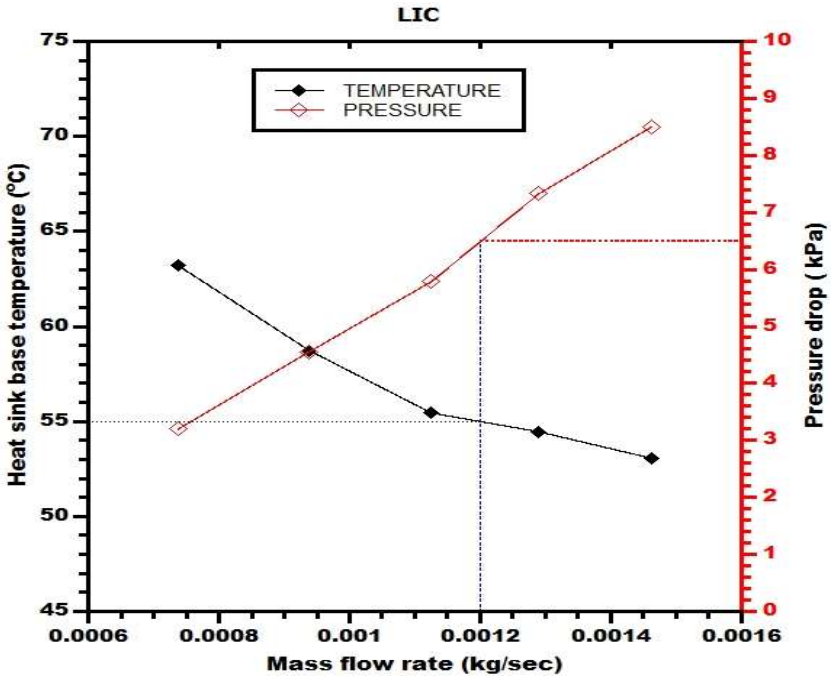

Fig 4.50 Variation of Heat Sink Base Temperature and Pressure Drop with the Mass Flow Rate (LIC)

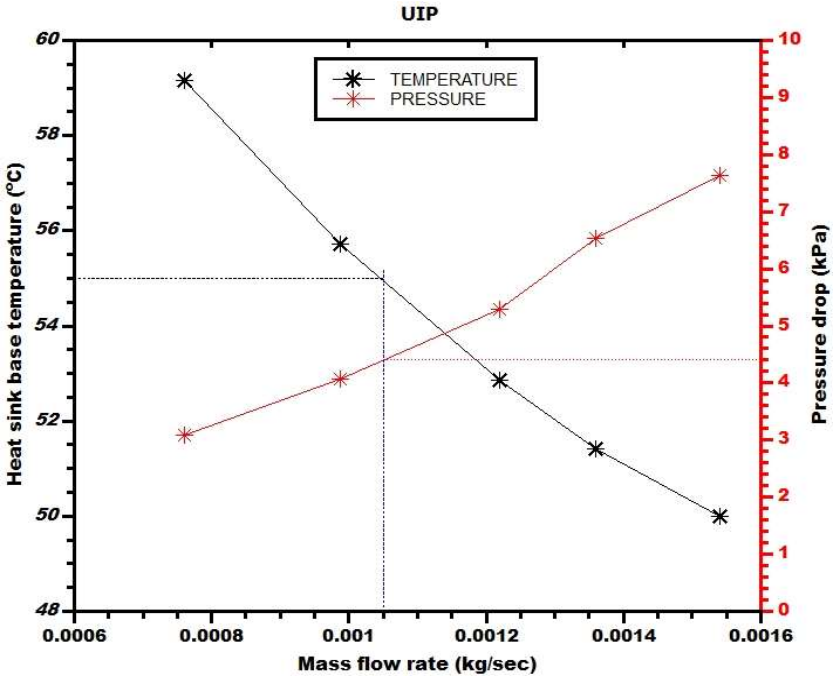

Fig 4.51 Variation of Heat Sink Base Temperature and Pressure Drop with the Mass Flow Rate (UIP)

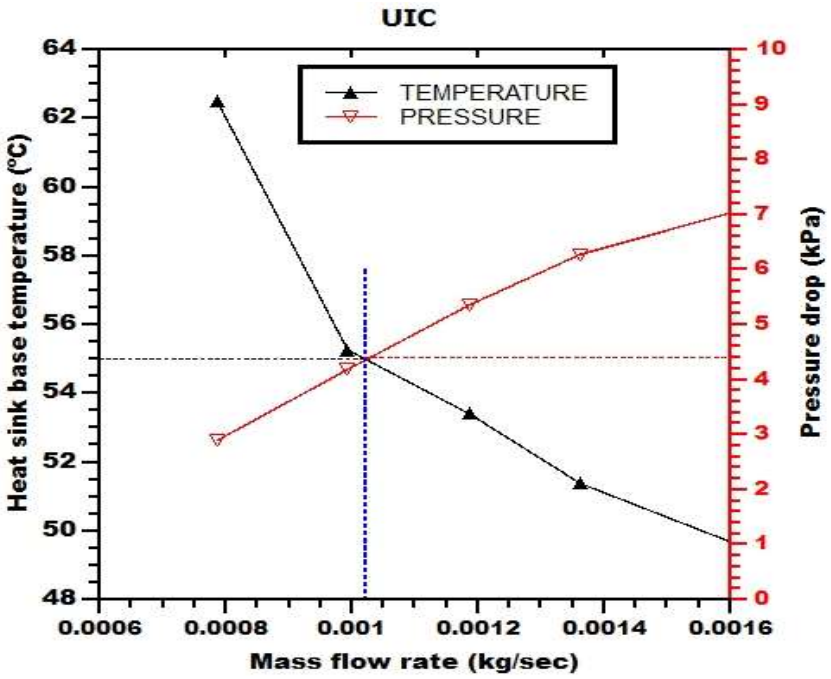

Fig 4.52 Variation of Heat Sink Base Temperature and Pressure Drop with the Mass Flow Rate (UIC)

This implies that the UIC flow configuration has required less mass flow rate to maintain this temperature with less pressure drop. Therefore the UIC configuration has the best one from the above four configurations for these heat sink base temperature and pressure drop.

4.7 SUMMARY

The flow and thermal performances of the double-layer circular microchannel heat sink were investigated numerically and experimentally. The investigation is conducted in single layer flow, parallel flow and counterflow configurations. The flow maldistribution study is conducted in parallel flow and counter flow configurations for turbulent and laminar flow condition. The pressure drop and thermal performance of the different series flow configurations like LIP, LIC, UIC and UIP are conducted.

CHAPTER 5
THE SUMMARY AND CONCLUSIONS

5.1 INTRODUCTION

This research was mainly focused to improve the cooling technique of the electronic equipment. For that, a new idea of the double layer circular microchannel heat sink is designed. This research aims to minimize the base temperature of the miniaturized chips. The novelty of the present study is the numerical and experimental analyses of the flow and thermal performances of the double layer stacked circular microchannel heat sink. With the help of the liquid cooling technique, the temperature at the base of the heat sink was reduced to an applicable range. A wide range of mass flow rate is analyzed to the effect of heat transfer and flow conditions.

The study was conducted with two different analysis namely (1) Numerical analysis and (2) Experimental analysis. The numerical analysis was conducted in two different flow conditions of laminar and turbulent. The numerical simulation of the double layer circular microchannel heat sink (DLCMC-HS) was modelled with the commercial CFD tool Ansys Fluent. The experimental analysis was done with the help of fabricating an experimental facility in our laboratory. The experiments were done with the help of two experiment setup (1) with the help of the peristaltic pump and (2) with the help of a gravity head application. The detailed summary of the results and findings are described in this chapter

5.2 FINDINGS FROM THE STUDY

The following are the major findings of the research work.

1. Numerically investigated the pressure drop, friction factor and heat transfer performance of a double layer circular microchannel heat sink with inlet velocity range from 0.4 m/s to 6.5 m/s with constant heat input.

- The pressure drop per unit length, pumping power and friction factor required was the same for CF and PF configurations.

- The outlet and convective wall temperature in the CF and PF configurations were the same and decrease with mass flow rate.

- The cabin temperature is under the range of 60^0 C.

- For the laminar condition, the CF has minimum thermal stress and heat sink base temperature.

- For the turbulent condition, the PF has minimum thermal stress and heat sink base temperature.

2. Analyzed the effect of flow maldistribution of a microchannel in both layers of the double layer circular microchannel heat sink in detail.

2.1 TURBULENT FLOW CONDITION

- At higher mass flow rate the maldistribution in the upper layer channel is significant.

- In CF analysis the lower layer microchannels have occurred equal flow distribution, while in the upper layer; the centre microchannel has a higher flow rate than the end microchannels.

- In PF analysis the lower layer microchannels also have occurred equal flow distribution. But in the upper layer, both end channels have less flow rate than the centre microchannel.

2.2 LAMINAR FLOW CONDITION

- Both in the CF and PF analysis, upper layer microchannels and lower layer microchannels have no effect of flow maldistribution

3. Experimentally investigated the pressure drop, friction factor and heat transfer performance of a double layer circular microchannel heat sink using the peristaltic pump with Single Layer flow (SL), parallel flow (PF), counterflow (CF) configuration. The mass flow rate of the deionized water ranges $1.5x10^{-3}$ kg/s to $14x10^{-3}$ kg/s with a constant heat input of 80W.

- The pressure drop per unit length, pumping power required was increased with the mass flow rate and friction factor is decreased with the mass flow rate.

- The pressure drop and pumping power required in single layer flow analysis is more than double layer flow with the same mass flow rate.

- The outlet and convective wall temperature decrease with the mass flow rate in all configurations.

- The CF has minimum thermal stress and heat sink base temperature.

4. Experimentally investigated the pressure drop, friction factor and heat transfer performance of a double layer circular microchannel heat sink using gravity feed system with Single Layer flow (SL), Parallel flow (PF), Counterflow (CF) configuration. The mass flow rate of the deionized water ranges $0.5x10^{-3}$ kg/s to $1.5x10^{-3}$ kg/s with a constant heat input of 100 W.

- The pressure drop per unit length, pumping power required was increased with the mass flow rate and friction factor is decreased with the mass flow rate.

- The pressure drop and pumping power required in single layer flow analysis is more than double layer flow with the same mass flow rate.

- The outlet and convective wall temperatures decrease with the mass flow rate for all configurations.

- The PF has minimum thermal stress and heat sink base temperature.

5. Experimented with copper-based circular microchannel with Lower Inlet Parallel series flow (LIP), Lower Inlet Counter series flow (LIC), Upper Inlet Parallel series flow (UIP), Upper Inlet Counter series flow (UIC) configuration with a mass flow rate of the deionized water ranges $0.5x10^{-3}$ kg/s to $1.58x10^{-3}$ kg/s to investigate the flow and thermal behaviour (using gravity feed system).

- The pressure drop per unit length required for all configurations was the same irrespective of heat input.

- The pressure drop increases with the mass flow rate in all configurations

- The friction factor is decreased with the mass flow rate. Friction factors were laid fewer than 10% error band.

- The maximum pumping power required among all configurations is 0.014W.

- UIC configuration required 29% less pressure drop compared to LIC configuration to attain 55^0C.

- UIC configuration required 39.5% less pressure drop compared to LIP configuration to attain 55^0C.

- The heat sink temperature for all configurations lies below 75^0C. Therefore all types of configurations are capable of avoiding the failure of an electronic chip.

- The heat sink base temperature was found the minimum for UIP and UIC configurations, and it is almost equal for UIP and UIC configurations.

- The temperature uniformity for UIC configuration is higher than UIP configuration and excess temperature found less for UIP configuration.

- By considering the overall performance UIC configuration is the best configuration among all.

5.3 SCOPE FOR FUTURE WORK

Certain studies are conducted with single layer microchannel as well as double-layer microchannel with different geometric configurations. The particular study aims to evaluate the flow and thermal behaviour of double-layer circular microchannel heat sink in detail**.** As future work, analysis of flow and heat transfer performance with crossflow arrangement of the microchannel layer can be done. Also, the study may be done with the channels arranged at an offset position.

5.4 SUMMARY

The present study delivered the new insight for the liquid cooling system applicable in the electronic applications. The novelty of this work is to analyze the flow and thermal performances of the double layer circular microchannel heat sink. This study includes the experimental work and the results are validated with numerical analysis. The numerical investigation was conducted in parallel flow and counterflow configurations. The flow maldistribution study was also conducted in parallel flow and counter flow configurations for laminar condition and turbulent condition. The experiments were conducted with the application of a pump and with the application of the gravity feed system. The flow and thermal performance of the different series flow configurations like Parallel flow (PF), Counterflow (CF), Lower Inlet Parallel series flow (LIP), Lower Inlet Counter series flow (LIC), Upper Inlet Parallel series flow (UIP), Upper Inlet Counter series flow (UIC) configurations are explained in detail.

REFERENCES

1. Adams T. M., S. I. Abddel-Khalik, S. M. Jeter and Z. H. Qureshi (1998) "An Experimental Investigation of single phase forced convection in Microchannels", *International Journal of Heat and Mass Transfer Vol. 41, P 851–857.*

2. Ahmed Hamdi E., M. I. Ahmed, (2016) "Experimental Investigation for sequential triangular double layered microchannel heat sink with nano fluids", *International Journal of Heat and Mass Transfer, Vol. 77 P104 - 115.*

3. Anbumeenakshy M. R and Thansekhar. (2016) "Experimental investigation of header shape and inlet configuration on flow maldistribution in micro channels" *Experimental Thermal and Fluid Science. Vol.75 P 156 - 161*

4. Ansys A.F.16 User's Guide, Ansys Inc.,2016

5. Appasaheb Rahul, B. N. Bhasme, R. S. Maurya (2016) "A numerical investigation of fluid flow maldistribution in inlet header configuration of plate fin heat exchanger" *Energy Procedia. Vol.90 P 267 - 275.*

6. Asadi M., Gongnan Xie, Bengt Sunden (2014) "A review of heat transfer and pressure drop characteristics of single and two-phase microchannels", *International Journal of Heat and Mass Transfer Vol.79, P 34 - 53.*

7. Attalla M., Hussein M, Maghrabie, and E. Specht (2016) "An experimental investigation on fluid flow and heat transfer of rough mini channel with rectangular cross section" *Experimental Thermal and Fluid Science, Vol. 75, P 199 - 210.*

8. Bucci. A, G. P Celata, M Cumo, E. Serra, G. Zummo, (2003) "Water single phase fluid flow and heat transfer in capillary tubes", in; *International Conference on Micro channels and Mini Channels*, *Paper 1037, ASME, Vol. 1, P 319 - 326.*

9. Chen Yu-Tang, Shung-Wen Kang, (2004) "Experimental Investigation of Fluid Flow and Heat Transfer in Microchannels", *Tam kang Journal of Science and Engineering Vol.7 No.1, P 11–16.*

10. Dai Baomin, Minxia Li, Chaobin Dang, Yital Ma, Qi Chen (2014) “Investigation on convective heat transfer characteristics of single phase liquid flow in multi port micro channel tubes”, *International Journal in Heat and Mass Transfer Vol.70, P 114 - 118.*

11. Danish Ansari and Kwang-Yong Kim, (2017). “Performance analysis of double layer micro channel under non-uniform heating conditions with random hot spots”, in *Micromachines, Vol. 54, P 1 - 20.*

12. Dario E. R., L. Tadrist, J. L. G. Oliveira, J. C. Passos. (2015) "Measuring maldistribution of two phase flows in multi parallel microchannels", *Applied Thermal Engineering, Vol. 91, P 924 - 937.*

13. Dede Ercan M. and Yan Liu, (2013) “Experimental and Numerical investigation of a multipass branching microchannel heat sink”, *Applied Thermal Engineering, Vol. 55, 51 - 60.*

14. Deng Daxiang, Guang, Weixum Zhang, Peng Wang and Ting Fu. (2018). “Numerical Study of Double –Layered Microchannel Heat Sinks with Different Cross-Sectional Shapes”, in *Entropy, Vol. 21, P 12 - 16.*

15. Esmaili Qadir, Ali Akbar Ranjbar, Soheil Porkhial (2018) “Experimental analysis of heat transfer in ribbed microchannel”, *International Journal of Thermal Science. Vol. 130, P140 - 147.*

16. Frank P. Incropera. David P. Dewitt, Theodore L. Bergman, and Adrienne S. Lavine (2014) “*Principles of Heat and Mass Transfer*” 7th edition, John Wiley & Sons, Inc. Hoboken. New Jersey.

17. Goldstein R. J, W. E. Ibele, S. V. Patankar, .W. Simon, T. H. Kuehn, P. J. Strykowski, K. K. Tamma, J. V. R. Heberlein, J. H. Davidson, J. Bischof, F. A. Kulacki, U. Kortshagen, S. Garrick, V. Srinivasn, K. Ghosh, R. Mittal (2010) “A review of 2004 literature”, *International Journal of Heat and Mass Transfer, Vol.53, P 4343 - 4396.*

18. Hetsroni G., A. Mosyak, E. Pogrebnyak, L. P. Yarin (2005) “Heat transfer in micro channels: Comparison of experiments with theory and numerical results”, *International Journal of Heat and Mass Transfer Vol.48, P 5580 – 5601.*

19. Hung Tu-Chieh and W. M. Yan Wei Ping Li, (2012) “Analysis of heat transfer characteristics of double layered microchannel heat sinks”, *International Journal of Heat and Mass Transfer. Vol. 55, P 3090 - 3099.*

20. Hung Tu-Chieh and W. M. Yan, (2012) “Optimal Design of Geometric Parameters of Double layered Microchannel Heat Sinks”, *International Journal of Heat and Mass Transfer. Vol. 55, P 3262 - 3272.*

21. Ji Zhang, Yanhua Diao, Yaohua Zhao, Yanni Zhang (2017) “An experimental investigation of heat transfer enhancement in mini channel; Combination of nano fluid and micro fin structure techniques” *Experimental Thermal and Fluid Science, Vol. 81, P 21 - 32.*

22. Jing Dalei and He Lei. (2018). “Thermal Characteristics of Staggered Double –Layer Microchannel Heat Sinks” in *Entropy, Vol. 20, P 537 - 541.*

23. Kandlikar S. G. and W. J. Grande, (2002) “Evolution of Microchannel flow passages - Thermohydraulic performance and fabrication technology”, *Heat Transfer Engineering, Vol.25 No.1, P 3 - 17.*

24. Kandlikar S. G. and W. J. Grande (2003) “Evolution of micro channel flow passages – thermo hydraulic performance and fabrication technology”, *Heat Transfer Engineering, Vol. 24, P 03 - 17.*

25. Kuppusamy Navin Raja, R. Saidur, N. N. N. Ghazali, H. A. Mohammed, (2014) “Numerical study of thermal enhancement in microchannel heat sink with the secondary flow”, *International Journal of Heat and Mass Transfer, Vol. 78, P 216 - 223.*

26. Lei N., P. Skandakumaran, and A. Ortega (2006) “Experimental and Modeling of Multilayer Copper Mini channel Heat sinks in Single –Phase Flow”, *0-7803-9524-7/6 IEEE.*

27. Lee Poh-Seng, Suresh V. Garimella, Dong Liu, (2005) "Investigation of heat transfer in rectangular micro channels", *International Journal of Heat and Mass Transfer, Vol. 48, P 1688 - 1704.*

28. Lee Seng Poh, Juay Choy Ho and Hong Xue (2002) "Experimental Study on Laminar Heat Transfer in Microchannel Heat sink", *IEEE Intersociety Conference of Thermal Phenomena, Vol. 23, P 379 - 385.*

29. Leng Chuan, Xiao-Dong Wang, Tian-Hu Wang, (2015) "An improved design of double-layered microchannel heat sink with truncated top channel", *Applied Thermal Engineering, Vol. 79, P 54 - 62.*

30. Levac, H. M. Soliman, and S. J. Ormiston *(2011) "*Three dimensional analysis of fluid Flow and heat transfer in single and two layered microchannel heat sinks", *Heat Mass Transfer - Springer, Vol. 47, 1375 - 1383*.

31. Li Gang, Lihao Huang, Leren Tao, (2017) "Experiment investigation of refrigerant condensation heat transfer characteristics in the horizontal micro fin tubes", *Applied Thermal Engineering, Vol. 123, P1484 - 1493.*

32. Li Zhuo, Ya-Ling He, Gui-Hua Tang, Wen-Quan Tao (2007) "Experimental and Numerical studies of fluid flow and heat transfer in microtubes" *International Journal of Heat and Mass Transfer, Vol. 50, P 3447 - 3460.*

33. Lijo Vincent, Heuy Dong Kim, Toshiakl Setoguchi (2012) "Effects of choking on flow and heat transfer in micro channels", *International Journal in Heat and Mass Transfer, Vol.55, P 701 - 709.*

34. Li Ming, Tariq S.Khan, Ebrahim Al-Hajri, Zahid H. Ayub (2016) "Single phase heat transfer and pressure drop analysis of a dimpled enhanced tube", *Applied Thermal Engineering, Vol. 101, P 38 - 46.*

35. Li W. and Zan Wu, (2010) “A general criterion for evaporative heat transfer in micro/mini channels”, *International Journal of Heat and Mass Transfer, Vol. 53 P 1967 - 1976.*

36. Lim Y.S, Simon Ching Man Yu,Jorg Uwe Schluter (2014) “Heat transfer characteristics of altering discrete flow in micro tubes”, *International Journal in Heat and Fluid Flow, Vol.74, P 333 - 341.*

37. Liu H-L, Xia-Khan A., Cong- Si Wang (2017) “Heat transfer performance of T-Y type micro channel heat sink with liquid GalnSn coolant.” *International Journal of Thermal Sciences, Vol. 120, P 203 - 219.*

38. Lu Bin, W J Meng and Fanghua Mei (2013) “Experimental Investigation of Cu-based double layered, microchannel heat exchangers”, *Journal of Micromechanics and Micro Engineering , Vol. 03, P 5017 – 19*

39. Mahendal S. S., A.M Jacobi, R. K. Shah, (2000) “Fluid flow and heat transfer at micro and meso scales with application to heat exchanger design”, *Applied Mechanical Rev*, *Vol. 53, P 175 - 193.*

40. Mahmoud M. M. and Tassos G. Karayiannis (2016) “Flow pattern transition models and correlations for flow boiling in mini tubes” *Experimental Thermal and Fluid Science, Vol. 70, P 270 - 282.*

41. Martin Mathieu, Chris Patton, John Schmitt, Sourabh V. Apte (2009) “Direct Simulation based model-predictive control of flow maldistribution in parallel microchannels”, *Journal of fluid Engineering, Vol. 143, P111201 - 17.*

42. Mirmanto (2014) “Heat transfer coefficient calculated using a linear pressure gradient assumption and measurement for flow boiling in micro channels”, *International Journal of Heat and Mass Transfer, Vol. 75, P 269 - 278.*

43. Moore, G. (1998). Cramming More Components On to Integrated circuits. *PROCEEDINGS OF THE IEEE, Vol. 86(1), P 82 - 85.*

44. Moradi H. V, Jerzy Maciej Floryan (2013) “Maximization of heat transfer across micro channels”, *International Journal in Heat and Fluid Flow, Vol.66, P 517- 530.*

45. Naphon Paisrn, Osod Khonseur. (2009) "Study on the convective heat transfer and pressure drop in the microchannel heat sink", *International Communications in Heat and Mass Transfer, Vol. 36, P 39 - 44.*

46. Nielsen K. K., K. Engelbrecht, C. R., H. Bhai (2013) “The influence of flow maldistribution on the performance of inhomogeneous parallel plate heat exchangers”, *International Journal of Heat and Mass Transfer. Vol.60, P 432 - 439.*

47. Osanloo Behzad, Akbar Mohammadi –Ahmar, Ali Solati, Mostafa Baghani. (2016) "Performance enhancement of the double-layered micro channel heat sink by use of tapered channels", Applied *Thermal Engineering, Vol. 102, P1345 - 1354.*

48. Owhaib Wahib and Bjorn Palm (2004) “Experimental investigation of single phase convective heat transfer in circular micro channels” *Experimental Thermal and Fluid Science*, *Vol. 28, P 105 - 110.*

49. Ozdemir Mehmed Rafet and Ali Kosar (2013) “Thermally developing single phase flows in micro tubes” *Journal of heat transfer, Vol.135, P 745021 - 745027.*

50. Patterson Michael K., Xiaojin Wei, Yogendra Joshi, Ravi Prasher (2004) “Numerical Study of Conjugate Heat Transfer in Stacked Microchannel”, *Inter Society Conference on Thermal Phenomena, IEEE, Vol. 8, P 357 - 362.*

51. Putra Nandy, Wayan Nata Septiadi, Gerry Julian, Ary Moulana, Ridho Irwansyah (2013) “An experimental study on thermal performance of nano fluids in micro channel heat exchanger”, *International journal of technology, Vol. 2, P167 - 177.*

52. Qu Jian, Xiaojun Li, Qian Wang, Feng Liu, Hongxian Guo (2017) “Heat transfer characteristics of micro grooved oscillating heat pipes” *Experimental Thermal and Fluid Science, Vol. 85, P 75 - 84.*

53. Qu Weilin, Issam Mudawar, (2002) "Analysis of three dimensional heat transfer in micro-channel heat sink*", International Journal of Heat and Mass Transfer, Vol. 45, P 3973 - 3985.*

54. Qui S. L., P. Zhang, R. Z Wang, L. X. Xu (2007), "Single phase pressure drop and heat transfer characteristics of turbulent liquid nitrogen flow in micro-tubes" *International Journal of Heat and Mass Transfer, Vol.50, P 1993 - 2001.*

55. Sahar Amirah M, Mehmed R. Ozdemir, Ekhlas M. Fayyadh Jan Wissink, Mohamed M. Mahmoud, Tassos G. Karayiannis, (2016) "Single phase flow pressure drop and heat transfer in rectangular metallic micro channels", *Applied Thermal Engineering, Vol. 93, P 1324 - 1336.*

56. Said S. A. M., Rached Ben-Mansour, M. A. Habib, M. U. Siddiqui (2015) "Reducing the flow maldistribution in a heat exchanger", *Computers and Fluids. Vol. 107, P 1 - 10.*

57. Sajadifar S. A, Arash Karimipour, Davood Toghraie (2017) "Fluid flow and heat transfer of non- Newtonian nano fluid in a micro tune considering slip velocity and temperature jump boundary conditions", *European Journal of Mechanics B/Fluids" Vol. 61, P 25 - 32.*

58. Siva V. Manoj, Arvind Pattamatta, Sarit K. Das (2014) "Effect of flow maldistribution on thermal performance of parallel micro channel cooling systems", *International Journal of Heat and Mass Transfer, Vol. 73, P 424 - 428.*

59. Sohel M. R., R .Saidur. Mohd Faizul Mohd Sabri, M. Kamalisarvestani, M. M. Elias, Ali Ijam (2013) "Investigating the heat transfer performance and thermo physical properties of nano fluids in circular micro channels", *International Communications in Heat and Mass Transfer, Vol.42, P 75 - 81.*

60. Sung M. K, Issam Mudawar, (2008) "Single phase and two phase heat transfer characteristics of low temperature hybrid microchannel/micro jet impingement cooling module*", International Journal of Heat and Mass Transfer, Vol. 51, P 3882 - 3895.*

61. Tam H. K. Lap Mou Tam, Afshi .J. Ghajar, Ping Chen, (2017) "Experiment study of the ultrasonic effect on heat transfer inside a horizontal mini tube in the laminar region", *Applied Thermal Engineering, Vol. 114, P 1300 - 1308.*

62. Thompson Scoot E., Srivatsan Parthasarathy (2014). "Moore's law; the future of Si microelectronics." In materials today journal, ISSN 1369 7021

63. Tuckerman D.B. and R.F.W.Pease, (1981) "High-performance heat sinking for VLSI", *IEEE Electron Device Letters EDL- Vol. 2, P 126 - 129.*

64. Vafai. K and Lu Zhu (1999) "Analysis of two layered microchannel heat sink concept in electronic cooling", *International Journal of Heat and Mass Transfer, Vol. 42, P 2287 - 2297.*

65. Vinoth R. and Senthil Kumar (2017) "Channel cross section effect on heat transfer performance of oblique finned micro channel heat sink", *International Communications in Heat and Mass Transfer, Vol.87, P 270 - 276.*

66. Wang J, Yong Li, Junjie Yan, Ronghai Huang, Xiping Chen (2015) "Condensation heat transfer of steam on vertical micro tubes.", *Applied Thermal Engineering, Vol. 88, P 185 - 191.*

67. Wang Sho-Lin, Xian-Yang Li, Xiao-Dong Wang, Gui Lu, (2018) "Flow and heat transfer characteristics in double layered microchannel heat sink with porous fins", *International Communication in Heat and Mass Transfer, Vol. 150, P 343 - 355.*

68. Wei Xiaojin and Yogendra Joshi (2004) "Stacked Microchannel Heat Sinks for Liquid Cooling of Microelectronic Components", *Transactions of ASME, Vol.126, P 60 - 66.*

69. Wei Xiaojin and Yogendra Joshi, Michael K. Patterson (2007) "Stacked Microchannel Heat Sinks for Liquid Cooling of Microelectronic Components", *Transactions of ASME, Vol.129, P 1432 - 1444.*

70. Wong. Kok-Cheong, Fashli Nazhirin, Ahmad Muezzin, (2013) "Heat transfer of a parallel flow two-layered microchannel heat sink", *International Communication in Heat and Mass Transfer, Vol. 02, P 862 - 865.*

71. Wu, J. Y. Zhao, K. J. Tseng (2014) "Parametric studies on the performance of double-layered microchannel heat sink", *Energy Conversion and Management, Vol. 80, P550 - 560.*

72. Xia G., Dandan Ma, Yuling Zhai, Yunfei Li, Ran Liu, Mo Du. (2015) "Experimental and numerical study of fluid flow and heat transfer characteristics in microchannel heat sink with complex structure.", *Energy Conversion and Management, Vol. 105, P 848 - 857.*

73. Xia Liang and Yue Chan (2015) "Investigation of the enhancement effect of heat transfer using micro channels", The 7th International Conference on Applied Energy-ICAE2015, *Science Direct Energy Proceedia, Vol. 75, P 912 - 918.*

74. Yadav V, Kuldeep Baghel, Ritunesh Kumar, S.T.Kadam (2016) "Numerical investigation of heat transfer in extended surface micro", *International Journal of Heat and Mass Transfer, Vol.93, P 612 - 622.*

75. Zhai Yuling, Zhouhang Li, Hua Wang, Jianxin Xu (2017) "Thermodynamic analysis of the effect of channel geometry on heat transfer in double-layered microchannel heat sink", *Energy Conversion and Management, Vol. 143, P 431 - 439.*

76. Zhao Hongxia, Zhigang Liu, Chengwu Zhang, Ning Guan, Honghua Zhao (2016) "Pressure drop and friction factor of a rectangular channel with staggered mini pin fins of different shapes", *Experimental Thermal and Fluid Science, Vol. 71, P 57 - 69.*

77. Zuo Wei, Jiaqiang E., Rongming Lin (2018) "Numerical investigations on an improved counter flow double channel micro combustor fueled with hydrogen for enhancing thermal performance", *Energy Conversion and Management, Vol. 93, P 41 - 47.*

LIST OF PUBLICATIONS

- Sagar M.Narayanan and Pradeep M. Kamath, (2019) "*Application of a Double Layer Circular Microchannel Heat Sink in Electronic Industry*" in International Journal of Innovative Technology and Exploring Engineering, *Vol. 8, Issue 12. P 1153 - 1158.*

- Sagar M.Narayanan and Pradeep M. Kamath, (2019) *"Influence of a Copper-Based Stacked Circular Microchannel Heat Sink in the Thermal Enhancement of Electronic Cooling*" in Advancement in Mechanical Engineering and Technology, *Vol. 2, Issue 2. P 14 - 26.*

- Sagar M.Narayanan and Pradeep M. Kamath, (2018) "*Numerical study of thermal enhancement in a stacked microchannel heat sink with different flow arrangement*s" in International Journal of Management Technology and Engineering, *Vol. 8, Issue XI. P 83 - 89.*

- Sagar M.Narayanan and Pradeep M. Kamath, *"Experimental analysis of pressure drop and heat transfer performance in a copper-based double layer circular microchannel heat sink"* in KETCON (2019) conducted by Kerala state Technological Congress 2019, organized at Government Engineering College, Thrissur.

- Sagar M.Narayanan and Pradeep M. Kamath, "*Numerical study of thermal enhancement in a stacked microchannel heat sink with different flow arrangement*s" in 4th International conference proceedings on Research Developments in Applied Science, Engineering and Management. Institution of Engineers, Chandigarh, India on 3rd November 2018.

APPENDIX - A

A.1 CALIBRATION OF THERMOCOUPLE

The calibration of the thermocouple is conducted during the experiment. The K-Type thermocouples used for the experiment are calibrated with a calibrated J-Type thermocouple.

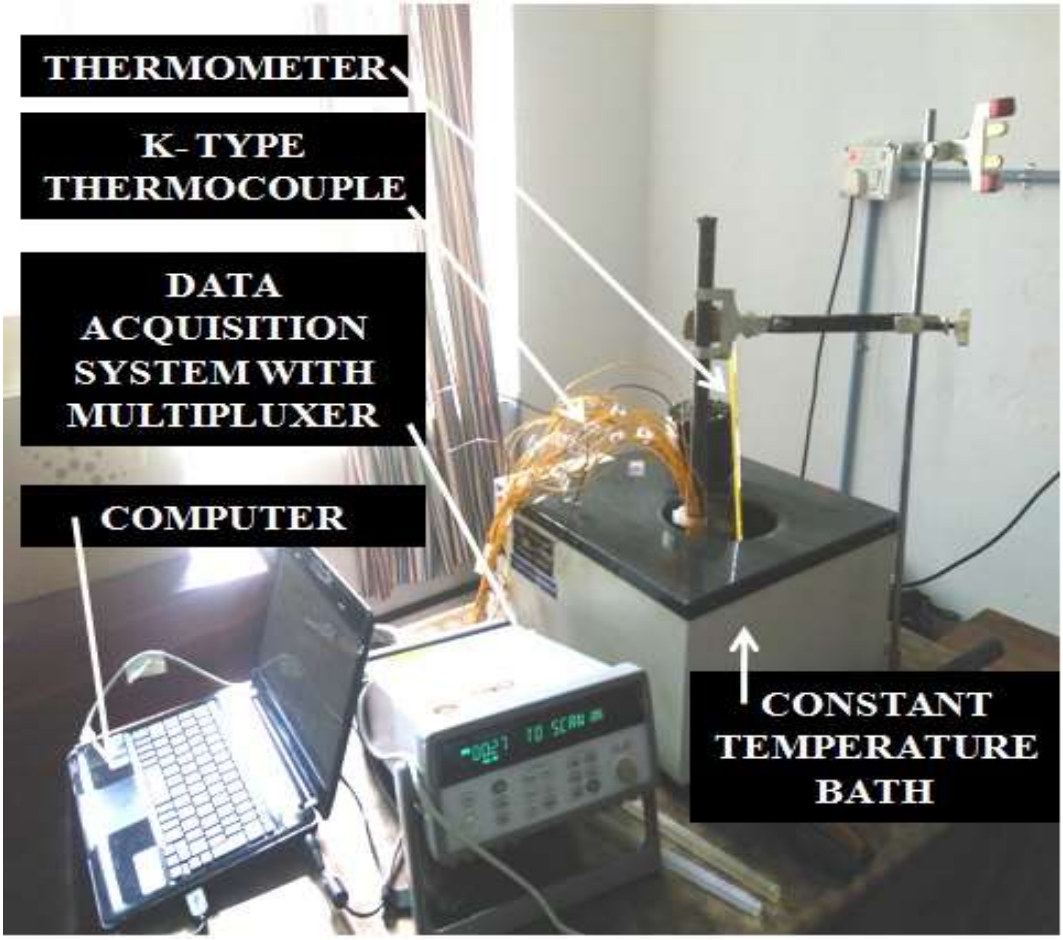

Fig A1 – 1, Pictorial view of the Thermocouple Calibration

The Fig.A1-1 shows the pictorial view of the thermocouple calibration. It consists of a constant temperature bath, thermometer, data acquisition unit with a multiplexer, and a computer. The data from the twenty three K-type thermocouples and a J-type

thermocouple is recorded in the computer and the variation is plotted in the Fig.A1- 2 and Fig.A1 - 3.

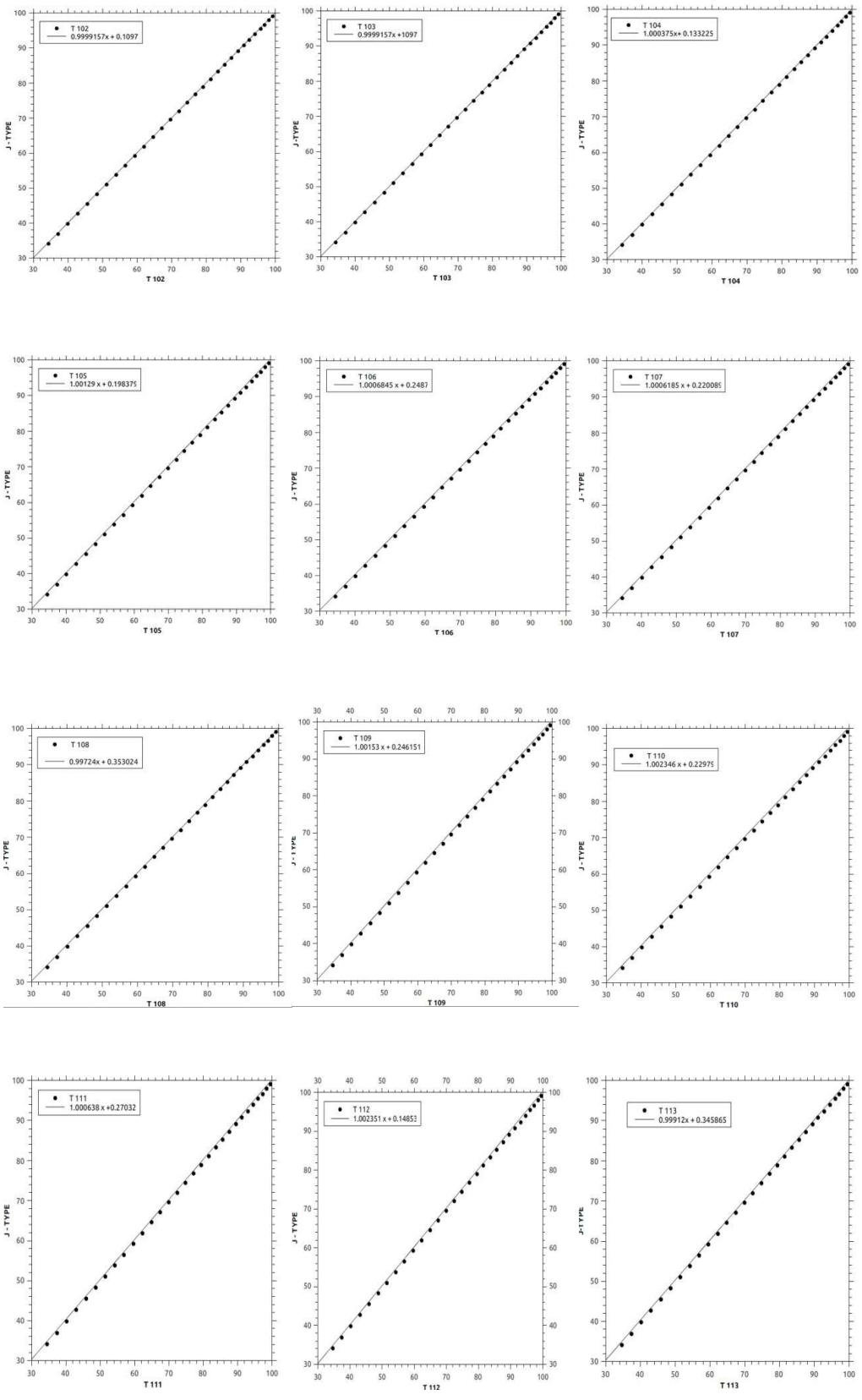

Fig A1 – 2, Thermocouple Calibration Curves

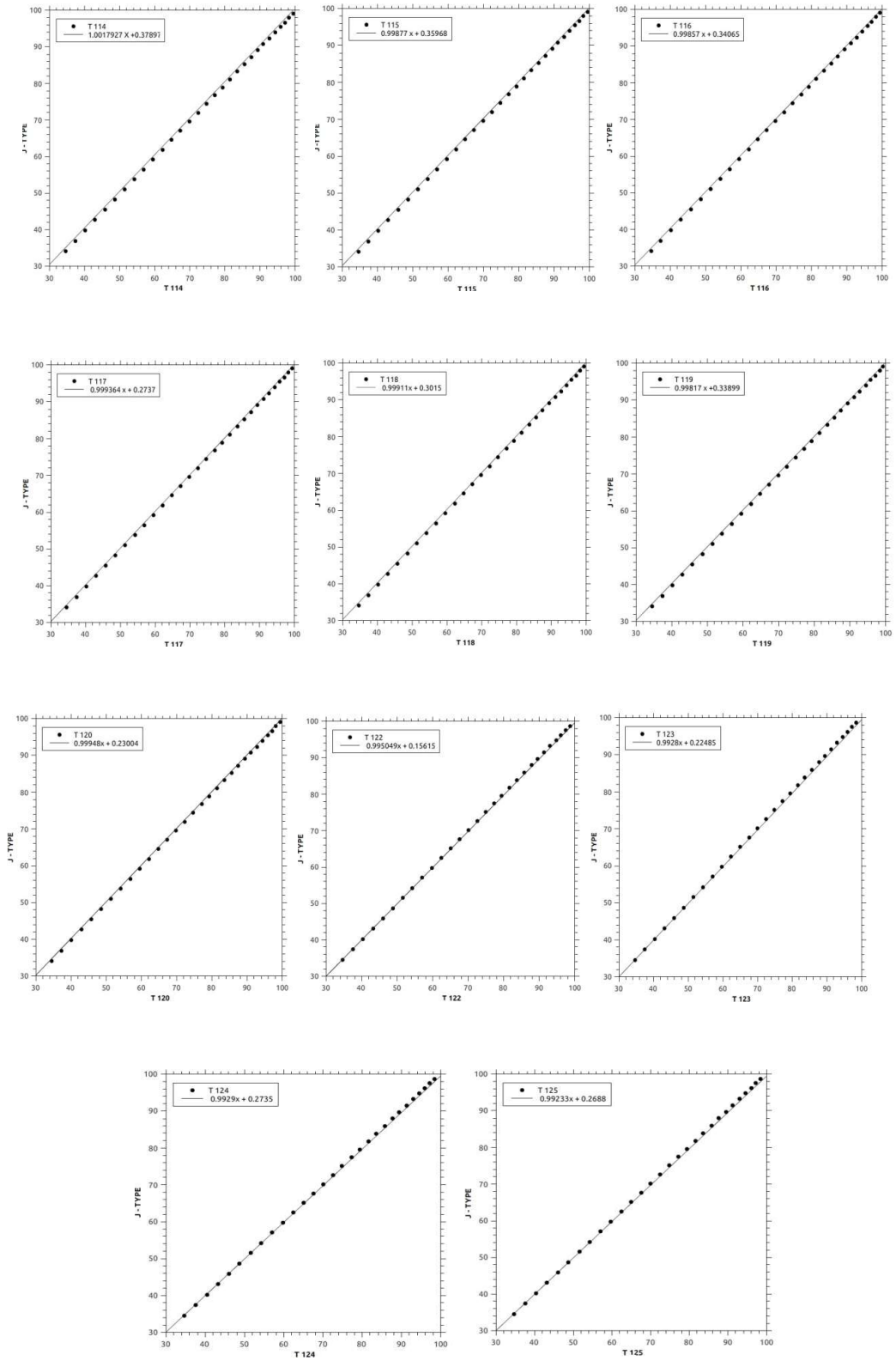

Fig A1 – 3, Thermocouple Calibration Curves

A.2 CALIBRATION OF DIGITAL MANOMETER

Fig A 2 – 1, Pictorial view of the digital manometer calibration

Fig. A 2-1 shows the pictorial view of the digital manometer calibration.

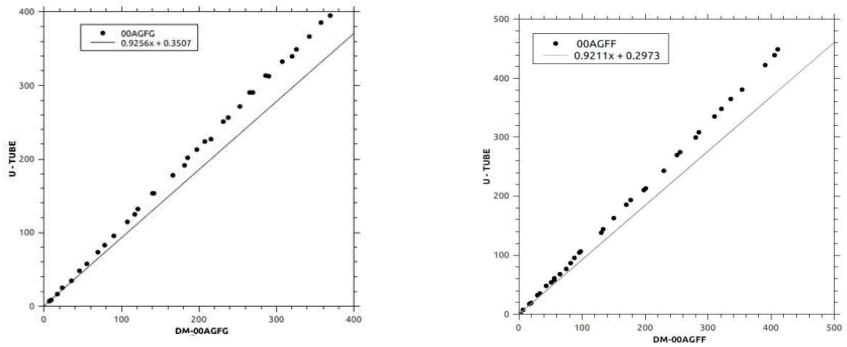

Fig A 2 – 2, Digital manometer calibration curves

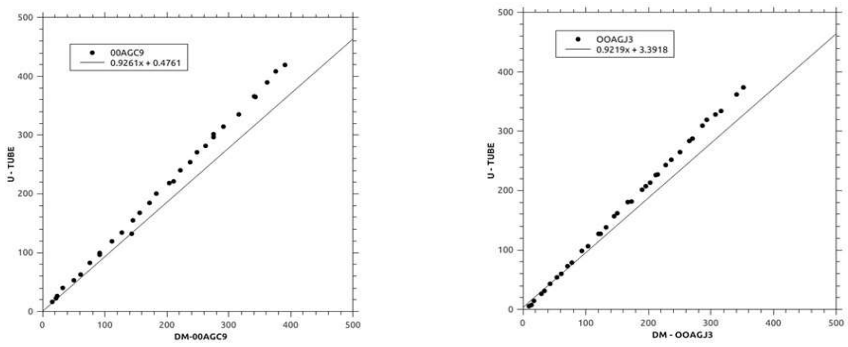

Fig A 2 – 3, Digital manometer calibration curves

The calibration is done with standard U-Tube manometer. The calibrated curves are plotted in Fig. A 2.2 and Fig. A 2.3.

APPENDIX - B

B.1 UNCERTAINTIES IN MEASUREMENTS

Table B.1 - 1 shows the uncertainties of the measurement.

Table B 1 - 1 Uncertainty of the Measurement

APPARATUS	UNCERTAINTY
U-tube Manometer	1 mm of Hg
Measuring Jar	1 ml
Digital Manometer	0.5% of the full-scale reading (2 bar)
Pressure Transducer	0.25% of the full-scale reading (2.5 bar)
Thermocouple	± 0.1 ^{0}C
Stopwatch	0.01 sec
GO-NO-GO Gauge	± 0.05 mm

For performing the error analysis the maximum uncertainties in determining the measured parameters are given in Table B1 - 1. The measurement uncertainty of the volume flow rate is one ml. The diameter of micro-channel is measured using GO-NO-GO gauge.

Table B.1 - 2 shows the derived uncertainties.

Table B1-2 Derived Uncertainties

DERIVED	UNCERTAINTY
Friction Factor	0.064
Discharge	0.01